COMPLIMENTARY COPY

AUSTRALIAN JOURNAL OF PHYSICS

VOLUME 13, NUMBER 4, DECEMBER 1960

REGISTERED IN AUSTRALIA FOR TRANSMISSION BY POST AS A PERIODICAL

AUSTRALIAN JOURNAL OF PHYSICS

Published by the Commonwealth Scientific and Industrial Research Organization. Volumes 1 to 5 of the Australian Journal of Physics and the Australian Journal of Chemistry issued as the Australian Journal of Scientific Research, Series A : Physical Sciences. Issued quarterly, £2 per annum.

BOARD OF STANDARDS

The Board of Standards for this Journal is appointed by the Commonwealth Scientific and Industrial Research Organization and the Australian Academy of Science and consists of Professor Sir Macfarlane Burnet (Chairman), Dr. N. S. Noble (Editor), Professor N. S. Bayliss, Dr. J. L. Pawsey, Professor W. P Rogers, and Professor J. S. Turner.

ADVISORY COMMITTEE

Acceptance of papers for this Journal is in the hands of an Advisory Committee appointed by the Board of Standards in consultation with the Institute of Physics (Australian Branch) and consisting of Dr. N. S. Noble (Chairman and Editor), Dr. G. H. Briggs, Emeritus Professor L. G. H. Huxley, Dr. J. L. Pawsey, and Professor H. C. Webster.

OTHER JOURNALS PUBLISHED BY C.S.I.R.O.

Australian Journal of Chemistry Australian Journal of Biological Sciences Australian Journal of Applied Science	Issued quarterly, £2 per annum
Australian Journal of Agricultural Research	Issued six times a year, £2 per annum
Australian Journal of Marine and Freshwater Research Australian Journal of Botany Australian Journal of Zoology	Not issued at regular intervals, 10/- per issue

The Organization is a signatory to the Fair Copying Declaration, details of which may be obtained from the office of the Royal Society, London.

All enquiries and manuscripts should be forwarded to :

The Editor,
Australian Journal of Physics,
Commonwealth Scientific and Industrial Research Organization,
314 Albert Street, East Melbourne, C.2, Victoria

MELBOURNE

FOCUSING OF RADIO WAVES REFLECTED FROM A ROUGH CURVED IONOSPHERE

By J. D. WHITEHEAD*

[*Manuscript received June* 8, 1960]

Summary

The reflection of radio waves from a partially rough, curved ionosphere is considered. The relationship between the amplitude of the echo, A, and phase path P when the ionosphere moves overhead with a horizontal velocity V at a height h is the same as that for a smooth curved ionosphere, i.e.

$$A^2 \propto 1 - \frac{h}{2V^2} \frac{\mathrm{d}^2 P}{\mathrm{d}t^2},$$

although because of the different physical conditions the large increases in echo amplitude observed when reflection takes place from a smooth ionosphere are not expected for reflection from a rough ionosphere.

A method of testing the relationship experimentally is suggested.

I. INTRODUCTION

It occasionally happens that the ionosphere behaves as a specular reflector of radio waves incident normally on it, so that for many purposes it may be treated as a smooth mirror. However, Munro (1950) and Bramley and Ross (1951) have shown that this smooth " mirror " is not plain but has ripples moving through it ; the ripples having a wavelength of about 100 km and an amplitude of a few kilometres. As they move overhead, the ripples have the effect of producing large increases in the amplitude of the reflected radio waves : this effect is known as focusing and the author (Whitehead 1956) has shown that, for vertical incidence, the amplitude A and phase path P are related by the equation

$$A^2 \propto 1 - \frac{h}{2V^2} \frac{\mathrm{d}^2 P}{\mathrm{d}t^2}, \quad \ldots\ldots\ldots\ldots\ldots\ldots \quad (1)$$

when h is the average height of the reflector and V is its horizontal velocity.

However, it is more usual for the ionosphere to be a rough reflector, so that the echo fades and the amplitude has a Rayleigh distribution (Mitra 1949). It is of interest to enquire whether " focusing " is to be expected under these circumstances if the rough reflector is curved. It is indeed found that the mean amplitude fluctuates slowly (Meadows and Moorat 1957), and it is of interest to see if there is a similar relationship to (1) between the mean amplitude and the phase path. It is the purpose of the present paper to derive this relationship. However, it is shown that the large increases in mean amplitude are not to be expected because of the difference in the physical situations.

* Radio Research Board Laboratory, Electrical Engineering Department, University of Sydney.

II. Derivation of the Equation

Briggs and Phillips (1950) have shown that, for radio wavelengths shorter than about 200 m, the ionosphere can usually be treated as a partially rough reflector so that most of the power returned to a transmitter on the ground is contained within a cone of semi-angle θ_0 if the ionosphere is flat. θ_0 was found to be about 5°, so that the effective area of the ionosphere for reflection is that contained within a circle of radius $\theta_0 h$, about 10–30 km, small compared with the wavelength of the ripples.

Now suppose the rough reflector is slightly curved concave downwards with a radius of curvature $R > h$, the curvature being in one dimension only so that it forms part of a cylinder. Power is now returned from a greater area of the ionosphere, an ellipse with semimajor axes $\theta_0 h$ and φh, where φ is the angle an incident ray makes with a line drawn perpendicular to the reflecting surface from the transmitter when the specularly reflected ray makes an angle $2\theta_0$ to the incident ray in the plane of curvature of the ionosphere (Fig. 1). Thus the power returned is increased in proportion to φ/θ_0. It is seen that

$$\frac{\sin \varphi}{R} = \frac{\sin \theta_0}{R-h},$$

therefore

$$\frac{\sin \varphi}{\sin \theta_0} = \frac{R}{R-h} = 1 + \frac{h}{R-h},$$

so that the square of the amplitude is given approximately by

$$A^2 \propto \varphi/\theta_0 \approx 1 + \frac{h}{R-h}.$$

This is identical with the relation derived for the amplitude of a wave reflected from a curved mirror: thus it follows that when the rough curved reflector moves with velocity V at right angles to the axis of the cylinder,

$$A^2 \propto 1 - \frac{h}{2V^2} \frac{\mathrm{d}^2 P}{\mathrm{d}t^2}.$$

In this equation A^2 and $\mathrm{d}^2P/\mathrm{d}t^2$ are to be interpreted as mean values taken over several rapidly fading cycles.

III. Discussion

Although the same equation has been derived for both rough and smooth ionospheres, there is an important physical difference. For a mirror reflection, the principal contribution to the amplitude comes from the first few Fresnel zones: the amplitude is proportional to the area of the zones, or for cylindrical curvatures, to the length of the (elongated) zones. However, for a rough reflector it is the power or the *square* of the amplitude which is proportional to the area, or length, of the effective reflecting part of the ionosphere. With a smooth flat reflector at a height of 200 km, the first Fresnel zone has a radius of about 5 km at a radio wavelength of 100 m: if the zone is elongated to a half length of 15 km, small compared to the wavelength of a ripple, the amplitude is increased by a factor of three. For a rough ionosphere at the same height, for which $\theta_0 = 5°$,

the radius of the effective area for reflection is 20 km : if the amplitude is to be increased by the same factor, the half length of the effective area has to be increased to 180 km, which is no longer small. Thus it is to be expected that equation (**1**) will apply to a rough ionosphere when the amplitude increases above normal are quite small : for large values of the right-hand side of equation (**1**), the amplitude will be less than that given by the equation.

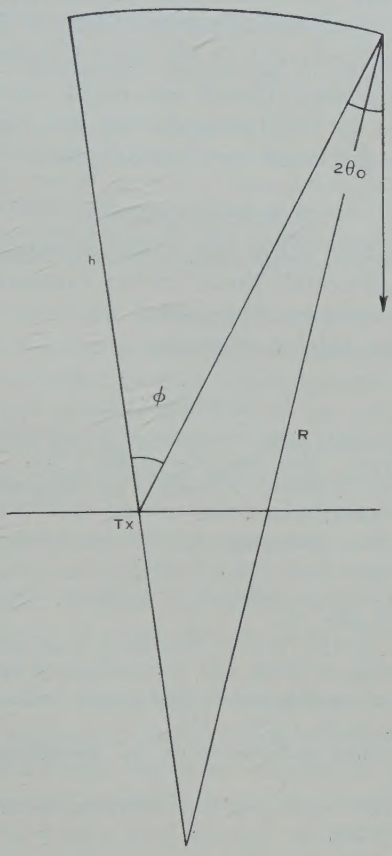

Fig. 1

IV. Proposed Experimental Test

The difficulty of testing the relationship is that, under rapid fading conditions, the changes in phase path are also rapid, and the usual method of measuring phase path (Findlay 1951) is unsatisfactory, partly because of the tedious work involved in counting wavelength changes from a confused film record and partly because the large and rapid changes in echo amplitude make it difficult to obtain a continuous record.

The Findlay method consists of beating an echo from a pulse transmitter with a c.w. oscillator output phase locked to the transmitter at a frequency of about 50 kc/s greater than the transmitter frequency. The rectified output is differentiated and recorded on film.

It is proposed to overcome the difficulties associated with this method by feeding the rectified output into a phase-sensitive rectifier whose comparison phase is derived from a 50 kc/s oscillator phased with respect to the original transmitted pulse by the rotation of a condenser. The output from the phase-sensitive rectifier will be used to drive the condenser in such a direction as to reduce this output. The rotation of the condenser will be recorded : this gives the changes in phase path. To ensure that a sufficiently pronounced beat is produced at the receiver output, the output amplitude of the c.w. radio-frequency oscillator will be made proportional to the echo amplitude.

This system of measurement should also enable us to distinguish between the rapid fading produced by small irregularities and that produced by a deep phase screen of the type discussed by Hewish (1951).

V. Acknowledgments

This work has been carried out as part of the investigations of this laboratory sponsored by the Radio Research Board of the Commonwealth Scientific and Industrial Research Organization. The author wishes to thank Dr. G. H. Munro and Mr. L. H. Heisler for helpful discussion.

VI. References

Bramley, E. N., and Ross, W. (1951).—Measurements of the angle of arrival of short radio waves reflected from the ionosphere. *Proc. Roy. Soc.* A **207** : 251.

Briggs, B. H., and Phillips, G. J. (1950).—A study of the horizontal irregularities of the ionosphere. *Proc. Phys. Soc. Lond.* B **63** : 907.

Findlay, J. W. (1951).—The phase and group paths of radio waves returned from the *E* region of the ionosphere. *J. Atmos. Terr. Phys.* **1** : 353.

Hewish, A. (1951).—The diffraction of radio waves in passing through a phase-changing ionosphere. *Proc. Roy. Soc.* A **209** : 81.

Meadows, R. W., and Moorat, A. J. G. (1957).—The effect of fading on the accuracy of measurement of ionospheric absorption. *Proc. Inst. Elect. Engrs.* B **105** : 27.

Mitra, S. N. (1949).—Statistical analysis of fading of a single downcoming wave from the ionosphere. *Proc. Inst. Elect. Engrs.* III **96** : 505.

Munro, G. H. (1950).—Travelling disturbances in the ionosphere. *Proc. Roy. Soc.* A **202** : 208.

Whitehead, J. D. (1956).—The focussing of short radio waves reflected from the ionosphere. *J. Atmos. Terr. Phys.* **9** : 269.

GEOMAGNETIC MICROPULSATIONS

By G. R. A. Ellis*

[*Manuscript received July* 11, 1960]

Summary

This paper describes simultaneous observations of geomagnetic micropulsations at three places ranging from 28° S. to 51° S. geomagnetic latitude. It is shown that there is no observable change in the micropulsation period with latitude although there is a monotonic increase in the amplitude with latitude for all periods between 10 and 100 sec. The interpretation of these results in terms of existing theories is discussed.

I. Introduction

The study of the micropulsations of the geomagnetic field has been intensified in recent years with the realization that these phenomena may provide evidence for the propagation of hydromagnetic waves in the outer atmosphere. Dungey (1954), for example, has suggested that micropulsations may be caused by standing hydromagnetic waves along the geomagnetic field lines, oscillating perpendicular to the meridian field. In the fundamental mode the period of these oscillations would increase with geomagnetic latitude as the length of the lines increased. Obayashi and Jacobs (1958) have reported that in middle and high latitudes the period of some micropulsations appears to increase with latitude and they calculated that the density of the outer atmosphere needed to support standing wave oscillations of the periods observed agreed fairly well with that obtained from the dispersion of whistling atmospherics (Storey 1953).

Dungey (1954) has suggested also that interplanetary gas, flowing over the surface of the Chapman-Ferraro boundary separating the terrestrial and interplanetary atmospheres, would generate waves in a similar way to the generation of waves on water by the wind ; propagating downwards as Alfvén waves, they would reach the ionosphere in the auroral regions. If their effects were localized, micropulsations due to this mechanism would not be observed at low and middle latitudes. However, it has recently been shown by Bomke *et al.* (1960) that magnetic disturbances caused by the Argus high altitude atomic explosions appeared to be propagated horizontally in hydromagnetic ducts between the ionosphere and a height of 2500 km. Such propagation would also be likely to spread micropulsations. In this case there would be a change in amplitude with latitude but not in period. It is relevant to this mechanism that observations at the boundary of the geomagnetic field with the Pioneer I space probe have shown the existence of large field fluctuations in this region (Sonett, Judge, and Kelso 1959).

* Upper Atmosphere Section, C.S.I.R.O., Camden, N.S.W. ; present address : Department of Physics, University of Tasmania, Hobart.

A third alternative has been put forward by Lehnert (1956) and Maple (1959), who, following Holmberg (1951), have suggested intra-layer hydromagnetic oscillations within the ionospheric E and F layers. The main objection to this hypothesis is that the high attenuation of hydromagnetic wave propagation under normal ionospheric conditions would appear to preclude such resonance effects (see, for example, Piddington 1959).

For the systematic study of these theories it would be necessary to record micropulsations simultaneously over large parts of the world. Nevertheless, it is clear that useful information would be obtained from a more limited investigation by comparing the amplitude and period of micropulsations recorded simultaneously at places in the same geomagnetic meridian, particularly at middle and lower latitudes where the disturbances of the auroral zone are less pronounced.

This paper presents the results of a series of observations over a range of geomagnetic latitudes extending from 28° S. to 51° S. for the period September 1959 to April 1960.

II. Observations

Micropulsations were recorded simultaneously at Townsville, Qld., Camden, N.S.W., and Hobart, Tas. These three places are at nearly the same geomagnetic longitude, but have geomagnetic latitudes of 28° S., 42° S., and 51° S. respectively. Each recorder used a 4-turn horizontal pick-up loop with an average area of 10 000 m^2. The loops were connected through galvanometer-photocell amplifiers to pen recorders with a chart speed of 6 in/hr. The frequency response of the amplifiers was flat from d.c. to 0·15 c/s, while the highest frequency which could be resolved by the recorders was 0·17 c/s. The deflection sensitivity of the three recorders for full scale deflection was normally 0·7, 0·5, and 0·3 γ/sec respectively, and the amplifier noise was less than 0·005/sec (1 $\gamma = 10^{-5}$ gauss). Each recorder was calibrated periodically, both with a calibration loop in the same trench as the pick-up loop and with a signal generator applied to the input terminals of the amplifier. The peak-to-peak amplitude of the third highest oscillation and the average period in 5-min intervals was measured, except when the period was greater than 50 sec, when 6 cycles were used. One hundred and nine individual occurrences of micropulsations occurring on 40 days during February, March, and April 1960 were used in the analysis ; 74 of these were in the day-time and 35 at night. Records obtained during magnetically active periods ($K_p > 6$) were not used because of the difficulty of separating the many different frequency components without a spectrum analyser.

Although a superficial inspection of the simultaneous records showed many occasions when there was an apparent large increase in period with latitude, closer examination showed that in all cases this was due to the superimposition of micropulsations of different periods but of different amplitudes at the three places. In general, those of longer period were stronger (compared with those of shorter period) at Hobart than at Townsville. This was shown clearly on occasions when bursts of relatively pure oscillations of different periods were recorded in succession. The periods were then always observed to be the same at all stations within the limits of measurement, which were estimated to be

± 5 per cent. On the other hand, the change in amplitude was often pronounced, particularly for the longer periods. Figure 1 shows sample records of micropulsations at Townsville, Camden, and Hobart on April 13, 1960. The two bursts of micropulsations at A and B on these records had periods of 30 and 17 sec respectively. The relatively greater amplitude of the shorter micropulsations at Townsville should be noted. Figure 2 shows the average amplitudes of simultaneous micropulsations of different periods at the three places and Table 1, the average ratios of their amplitudes at Hobart and Townsville.

TABLE 1

THE RATIO BETWEEN MICROPULSATION AMPLITUDES AT HOBART AND TOWNSVILLE

Period range (sec) ..	10–20	20–30	30–45	45–60	60–100
Amplitude at Hobart / Amplitude at Townsville	$1{\cdot}75\pm0{\cdot}8$	$1{\cdot}75\pm0{\cdot}5$	$4{\cdot}0\pm1{\cdot}5$	$4{\cdot}1\pm1{\cdot}25$	$4{\cdot}0\pm1{\cdot}4$
No. of observations ..	28	24	14	17	26

III. Discussion

It is clear from the observations that the variation of period with latitude was very small between 28° S. and 51° S. To see how this result compared with the predictions of the standing-wave theory, the fundamental period of oscillation of the geomagnetic field lines was calculated using recent data on the density of the outer atmosphere. For a line of length l, passing through a fully ionized medium of mass density ρ, the period is

$$T=\int_0^l \frac{2\mathrm{d}s}{V(s)},$$

where $\mathrm{d}s$ is the line element and $V(s)$ the Alfvén velocity,

$$V(s)=H(s)(4\pi\rho(s)^{-\frac{1}{2}}. \quad \text{(Dungey 1954)}$$

$H(s)$ is the magnetic field intensity. In the lower parts of the outer atmosphere the density of neutral atoms is not negligible and it is necessary to modify the expression for the velocity. Piddington (1959) has shown that the propagation constant is then

$$K=H^{-1}(4\pi\rho)^{+\frac{1}{2}}(\omega/2\tau)^{\frac{1}{2}}(1-i),$$

which describes waves travelling with velocity

$$H(4\pi\rho)^{-\frac{1}{2}}(2\omega\tau)^{\frac{1}{2}}$$

and with attenuation

$$k=H^{-1}(4\pi\rho)(\omega/2\tau)^{\frac{1}{2}}.$$

τ is the period needed to accelerate neutral atoms to the same velocity as the ions (see Piddington 1957, Appendix I).

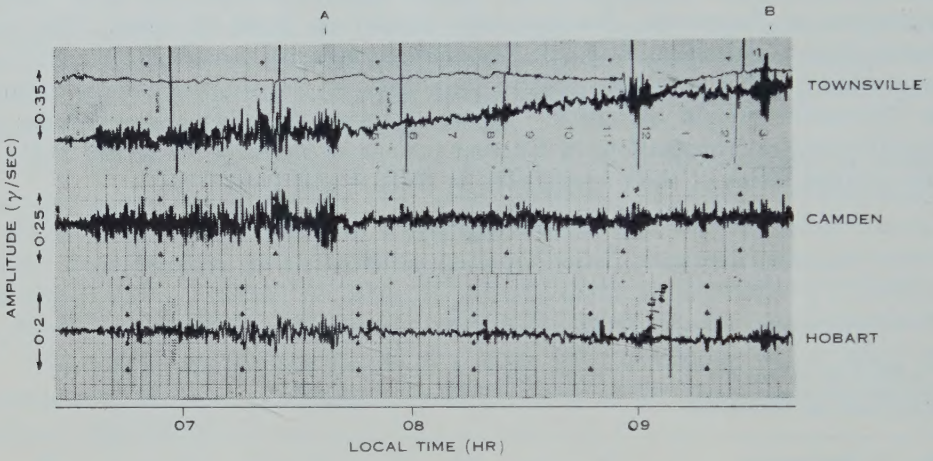

Fig. 1.—Records of micropulsations at Townsville, Camden, and Hobart on April 13, 1960. The individual oscillations were resolved on the original records.

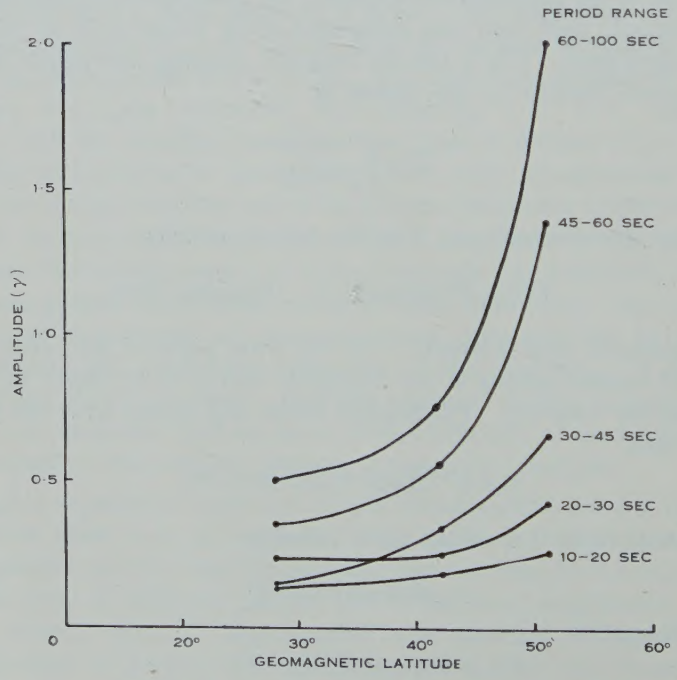

Fig. 2.—The observed variation in amplitude with geomagnetic latitude of micropulsations with different periods.

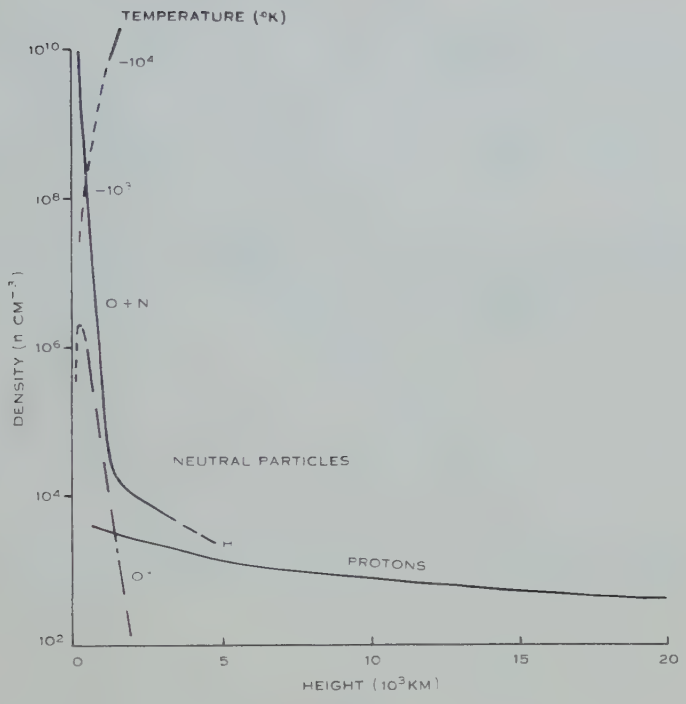

Fig. 3.—Assumed model of the outer atmosphere.

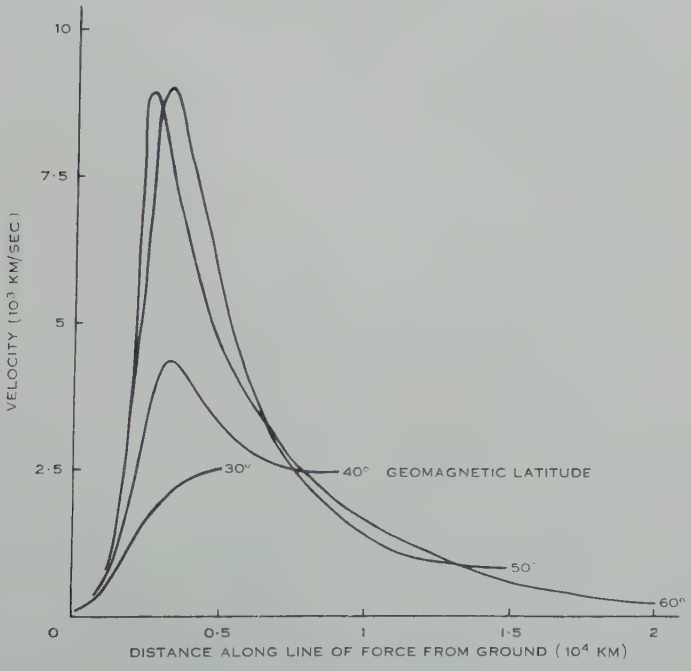

Fig. 4.—The variation of the Alfvén velocity along different geomagnetic field lines.

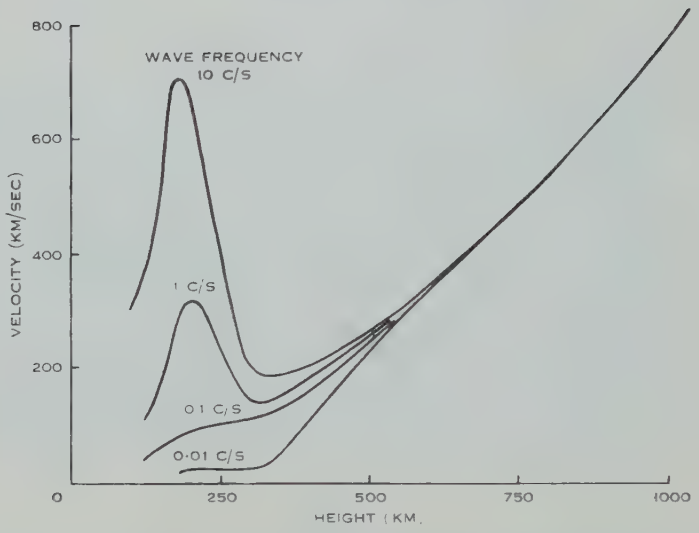

Fig. 5.—The variation of hydromagnetic wave velocity below 1000 km height when the effect of neutral atoms is taken into account.

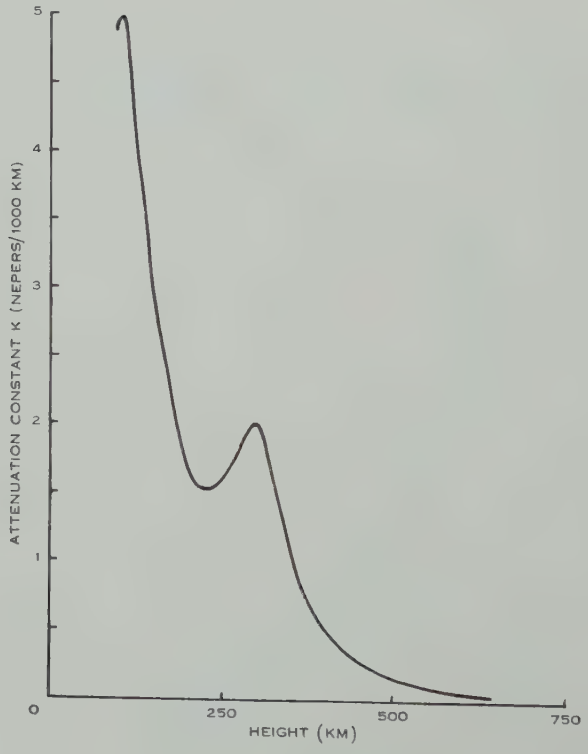

Fig. 6.—The attenuation below 1000 km height for a wave frequency of 0·01 c/s when neutral atoms are taken into account. The attenuation is proportional to (frequency)$^{\frac{1}{2}}$.

The velocity of propagation along field lines ending at different latitudes was computed assuming a dipole form for the geomagnetic field and using the model of the outer atmosphere recently proposed by Johnson (1960) (Fig. 3). Figures 4 and 5 show the velocity profiles obtained. Figure 6 shows the high attenuation for propagation within the ionosphere when neutral atoms are taken into account, and Figure 7 shows the variation of the fundamental period with latitude.

With this model the period would be 30 sec at 28° S. increasing to 55 sec at 51° S. An earlier exponential model of the outer atmosphere with greater densities between 2000 and 10 000 km heights (Obayashi and Jacobs 1958) gave periods of 45 and 70 sec at 28° S. and 51° S. respectively.

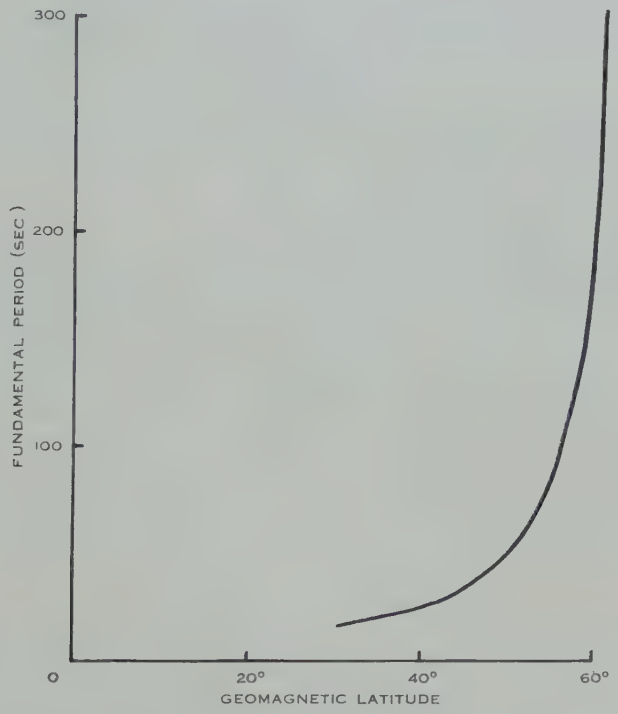

Fig. 7.—The calculated variation of the fundamental period of oscillation of geomagnetic field lines using the model of Figure 3.

The absence of any observed variation in the period over this range of latitudes would therefore appear to point to some other cause of micropulsations. The monotonically increasing amplitude with latitude, on the other hand, suggests strongly that they originate at higher latitudes and are propagated towards the equator, with greater attenuation at the longer periods. The rapid decrease in the propagation velocity of longitudinal hydromagnetic waves below 3000 km (Fig. 4) supports the idea of suitable horizontal hydromagnetic ducts such as Bomke *et al.* proposed. Although the fundamental periods of standing waves along high latitude field lines would be much greater than the periods

observed, it should be noted that the considerable variation in velocity along these lines would favour the generation of many higher order oscillations with periods not integral submultiples of the fundamental.

As in the case of Dungey's hypothesis of ripples in the Chapman-Ferraro surface, micropulsations due to higher order oscillations of the longer field lines would first appear in the auroral zone. Lower latitude observations could not distinguish between these two possibilities. However, very accurate measurements of the phase difference between micropulsations at slightly different latitudes should provide information about their horizontal propagation.

IV. Acknowledgments

The author wishes to thank Mr. R. Conway of the Ionospheric Prediction Service, Townsville, for operating the Townsville recorder.

V. References

Bomke, H. A., Ramm, W. J., Goldblatt, S., and Klemas, V. (1960).—*Nature* **185** : 299.
Dungey, J. W. (1954).—" The Physics of the Ionosphere." p. 229. (Phys. Soc. : London.)
Holmberg, E. R. R. (1951).—Ph.D. Thesis, University of London.
Johnson, F. S. (1960).—*J. Geophys. Res.* **65** : 577.
Lehnert, B. (1956).—*Tellus* **8** : 241.
Maple, E. (1959).—*J. Geophys. Res.* **64** : 1405.
Obayashi, T., and Jacobs, J. A. (1958).—*Geophys. J.* **1** : 53.
Piddington, J. (1957).—*Aust. J. Phys.* **10** : 515.
Piddington, J. (1959).—*Geophys. J.* **2** : 173.
Sonett, C. P., Judge, D. L., and Kelso, J. M. (1959).—*J. Geophys. Res.* **64** : 941.
Storey, L. R. O. (1953).—*Phil. Trans.* A **246** : 908.

PHOTOMETRIC OBSERVATIONS OF 5577 Å AND 6300 Å AIRGLOW DURING THE I.G.Y.

By R. A. Duncan*

[*Manuscript received July* 25, 1960]

Summary

Twenty-one months' observation of the airglow from near Sydney, Australia, shows that (*a*) aurorae are detected 10° above the southern horizon at 6300 Å whenever the magnetic disturbance index (K) reaches 5 but K must reach 7 before detection is certain at 5577 Å; (*b*) the 6300 Å zenith intensity increases rapidly with K once this equals or exceeds 4, but the 5577 Å zenith intensity is independent of magnetic disturbance; (*c*) the zenith intensity of 5577 Å tends to be a maximum at 03 hr local time; (*d*) the zenith intensity of 6300 Å drops rapidly from dusk till 01 hr and then rises till dawn.

I. Introduction

As part of the I.G.Y. programme a nightglow photometer, lent by the American National Bureau of Standards, has been operated at Camden, near Sydney (geographic lat. 34° S., geomagnetic lat. 42° S.), since March 1957.

The intensity of the green oxygen emission at 5577 Å was monitored on 280 clear nights from March 1957 till July 1958. After July 1958 attention was concentrated mainly on the red oxygen emission at 6300 Å. Sixty-six clear nights' observation of the red nightglow were obtained to the end of 1958.

In the present paper these observations are studied for dependence on magnetic and ionospheric parameters and for nocturnal behaviour. The results are compared with those of similar studies in the northern hemisphere.

II. The Instrument

The photometer has been described by St. Amand (1955). It has high spectral purity, successfully eliminating the continuous background even during bright moonlight. It scans the sky in a series of horizontal circles at successive zenith distances of 80, 75, 70, 60, 40, and 0°, a complete sky scan taking about four minutes, and usually being repeated each quarter hour.

The photometer sensitivity was calibrated by Roach (1958) against a portable standard photometer, thus permitting comparison with nightglow photometric observations in other parts of the world.

III. Photometric Observations of Auroras

Auroras show clearly on the photometric records as pronounced brightening to the south or as structures such as arcs and rays (Duncan 1959). Figure 1 shows the probability of detecting an auroral form, as a function of the magnetic

* Upper Atmosphere Section, C.S.I.R.O., Camden, N.S.W.

disturbance index (K). It will be seen that the red line is much more prone to auroral excitation than the green. Auroras are always detected at 6300 Å when the magnetic index K reaches 5 but K must reach 7 before we can be sure of detecting an aurora at 5577 Å. This accords with the common observation (e.g. Seaton 1956) that middle latitude auroras are predominantly red.

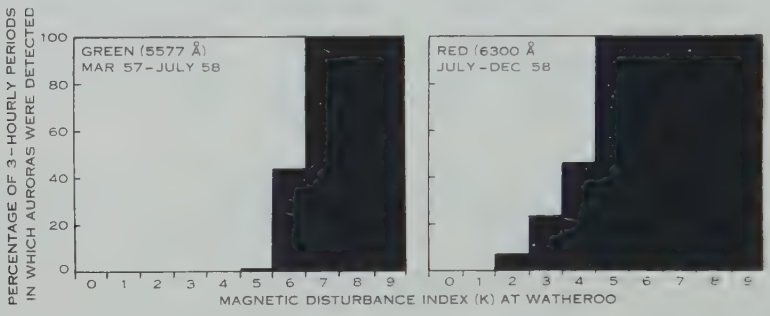

Fig. 1.—The percentage of 3-hourly observing periods during which auroral forms were detected by the photometer against the magnetic disturbance index (K) at Watheroo.

IV. Airglow and Magnetic Disturbance

It may be asked whether auroras make an appreciable contribution to the zenith airglow intensity. A study of the relation between airglow and the magnetic disturbance index K probably has some bearing on this problem.

It will be seen from Figure 2 that, except for the sporadic effect of a few great auroras, the zenith green airglow intensity is independent of the magnetic disturbance index K.

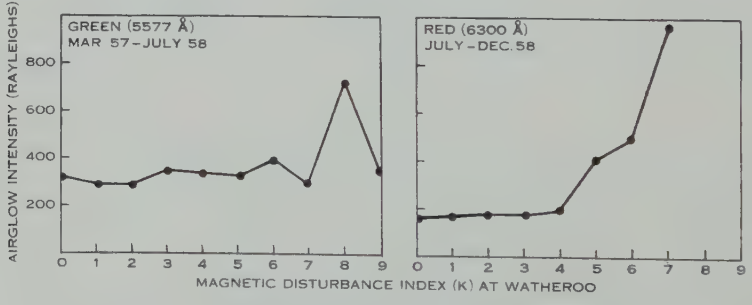

Fig. 2.—The mean zenith airglow intensity against the magnetic disturbance index (K) at Watheroo.

The zenith red airglow intensity, on the other hand, while independent of the magnetic disturbance index K so long as this is less than 4, increases rapidly with larger K. It would seem that the red airglow has a basic non-auroral level of about 175 rayleighs, plus a substantial auroral component on magnetically disturbed nights.

Recently, Roach (1960) has shown that, although the mean intensity at 5577 Å is not significantly increased, there is a tendency for sporadic high 5577 Å

TABLE 1
LOCAL TIMES OF MAXIMUM 5577 Å EMISSION

Station	Latitude	Time of Maximum	Observers
Haute Provence, France ..	44° N.	23·7	Barbier, Dufay, and Williams (1951)
Mt. Elbrus, Russia ..	43° N.	01·6	Rodionov, Pavlova, and Rdultoskava (1949)
Cactus Peak, U.S.A. ..	36° N.	00·2	Roach, Williams, and Pettit (1953)
Flagstaff, U.S.A.	35° N.	01·5	McLennon, McLeod, and Ireton (1928)
Camden, Australia ..	34° S.	03	Duncan
Sacramento Peak, U.S.A...	33° N.	23–01	Manring and Pettit (1958)
Poona, India	18° N.	Minimum 01	Karandikar (1934)

intensities to occur at times of high K-index. Camden data support this conclusion. McCaulley, Roach, and Matsushita (1960) have shown that the lack of correlation between 5577 intensities and magnetic disturbance index K is largely due to the imprecise nature of the K-index. They found a good correlation between 5577 intensities and the horizontal component of the geomagnetic field measured on a nearby magnetometer.

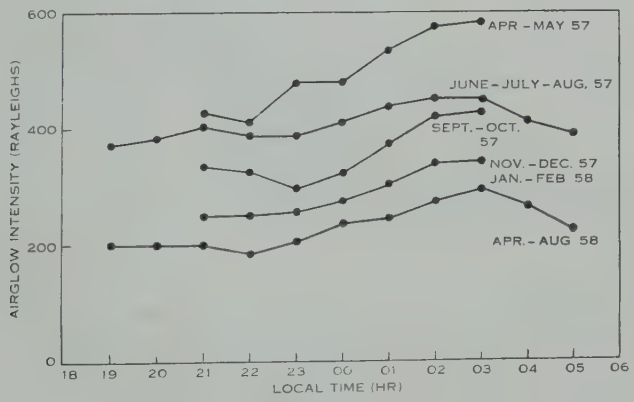

Fig. 3.—Mean nocturnal variation of the zenith green (5577 Å) airglow.

V. Nocturnal Variation of the Green (5577 Å) Airglow

The nocturnal variation of the zenith green airglow has been studied by a number of workers. Their results are summarized in Table 1. Observations at Camden confirm previous reports that the diurnal variation varies greatly from night to night. The mean nocturnal variations for each season, however, show a consistent pattern (Fig. 3). In winter a maximum is found at 03 hr. In summer observations run only from 21 to 03 hr, but within this time interval the nocturnal behaviour seems similar to that found in winter.

Observers at middle latitudes in the northern hemisphere (Table 1) have found maxima between 23 and 01 hr.

VI. Nocturnal Variation of the Red (6300 Å) Airglow

The zenith red (6300 Å) airglow shows a far more pronounced and consistent nocturnal variation than the green (Fig. 4). Earlier workers (Elvey and Farnsworth 1942 ; Barbier 1957*a*) have described a dusk and dawn enhancement of the red airglow, but as a transient effect superimposed upon, and easily distinguishable from, the " true " nightglow. It would appear from Figure 4 that the dawn and dusk enhancements are simply parts of a smooth nocturnal variation. If this variation were to be explained entirely in terms of resonance scattering of sunlight, the terrestrial atmosphere would need to be effective at heights as great as 2000 km, for the winter dawn increase is already apparent at 03 hr. The nocturnal variation (Fig. 4) is not symmetrical about midnight. It is about twice as bright at dusk as at dawn, and the lowest intensity occurs not at midnight

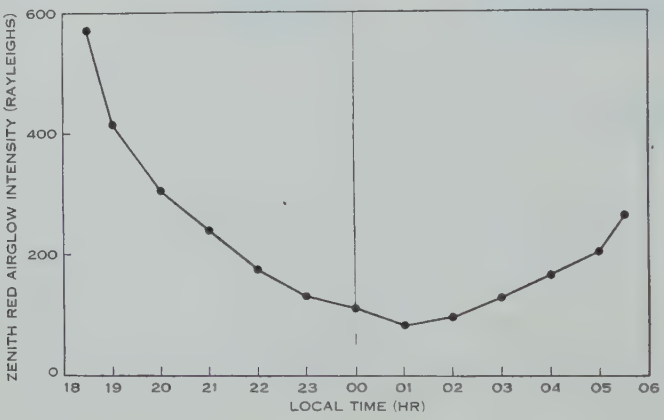

Fig. 4.—The nocturnal variation of the zenith red (6300 Å) airglow intensity. Mean for 20 nights during July and August 1958.

but at 01 hr. This suggests that, in addition to an airglow component dependent on the solar zenith angle, there is a component which decreases steadily from dusk to dawn. Possibly this is due to the dissipation (as airglow) of solar energy absorbed by the upper atmosphere during the day.

Bates and Massey (1946) have suggested that both the red airglow and the decay of the F_2 region could result from the reaction

$$O_2^+ + e \rightarrow O' + O''. \quad \ldots\ldots\ldots\ldots\ldots\ldots \quad (1)$$

In support of this Barbier (1957*b*) found, for the first half of the night, an empirical relation

$$I = (5 \cdot 83 \times 10^6)(f_0)^2 \exp\{(-h' - 200)/88\} \quad \ldots\ldots\ldots \quad (2)$$

between the red airglow intensity I and the ionospheric height h' and critical frequency f_0. A comparison of Camden ionosonde and airglow records gives no support to this finding. Certainly there is support of a kind in the fact that both the red airglow intensity I and f_0F_2 decrease during the first half of the night. However, the airglow intensity at a given hour varies by a factor of 2 or 3 from

night to night and these fluctuations bear no direct relation to ionospheric parameters. Part of the variability is due to magnetic disturbance. As Figure 2 shows, the average red airglow intensity I increases with magnetic disturbance while, as is well known, magnetic storms cause f_0F_2 to decrease and $h'F_2$ to increase. These changes are in opposite directions to those required by equation (2).

Barbier also found that the second half of the night was characterized by an enhanced glow which appeared to the north and gradually spread over the entire sky. This phenomenon has never been seen to the south at Camden.

VII. Acknowledgments

This work formed part of the I.G.Y. programme of the Upper Atmosphere Section of the Commonwealth Scientific and Industrial Research Organization, and was done under the direction of Dr. D. F. Martyn. The photometer was lent by the American National Bureau of Standards.

VIII. References

Barbier, D. (1957*a*).—*C.R. Acad. Sci., Paris* **244**: 1809.
Barbier, D. (1957*b*).—*C.R. Acad. Sci., Paris* **244**: 2077.
Barbier, D., Dufay, J., and Williams, D. R. (1951).—*Ann. Astrophys.* **14**: 399.
Bates, D. R., and Massey, H. S. W. (1946).—*Proc. Roy. Soc.* A **187**: 261.
Duncan, R. A. (1959).—*Aust. J. Phys.* **12**: 197.
Elvey, C. T., and Farnsworth, A. H. (1942).—*Astrophys. J.* **96**: 451.
Karandikar, J. V. (1934).—*Indian J. Phys.* **8**: 547.
McCaulley, J. W., Roach, F. E., and Matsushita, S. (1960).—*J. Geophys. Res.* **65**: 1499.
McLennan, J. C., McLeod, J. H., and Ireton, H. J. C. (1928).—*Trans. Roy. Soc. Can.* **22**: 397.
Manring, E. R., and Pettit, H. B. (1958).—*J. Geophys. Res.* **63**: 39.
Roach, F. E. (1958).—U.S. Nat. Bur. Standards Rep. 5591.
Roach, F. E. (1960).—*J. Geophys. Res.* **65**: 1495.
Roach, F. E., Williams, D. R., and Pettit, M. P. (1953).—*J. Geophys. Res.* **58**: 73.
Rodionov, S. F., Pavlova, E. N., and Rdultoskava, E. V. (1949).—*C.R. Acad. Sci. U.R.S.S* **66**: 55.
St. Amand, P. (1955).—*Ann. Géophys.* **11**: 435.
Seaton, M. J. (1956).—"The Aurorae and the Airglow." Pergamon Press: London.)

A NOVEL TYPE OF HIGH POWER PULSE TRANSMITTER

By K. Landecker* and K. S. Imrie*

[*Manuscript received June* 14, 1960]

Summary

A system of generation of radio waves is described which makes use of a symmetrical circular array of condensers charged through resistors and discharged through spark gaps in the manner of the Marx impulse generator. It is shown that exponential wave-trains of very high peak powers, of the order of 10,000 MW, may be radiated. The radiation resistance and radiation field of the structure are given and modification of the field pattern by parasitic elements is considered. Formulae and graphical aids are given which facilitate the design of such transmitters and experiments with various model transmitters are described. Consideration is given to circuit losses, particularly spark losses, and means are described to minimize these losses.

I. Introduction

In recent years a demand for high power pulses of radio-frequency waves has arisen in various branches of physics, as for example in ionospheric and cosmic research as well as in radio direction-finding, radar, and communication. However, the generation of large radio-frequency pulses by means of conventional transmitters is at present limited to peak powers of the order of 1 MW. Transmitters for powers much in excess of this limit would become prohibitively costly. The rapidly increasing difficulty in the construction of large pulse transmitters is not only governed by the increase in the size and cost of the constructional elements, that is, the transmitting valves and their associated circuits, the aerial system, and the coupling elements between the transmitter and the aerial system, but also by the fact that new phenomena come into play which are not present in transmitters designed for moderate powers. We here merely point out one particular difficulty, namely, the power loss from corona discharges in the atmosphere surrounding the aerial system.

The purpose of the present paper is to report on the results of experiments with various models of a novel type of pulse transmitter, which indicate that it is quite feasible to generate pulses of a peak power of the order of 10 000 MW at a small fraction of the cost of a corresponding conventional transmitter. In addition we shall refer below (in Section VI) to certain aspects of this principle of wave generation which appear to indicate that there exists a fundamental upper limit to the maximum power that, with materials available at present, may be radiated from a point in space.

II. Description of the Principle of Transmission

The principle of transmission may be conveniently explained with the aid of the schematic diagram Figure 1. A number of sets of electrical components $\bar{L}$, $\bar{C}$, $\bar{R}$, and S are shown arranged in circular form. The eight capacitors $\bar{C}$

* Department of Physics, The University of New England, Armidale, N.S.W.

are representative of an arbitrarily large number of condensers whose series combination forms the tuning capacity, while the corresponding tuning inductances $\overline{L}$ are located symmetrically with respect to the condensers and spark gaps S and may, at higher frequencies, be formed solely by the connecting leads. In a limiting case they may even degenerate into the internal inductances of the condensers. The total tuning inductance is then the inductance of the circular current path through the condensers and spark gaps, and it will presently become clear that this is the desirable condition for maximum energy storage.

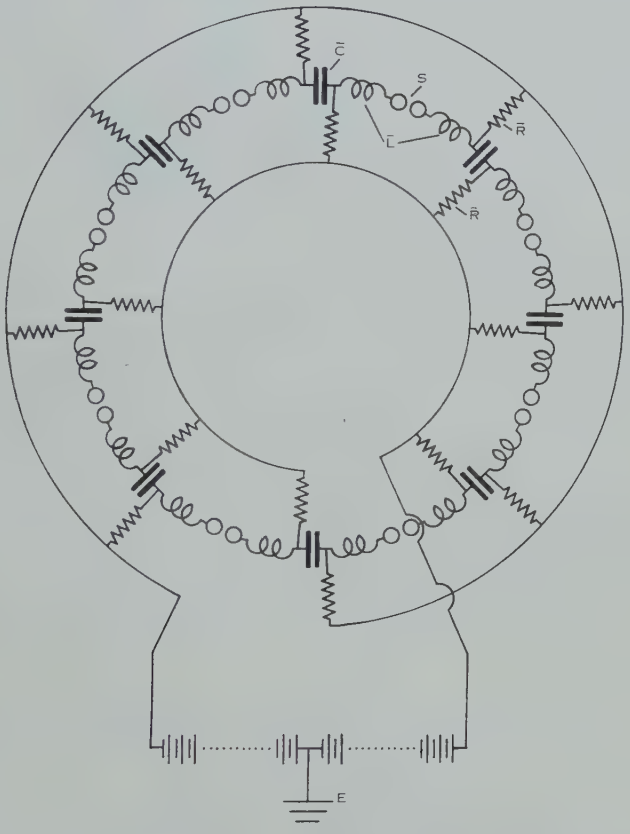

Fig. 1.—Schematic circuit diagram of the transmitter.

The condensers $\overline{C}$ are charged in parallel through the resistors $\overline{R}$ and discharged in series through the spark gaps S in the manner of the well-known Marx impulse generator (Edwards, Husbands, and Perry 1951; Craggs and Meek 1954). However, the structure described forms not only the tank circuit of the transmitter but also is extended spatially so as to form at the same time a magnetic dipole or loop aerial which itself radiates the radio-frequency energy. A variation of this principle using parasitic elements in addition to the main oscillatory circuit will be referred to below.

Anticipating the results of calculations and experiments quoted below, which show that this system of transmission may be made to function and that very large power pulses may in fact be radiated, we enumerate some advantageous properties of this scheme:

1. The energy stored in the tuning condensers is transformed into radiation in a most direct manner. This outweighs the fact that higher electrical energies may possibly be stored in unit volume by other means, for example by homopolar generators and the like, than it is possible to store in condensers with present-day dielectric materials.

2. In the presence of an atmosphere a magnetic dipole is inherently superior as a radiator to an electric dipole. A magnetic dipole fails at high power because it ultimately gives rise to an electrodeless discharge in the surrounding air. An electric dipole causes a corona discharge at the field boundaries (the "ends" of the aerial wire) long before an electrodeless discharge can be initiated. The circular array of condensers of Figure 1 approaches a perfect magnetic dipole as the number of condensers is increased and their individual capacities increased simultaneously beyond all limits in such a way that the LC product of the entire circuit remains at a constant desired value. In practice it is sufficient to subdivide the condenser bank to such an extent that the individual condensers are able to withstand their charging potentials. The latter are the only scalar potentials that arise in the circuit. This statement is related to a well-known electrodynamic theorem which has been frequently mentioned in the literature (Howe 1945) and according to which no scalar potential difference exists between any two points of a conducting annulus situated in a varying magnetic field of axial symmetry. Experience indicates that with slight departures from a perfectly circular form and from perfect symmetry there is still little tendency for a corona discharge or flashover to occur.

3. Since no point of the structure is necessarily at ground potential, it is possible to ground the electrical centre of the voltage supply. The latter therefore need only be insulated for one-half of the condenser charging voltage.

III. Calculation of the Power of the Emitted Wave-train

The stored energy will be radiated in the form of exponentially decaying wave-trains. To obtain an estimate of the power that such a system is capable of radiating we begin by calculating three characteristic quantities of the emitted wave-train: the average power during the first half cycle, the peak power of the entire wave-train which occurs instantaneously at the current maximum of the first half cycle, and the approximate average power of the total wave-train.

Assuming that N condensers each of capacity $\overline{C}$ are distributed around the circumference of the circuit, and that they are designed to withstand a maximum charging voltage V, the total energy E_{tot} stored in the condenser bank is related to the current in the circuit through

$$E_{\text{tot}}=\tfrac{1}{2}N\overline{C}V^2=\int_0^\infty I_0^2 \sin^2 \omega t \, \mathrm{e}^{-2kt}R\mathrm{d}t, \quad \ldots\ldots\ldots \quad (1)$$

where $k=R/2L$, L is the circuit inductance, $\omega=(N/L\bar{C}-R^2/4L^2)^{\frac{1}{2}}$, R is a resistance representing radiation and circuit losses, and I_0 is the current in the circuit in the absence of damping ($R\to 0$).

From equation (**1**) we obtain

$$\frac{N\bar{C}V^2}{I_0^2R}=\int_0^\infty e^{-2kt}(1-\cos 2\omega t)\,dt$$

$$=\left[\frac{e^{-2kt}}{-2k}\right]_0^\infty-\int_0^\infty e^{-2kt}\cos 2\omega t\,dt$$

$$=\frac{1}{2k}-\int_0^\infty e^{-2kt}\cos 2\omega t\,dt, \quad \ldots\ldots\ldots\ldots\ldots (2)$$

and, integrating the second term by parts,

$$\frac{N\bar{C}V^2}{I_0^2R}=\frac{1}{2k}-\frac{k}{2\omega^2}+\int_0^\infty \frac{k^2}{\omega^2}e^{-2kt}\cos 2\omega t\,dt. \quad \ldots\ldots\ldots (3)$$

On multiplying (**2**) by k^2/ω^2 and adding to (**3**) there results

$$\frac{N\bar{C}V^2}{I_0^2R}\left(\frac{k^2}{\omega^2}+1\right)=\frac{1}{2k}, \quad \ldots\ldots\ldots\ldots\ldots (4)$$

from which follows

$$I_0=NV/\omega L, \quad \ldots\ldots\ldots\ldots\ldots (5)$$

and therefore the average power during the first half cycle is closely

$$P_{0\,(av)}=\tfrac{1}{2}I_0^2R=\tfrac{1}{2}R(NV/\omega L)^2. \quad \ldots\ldots\ldots\ldots (6)$$

In all cases of practical interest $\omega\approx(N/L\bar{C})^{\frac{1}{2}}$, that is, $\omega L\approx N/\omega\bar{C}$. Introducing the Q-factor of the circuit $Q=\omega L/R=N/\omega\bar{C}R$, the average power during the first half cycle may also be expressed as

$$P_{0\,(av)}=\tfrac{1}{2}N\bar{C}V^2\omega/Q=E_{tot}\omega/Q \text{ watts}, \quad \ldots\ldots\ldots (7)^*$$

when $\bar{C}$ is given in farads, V in volts, and E_{tot} in joules. The instantaneous peak power at the first current maximum is double this value, that is,

$$P_{0\,(peak)}=2E_{tot}\omega/Q \text{ watts}. \quad \ldots\ldots\ldots\ldots (8)$$

Lastly, in order to determine the approximate average power during one wave-train, we assume that the wave-train may be considered as terminated when the current amplitude has decreased to 1 per cent. of its initial value (Fleming 1919). Under these conditions the duration τ of the wave-train is given by

or
$$\left.\begin{aligned} e^{-k\tau}&=0\cdot 01,\\ -k\tau&=\ln 0\cdot 01=-4\cdot 6,\end{aligned}\right\} \quad \ldots\ldots\ldots\ldots\ldots\ldots (9)$$

* The same expression for $P_{0\,(av)}$ (except for a factor $(1-e^{-\delta/2})$ not very much different from unity) is obtained by considering the wave-train to consist of a succession of half sinoids of amplitudes I_0, I_1, I_2, . . ., where successive amplitudes are related by the logarithmic decrement $\delta=\pi/Q$ through $I_0/I_1=I_1/I_2=I_2/I_3=\ldots=e^{\delta/2}$.

but, since

$$k=R/2L=\omega/2Q, \quad \ldots\ldots\ldots\ldots\ldots\ldots\ldots\ldots \quad (10)$$

we obtain for the duration of the train the value

$$\tau=4\cdot6/k=4\cdot6\times2Q/\omega=9\cdot2Q/\omega\sim10Q/\omega \text{ seconds.} \quad \ldots \quad (11)$$

The average power of the whole train is therefore given with sufficient accuracy by

$$P_{\text{tr (av)}}=\tfrac{1}{2}N\bar{C}V^2\omega/10Q=E_{\text{tot}}\omega/10Q \text{ watts.} \quad \ldots\ldots\ldots \quad (12)$$

Finally we note that from (11) there follows the useful expression for the number of cycles in the train

$$n=\omega\tau/2\pi=9\cdot2Q/2\pi=1\cdot46Q\sim1\cdot5Q. \quad \ldots\ldots\ldots \quad (13)$$

It is necessary to show that it is sufficiently accurate to include the radiation resistance in the total circuit resistance R of equation (1) as a part that is independent of frequency.

So far in this discussion we have assumed that the wave-trains are generated in the manner described in Section II, without going into the process of transmission in detail. This process depends fundamentally on the Fourier composition of the train. Fortunately, the frequency composition of an exponentially decaying wave-train may be stated in very simple terms. It is well known that the Fourier transform of such a train is identical with the frequency response of a tuned *LRC* circuit.* However, the radiation resistance of a transmitting aerial is a function of frequency and also a function, unfortunately not at all simple, of the spatial configuration of the aerial. The general problem of transmission and reception of arbitrary wave shapes is in fact exceedingly difficult. However, it will be shown in the following section that, though the radiation resistance of a circular loop exhibits a general increase with diameter but oscillates for large diameters, it nevertheless shows a simple monotonic increase within the range of interest (see Fig. 2). For all loop diameters which are practical the radiation resistance increases approximately with the fourth power of the diameter (see Fig. 3). From the foregoing it follows that it is permissible to assume that the frequency components of the radiation field have appreciable values only in the neighbourhood of the frequency of oscillation of the wave-train, provided that the train is not too short. It has in fact always been found that under these conditions the radiation field of a spark transmitter is a time function closely similar to the aerial current. The circumstance that in reality, in the process of radiation from our transmitting loop, the higher frequency components are always favoured compared to the lower frequency components, makes the above assumption of minor importance in practice, but this simplification greatly reduces the complexity of the problem.

* See, for example, the Fourier pairs Nos. 448 and 449 in Campbell and Foster (1931).

Finally, it should be noted from equations (7), (8), and (12) that the power of the wave-train is simply inversely proportional to the Q-factor of the circuit, which is solely determined by radiation and circuit losses. It will be shown in the following that the circuit may always be adjusted so that the radiation losses may have any desired value, and that the circuit losses may be minimized by various means. The question of which particular value of the Q-factor is desirable will largely depend on the specific application of the emitted energy. For example, the wave shape most suitable for producing changes in an ionized medium will not be the same as that of a signal to be received against a strong background of noise. In transmitting practice it is accepted that the loaded Q of a transmitter should be at least 10 in order to ensure that the major part of the wave energy is radiated near the fundamental frequency. It can only be estimated that in general the choice of the factor will range between values of 10 and 50, and in the following we shall consider numerical examples in this range only.

IV. The Radiation Resistance of the Circuit

In the previous section the significance of the Q-factor was emphasized. It is therefore of importance to determine what fraction of the total damping resistance is made up of undesirable circuit losses. As will be shown below, the major portion of these losses is accounted for by losses in the sparks and means will be mentioned to minimize these losses. In order to render the problem manageable we therefore initially disregard the circuit losses and deal first with the radiation resistance.

It is not immediately obvious that when a desired frequency of transmission and a maximum condenser voltage are specified the circuit constants may be made to converge towards values which are practicable and which ensure a large output of radiated power. The frequency fixes in the first instance the LC product in which the factor C should ideally be obtained from the largest number of series capacities it is possible to accommodate along the circumference of the circuit, allowing sufficient space for the spark gaps. The factor L, on the other hand, is a function of the diameter of the circuit and depends only weakly on the average cross section of the current path. The diameter of the circuit, however, also determines the radiation resistance but, as mentioned in Section III, the latter unfortunately is not a simple function of the former. If a suitable radiation resistance (a suitable Q-factor) is chosen, then the loop diameter, the tuning inductance, and the tuning capacity are determined. The number (N) of condensers is limited by space requirements and it might well have been that the energy stored in the condenser bank and therefore also the radiated power were small. That the power is in fact large can only be shown by numerical examples or by the dimensional reasoning adopted in Section VI.

The radiation resistance of circular current loops whose diameter is an appreciable fraction of a wavelength has been calculated by various authors (Foster 1944 ; Moullin 1946) and, in addition, the field distribution around such loops has also been worked out.

The radiation resistance is given by

$$R^* = \tfrac{1}{2}\pi\mu_0 ck \int_0^{2k} J_2(x)\mathrm{d}x \text{ ohms}, \quad \ldots\ldots\ldots\ldots \quad (14)$$

where $\mu_0 = 1{\cdot}26 \times 10^{-6}$ henry/m, c = velocity of light 3×10^8 m/sec, $k = 2\pi a/\lambda$, a = radius of loop, λ = wavelength, and $J_2(x)$ is the Bessel function of the first kind and second order (Fig. 2).

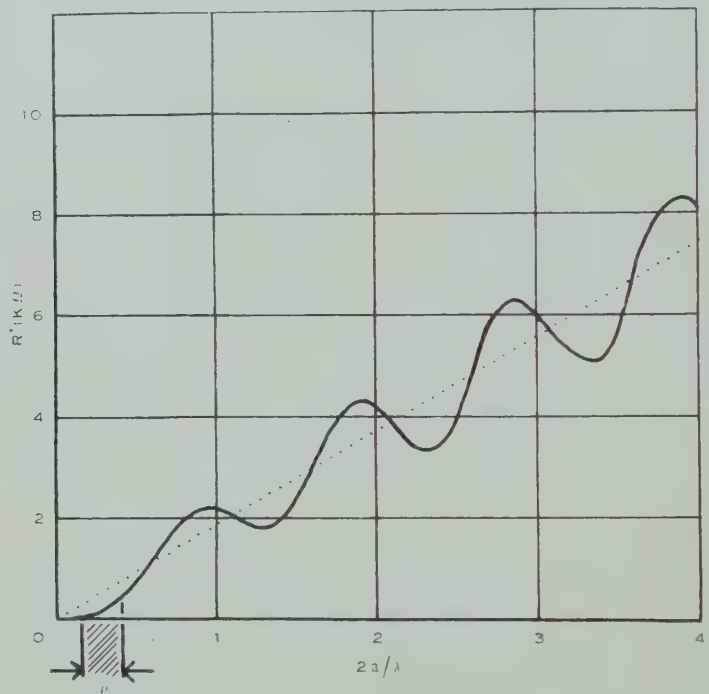

Fig. 2.—The radiation resistance of a circular loop as a function of its diameter (in wavelengths). ρ indicates the region of interest (see text).

This may also be written in the form of a power series in k as

$$R^* = 20\pi^2 k^4 \left(1 - \frac{k^2}{5} + \frac{k^4}{56} - \ldots\right), \quad \ldots\ldots\ldots \quad (14a)$$

which shows that the radiation resistance of a loop which is small compared to the wavelength approximates to

$$R^* = 20\pi^2 k^4 = 320\pi^6 (a/\lambda)^4. \quad \ldots\ldots\ldots\ldots\ldots \quad (14b)$$

Equation (**14b**) still holds within 20 per cent. up to a value of $k=1$. Using the three terms of the power series in (**14a**) gives R^* within a few per cent. at $k=1$.

From equation (**14**) the radiation resistance R^* of the loop has been plotted as function of the diameter in wavelengths in Figure 3 over the range which will be shown to be of interest to us.

The inductance L of the circular loop which together with the resistance R^* of equations (**14**), (**14a**), or (**14b**) enters the Q-factor is given by

$$L=\mu_0 a\{\ln(8a/b)-1\cdot75\}, \quad \ldots\ldots\ldots\ldots \quad (15)$$

where a=loop radius, as before, and b=(average) radius of the cross section of the current path.

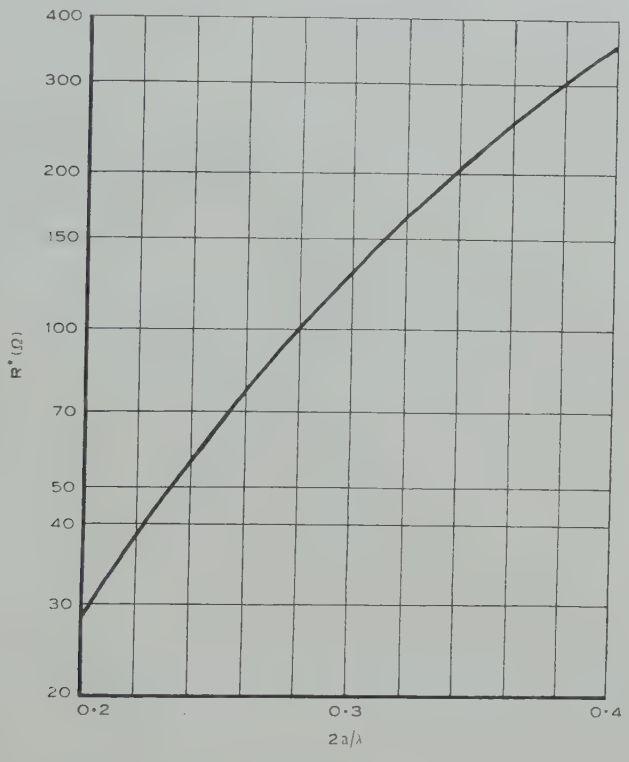

Fig. 3.—The radiation resistance of the loop within the range of interest (see text).

Since the ratio a/b and therefore also the term $\ln(8a/b)$ are restricted by practical considerations to a range with rather definite limits the inductance may be written in an approximate form

$$L\approx D\mu_0 a, \quad \ldots\ldots\ldots\ldots\ldots \quad (15a)$$

where D is a constant.

Since the loop radius a enters equations (**14b**) and (**15a**) through the fourth and first power respectively it follows that a desired Q-factor may always be realized. Using (**14**) and (**15**) the Q-factor may be written

$$Q=\left\{\frac{2}{\pi}\left(\ln\frac{8a}{b}-1\cdot75\right)\right\}\left\{\left\{\int_0^{2k} J_2(x)\,dx\right\}^{-1}\right\}. \quad \ldots\ldots \quad (16)$$

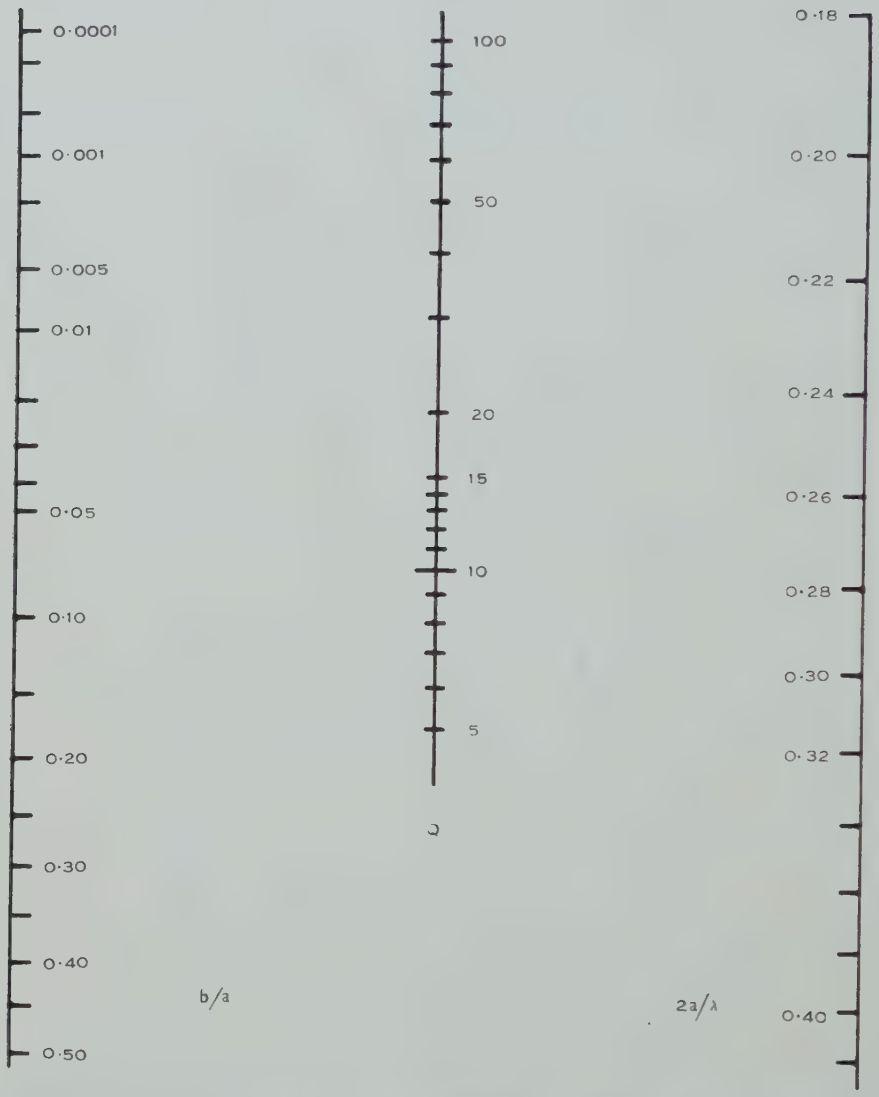

Fig. 4.—Nomogram relating the circuit diameter as a fraction of the loop diameter, the Q-factor, and the loop diameter in wavelengths.

This equation may be put into the form

$$\log Q = \log f(b/a) + \log g(2a/\lambda), \quad \ldots\ldots\ldots\ldots\ldots\ldots \quad (16a)$$

where f and g are functions following from (**16**), and therefore a nomogram of Q, b/a, and $2a/\lambda$ may be constructed as shown in Figure 4. The nomogram shows at a glance that practical loop diameters will mainly be restricted to the range from $0{\cdot}2\lambda$ to $0{\cdot}3\lambda$.

V. The Radiation Field of the Loop and the Effect of Parasitic Elements

The electric and magnetic vectors of field strength E and B, at a distance r from the centre of a circular loop of radius a, have the following magnitudes (Foster 1944; Moullin 1946)

$$E=\tfrac{1}{2}\mu_0 c I_a k \mathrm{J}_1(k\cos\varphi)\cdot\frac{1}{r}\sin\left(\omega t-\frac{\omega r}{c}\right), \quad \ldots\ldots\ldots \quad (17)$$

and

$$B=-\tfrac{1}{2}\mu_0 I_a k \mathrm{J}_1(k\cos\varphi)\cdot\frac{1}{r}\sin\left(\omega t-\frac{\omega r}{c}\right), \quad \ldots\ldots \quad (18)$$

where I_a is the amplitude of the current in the loop, $r\gg a$, φ is the angle between the plane of the loop and the radius vector to the reference point, $\mathrm{J}_1(x)$ is the Bessel function of the first kind and first order, and the other symbols have the same meaning as before.

With the plane of the loop considered as an equatorial plane, the electric vector oscillates tangentially to a circle of latitude and the magnetic vector tangentially to a meridian. This should be noted when comparing the radiation field of the loop with that of an electric dipole.

When the diameter of the loop is much smaller than a wavelength, that is, when $k\ll 1$, these expressions approximate to

$$E=\tfrac{1}{4}\mu_0 c I_a k^2\cos\varphi\cdot\frac{1}{r}\sin\left(\omega t-\frac{\omega r}{c}\right), \quad \ldots\ldots\ldots \quad (19)$$

$$B=-\tfrac{1}{4}\mu_0 I_a k^2\cos\varphi\cdot\frac{1}{r}\sin\left(\omega t-\frac{\omega r}{c}\right). \quad \ldots\ldots\ldots \quad (20)$$

These approximations are correct to within about 10 per cent. even up to $k=1$, so that even when the loop is one wavelength in circumference the radiation field is still very like that of a small magnetic dipole. For reasons stated in Section IV this will nearly always be so for the transmitting loop we are considering.

It should be noted that, whenever the Bessel function $\mathrm{J}_1(x)$ passes through zero, extinction angles occur near the equatorial plane and progress towards the zenith with increasing radius of the loop until the entire quadrant is divided into lobes. The first zero of the Bessel function occurs for the argument $x=3\cdot83$, that is, an extinction angle occurs for the first time when $x=2\pi a/\lambda=3\cdot83$ or $2a/\lambda=3\cdot83/\pi=1\cdot22$. But since we are here always restricted to the condition $0\cdot2<2a/\lambda<0\cdot3$ this means that we have always only a single lobe.

There are various possibilities of arranging parasitic elements (reflectors and directors) in the neighbourhood of the main loop for the purpose of modifying the radiation pattern. Some of these are shown schematically in Figure 5.* C represents a biconical reflector suggested by Moullin (1946) and D represents

* Various configurations like the closed coplanar rings A and coaxial rings B call to mind various electric counterparts, such as broadside, endfire, Yagi array, etc., but it is doubtful whether any useful inferences may be made from these analogies.

a parabolic reflector. It is to be noted that all axially symmetrical elements such as A and B share the property with the main circuit that no scalar potential arises between any two points of the circumference.

The question whether it is possible to induce sufficient current into any of these parasitic elements and still effect a worth-while modification of the polar pattern by placing the element at a suitable distance is in general difficult to analyse and is best decided by experiment. The tuned secondary circuit mentioned in Section VII will also affect the radiation pattern to some extent and a choice may have to be made regarding its position with respect to the main circuit and whether more than one secondary circuit should be used.

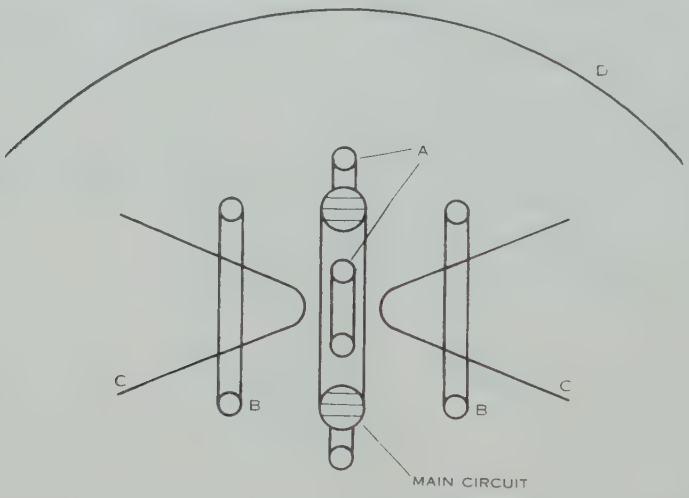

Fig. 5.—Various forms of parasitic elements used in conjunction with the main driving circuit.

VI. Numerical Examples. Some Considerations regarding the Maximum Amount of Wave Power that may be produced in Space

We now turn to some numerical examples and assume to begin with that a wave of a frequency of 1 Mc/s is to be produced and that the condensers will be designed to withstand a charging voltage of $V=200$ kV. Condensers for such a voltage may today be considered to be standard items in engineering practice. The Q-factor will be taken to be 10, and initially we shall ignore circuit losses. Selecting a value of (diameter of loop)/(wavelength) of $0{\cdot}28$, the nomogram (Fig. 4) gives a diameter of the current path of $0{\cdot}06$ of the loop diameter and we see that a circular structure of 80 m diameter and a cross section of the current path of $4{\cdot}8$ m diameter is required. This would call for large tubular condensers with air or possibly polythene ribbon as a dielectric. The loop will have an inductance of $L=170$ μH and therefore requires a tuning capacity of $\overline{C}/N=1{\cdot}5\times10^{-4}$ μF. We now suppose that $N=50$ condensers are distributed around the circumference, that is, that $\sim$5 m of circumference are available for each condenser and its associated spark gap, though a design as shown schematically in Figures 6 (a) and 6 (b) would allow us to accommodate

many more units around the circumference, even when the spark gaps are operated at atmospheric pressure. The capacity of each of the 50 units is then $\bar{C}=50\times1\cdot5\times10^{-4}=7\cdot5\times10^{-3}$ μF, and the capacity of the whole condenser bank $N\bar{C}=50^2\times1\cdot5\times10^{-4}=3\cdot75\times10^{-1}=0\cdot375$ μF. The energy stored in the total capacity is given by

$$E_{\text{tot}}=\tfrac{1}{2}N\bar{C}V^2=0\cdot5\times0\cdot375\times10^{-6}\times(2\times10^5)^2=7\cdot5\times10^3\text{ J}.$$

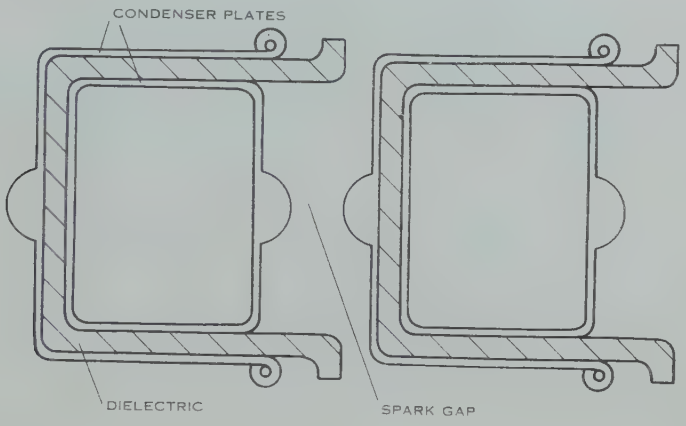

a

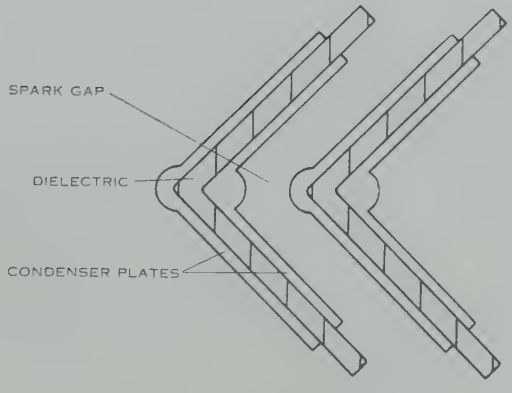

b

Fig. 6.—Schematic diagram of space-saving arrangement of condensers.

We then obtain from equations (7), (8), and (12) of Section III:
Average power during the first half cycle

$$P_{0\,(\text{av})}=7\cdot5\times10^3\times6\cdot28\times10^6/10=4\cdot7\times10^9\text{ J/sec}$$
$$=4700\text{ MW}.$$

Peak power at first current maximum

$$P_{0\,(\text{peak})}=2P_{0\,(\text{av})}=9400\text{ MW}.$$

Average power during the wave train

$$P_{\text{tr (av)}}=P_{0\text{ (av)}}/10=470\text{ MW},$$

and equation (**13**) shows that the train lasts for $n=1\cdot5Q-15$ cycles.

This example shows that it is quite feasible to obtain with this arrangement and a condenser voltage slightly larger than 200 kV peak powers of the order of 10 000 MW. The structure is, however, very large, even if it should be possible the reduce the dimensions by improvements in design and judicious use of parasitic elements, as discussed in Section V. Nevertheless, it covers no more ground than a conventional aerial array at this frequency. If used for ionospheric work it might be advantageous to erect the transmitter at or near the bottom of a natural valley in order to direct the radiation upwards.

We next consider a more readily realizable example and assume a desired frequency of 30 Mc/s, a maximum condenser voltage of 200 kV, and a Q-factor of 15. Proceeding as before, we select from the nomogram a loop diameter of 2·8 m, which fixes the diameter of the current path at about 4 cm and its inductance at $L=16$ μH. This requires a tuning capacity of $\bar{C}/N=1\cdot75$ μμF. Accommodating $N=40$ condensers around the circumference allows 22 cm for the space to be occupied by one condenser and its associated spark gap, which is ample. Proceeding as in the previous example we obtain :

$$\begin{aligned}
\bar{C}&=40\times1\cdot75\times10^{-12}=70\text{ μμF},\\
N\bar{C}&=2800\text{ μμF},\\
E_{\text{tot}}&=\tfrac{1}{2}\times2800\times10^{-12}(2\times10^{5})^{2}=56\text{ J},\\
P_{0\text{ (av)}}&=56\times6\cdot28\times30\times10^{6}/15=700\text{ MW},\\
P_{0\text{ (peak)}}&=2\times P_{0\text{ (av)}}=1400\text{ MW},\\
P_{\text{tr (av)}}&=P_{0\text{ (av)}}/10=70\text{ MW},\\
n&=1\cdot5\times15\approx22\text{ cycles}.
\end{aligned}$$

We again note that very large powers are radiated and yet the circuit is very easy to construct. This example was selected because a transmitter approximating to these specifications is at present being designed and constructed in this laboratory.

Finally, we consider the maximum peak power that it is possible to radiate with this type of transmitter. For this purpose it is convenient to rewrite equation (**8**) of Section III as follows

$$P_{0\text{ (peak)}}=(NV)^{2}/Q^{2}R\text{ watts.}\quad\ldots\ldots\ldots\ldots\ (\mathbf{8a})$$

We now assume that for the construction of the condensers a low-loss dielectric material with a breakdown strength of $\Delta=5\times10^{7}$ V/m is available (this is about the breakdown strength of polystyrene), that one-quarter of the circumference of the transmitting loop is taken up by dielectric, and that the other three-quarters is occupied by the spark gaps and the condenser plates. It will be shown in Section VII that it is quite feasible to control the spark length by pressurization of the spark gaps and that the above allocation of space for the spark gaps is ample. The charging voltage of the condensers may be expressed as $V=\frac{1}{2}\pi a\Delta/N$ and, since it follows from the foregoing that in any practical

design it is not possible to deviate much from the values $2a \sim 0 \cdot 29\lambda$, $Q \sim 10$, $R \sim 100\ \Omega$, equation (**8a**) becomes

$$P_{0\,(\text{peak})} = (\tfrac{1}{2}\pi a\Delta)^2/Q^2R = (\tfrac{1}{4}\pi \times 0 \cdot 29\lambda\Delta)^2/Q^2R$$
$$= (1 \cdot 2 \times 10^7\lambda)^2/10^4 = 10^{10}\lambda^2 \text{ watts.} \quad \ldots\ldots\ldots \quad (8b)$$

From (**8b**) it follows that it should be possible to produce peak powers of the order of 10^4, 10^6, and 10^8 MW at wavelengths of 1, 10, and 100 m respectively. Even when circuit losses are taken into account this calculation demonstrates that very large peak powers may be produced. Further, this result seems to us to have also a fundamental significance. Unless entirely new methods of radiating electrical energy from a point into space are discovered, equation (**8b**) may represent a limiting value for such radiation with present-day dielectric materials and insulating techniques.

VII. Experiments with Various Scale Models

In order to verify the feasibility of this principle of transmission and the calculations of the previous sections, experiments have been carried out with two transmitters. The first operated at a frequency of 10 Mc/s and used 6 tubular air-insulated condensers. The average loop diameter was about 2 m, that is, only 1/15 of a wavelength, and so the radiation resistance was very low. This transmitter was mounted in the open on a low wooden tower. It proved very difficult to protect it from the weather. A second transmitter was constructed working at a frequency of 70 Mc/s. It uses 18 parallel-plate condensers with a dielectric of polystyrene and 18 associated spark gaps. The mean loop diameter is approximately 1 m, which corresponds to a radiation resistance of about 100 Ω. This transmitter is small enough to be operated in the laboratory. Both transmitters must be considered to be scale models because the condensers in the 10 Mc/s transmitter are not able to withstand a charging voltage of more than 5 kV and those in the 70 Mc/s transmitter more than 15 kV. The charging resistances each had a value of 10 MΩ in both models. In addition to experiments with these transmitters, many observations were made on simple tuned circuits.

The results of these experiments may be summarized as follows :

(i) It was found that the spark gaps of the transmitters could be adjusted to fire quite regularly and strong signals were received at distances of many wavelengths from both transmitters. It was immediately established that the transmitting loops exhibited the radiation pattern of a dipole and that the field vectors had the correct orientations. The signal strength was of the expected order of magnitude, but experience with these model transmitters has shown that accurate measurement of the field strength of short, strongly damped, high frequency pulses presents a special problem, and various detectors are being designed for this purpose.

(ii) Near the transmitters the signals are easily displayed on the screen of a cathode-ray tube. Observations of the pulse length indicate that by far the largest part of the circuit losses is accounted for by spark losses, and various attempts were made to minimize these losses. The most effective means of controlling the pulse length proved to be the coupling of a tuned secondary

circuit with the main driving circuit. This of course used to be standard practice in spark telegraphy, but with the arrangement we are considering the problems are somewhat different from those encountered in spark telegraphy. The tuned secondary takes the place of one of the untuned parasitic elements of type A or B in Figure 5 (Section V). The radiation resistance of such a passive element by itself will be either exactly or nearly exactly the same as that of the main circuit. If an untuned parasitic reflector is coupled to the main circuit it modifies the radiation pattern and also increases the radiation resistance of the whole combination.* A tuned secondary, on the other hand, in addition reduces the energy losses in the whole system because while being driven by the main circuit it abstracts oscillatory energy from this circuit and continues to radiate after the sparks are extinguished. It was found that such a tuned secondary controlled the pulse length very effectively. Experiments with single tuned circuits at a frequency of 10 Mc/s showed that the pulse length could be extended by this means by at least a factor of 10 without significantly affecting the peak amplitude. Maximum improvement occurs at slightly below optimum coupling. Finally, it should be noted that the tuned secondary circuit shares with the main circuit the property that no scalar potential differences appear between any two points of its circumference provided the tuning condensers are able to withstand the oscillating voltage.

The spark discharge was also studied at pressures higher than atmospheric and an adjustable spark gap was constructed which is capable of being pressurized up to 100 atmospheres. The most useful gas for this purpose proved to be nitrogen, in agreement with various statements in the literature. Replacing a spark gap working at atmospheric pressure in an oscillating circuit by a pressurized gap with the same breakdown voltage always increased the pulse length ; that is, no combination of circuit constants was found in which pressurization reduced the pulse length. The actual increase in pulse length depends very much on the circuit constants and may be as much as by a factor of 2. Such a factor is very desirable but the main advantage of pressurization for us seems to be the possibility of reducing the space requirements of the spark gaps and, incidentally, also the noise from the sparks. Moreover, a design shown schematically in Figure 7, which is quite feasible at frequencies above 10 Mc/s, would protect the circuit from humidity and dust and from the effects of high altitude. We are at present constructing a 35 Mc/s transmitter according to this design.

(iii) According to the calculations of Section IV the optimum diameter of the loop will practically always be within the limits of 0·2–0·3 of one wavelength, so that the firing impulse propagates from one spark gap to the next along the circumference in a finite time which is an appreciable fraction of a period. It was therefore anticipated that a separate firing impulse might have to be applied, by some means from the axis of the loop, so as to arrive simultaneously at all the spark gaps. However, it was noted from the beginning that the firing of

* Here and in the following the radiation resistance is referred to the driving current in the main circuit. Detuning of the main circuit due to the coupled reactance is of no practical importance.

all the gaps seemed to take place surprisingly decisively, though one could not be sure that the circuit did not support some unwanted mode along its circumference. This was tested, using the 70 Mc/s transmitter, by firing all gaps simultaneously by means of a flash of ultraviolet light from an auxiliary bright spark between aluminium electrodes situated at the centre of the loop. No significant difference in operation could be detected with and without the auxiliary spark. It therefore appears that the desired principal current mode established itself within a sufficiently short time by the mechanism that is responsible for the operation of the Marx impulse generator.

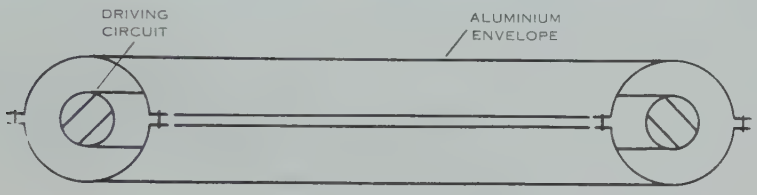

Fig. 7.—Schematic drawing of cast aluminium envelope for pressurization of the circuit.

VIII. Conclusion

Summarizing, we can state that theoretical and experimental work on this problem has at the time of writing reached a stage where the mode of operation and the limitations of this transmitter are well understood and the properties of a practical design may be predicted with sufficient accuracy. We are at present constructing a 60 ft diameter parabolic reflector for a 35 Mc/s transmitter with the aim of radiating pulses with a peak power of about 1000 MW for a programme of ionospheric and cosmic research.

In this work we have been led to numerous other problems whose investigation has had to be postponed. These include the possibility of using lengths of transmission line in place of the condensers in the circular array and the possible use of electronic or ionic valves with negative current-voltage characteristics, instead of the simple spark gaps, with the aim of generating continuous or modulated waves. Though oscillating circuits in which the energy is fed into the tuned circuit in parallel are highly developed, there seems to be no reason why series-fed circuits should not find equally useful applications in certain cases.

The principle of transmission described here has been the subject of a patent application by the University of New England (1958). It is hoped that the transmitter described will find use as a research tool.

IX. Acknowledgments

We are greatly indebted to Professor J. M. Somerville, Professor of Physics in the University of New England, and to Professor V. A. Bailey, Research Professor in the University of Sydney, for advice and encouragement with this work. We gratefully acknowledge the benefit derived from discussions with Dr. F. H. Hibberd. Mr. A. W. Findlay has assisted with experimental work.

Thanks are also due to the Laboratory and Workshop Manager of this department, M . D. A. Atkinson, and to several members of the workshop staff, in particular Mr. A. Sowasko, for continued assistance with design and construction work. The project has received financial assistance from the Radio Research Board of Australia. The Royal Australian Navy has kindly made available a surplus gun turret as a base for the parabolic reflector. One of us (K.S.I.) is the recipient of an I.C.I.A.N.Z. Research Fellowship.

X. References

Campbell, G. A., and Foster, R. M. (1931).—" Fourier Integrals for Practical Applications." Bell Monograph B584. (Bell Telephone Lab. : New York.)

Craggs, J. D., and Meek, J. M. (1954).—" High Voltage Laboratory Technique." (Butterworths : London.)

Edwards, F. S., Husbands, A. S., and Perry, F. R. (1951).—*Proc. Instn. Elect. Engrs.* **98** : 155.

Fleming, J. A. (1919).—" The Principles of Electric Wave Telegraphy and Telephony." (Longmans : London.)

Foster, D. (1944).—*Proc. Inst. Radio Engrs., N.Y.* **32** : 603.

Howe, G. W. O. (1945).—*Wireless Engineer* **22** : 53.

Moullin, E. B. (1946).—*J. Instn. Elect. Engrs.* **93** (III) : 345.

University of New England (1958).—Aust. Provisional Patent Application No. 42451.

VERTICAL CHARACTERISTICS OF TRAVELLING IONOSPHERIC DISTURBANCES

By L. H. Heisler*

[*Manuscript received December* 17, 1959]

Summary

The vertical dimensions of travelling disturbance phenomena have been investigated by derivation of the associated true height distributions of ion density. The height at which they appear often has an upper limit which may fluctuate in height from day to day.

It appears that direction of travel is related mainly to season, with the possibility of some additional form of solar control only evident at times of sunspot maximum.

During a particular season, there is no obvious change of direction of travel with height in the height range under observation.

No definite variation of speed with height is evident in the ionospheric region considered, which extends from 160 to 230 km.

I. Introduction

Munro (1950, 1953) has described disturbances on 5·8 Mc/s fixed-frequency records, using a three-station triangulation to determine speed and direction, and has recently published (Munro 1958) comprehensive statistical data of eight years' results. Munro and Heisler (1956*a*, 1956*b*) have described large disturbances which occur in variable-frequency ionosonde records, and Heisler (1958), comparing records from Australian ionosonde stations, has shown that these disturbances travel distances of at least 3000 km, with fronts possibly broader than 1000 km. The existence of similar disturbances in the northern hemisphere, first mentioned by Munro (1957), has recently been confirmed by Valverde (1958), using backscatter techniques.

Recently there has been an increasing appreciation by many workers of the importance of $N(h)$ electron density profiles in ionospheric research. The usual ionosonde presentation, which relates virtual height to frequency, has many shortcomings when used for investigating ionospheric phenomena and, in fact, can give rise to entirely misleading results. For the purpose of many investigations, it is the knowledge of the true height at which a certain ionospheric event occurs, and of the change in electron density N at this point, which is of importance. In particular, recent probings of the ionosphere by rockets and artificial satellites have necessitated a knowledge of true heights of ionospheric layers for comparison with experimental measurements. Furthermore, the derived $N(h)$ curve may be used to estimate n, the total ion content of the layer up to maximum ion density, and variations in this quantity give valuable information on ionization and recombination processes, as shown in applications by Ratcliffe (1951).

Many methods have been developed to obtain the necessary $N(h)$ curves from the available $h'f$ presentation, and as early as 1938 Booker and Seaton

* Radio Research Board Laboratory, Electrical Engineering Department, University of Sydney.

suggested a simple technique based on a parabolic distribution of electron density with height, neglecting the effect of the Earth's magnetic field (Booker and Seaton 1938). This has been superseded by the more accurate integral methods of Manning (1947) and of Kelso (1954), the latter method including the magnetic field correction. These analyses and others are discussed in an excellent survey by King (1957).

The complicated and tedious calculations necessary, particularly in accounting for the magnetic field, have always been a deterrent in employing these methods for ionospheric research. However, Jackson (1956), King (1957), and more recently Duncan (1958), have developed techniques which are especially suitable for programming automatic electronic computers, and a program prepared by Duncan has been used by this laboratory in SILLIAC, the electronic computer situated at the Physics Department of Sydney University. The data consisting of virtual heights and corresponding frequencies from the ionosonde record, enough readings to sufficiently describe the curve, are supplied to the machine on punched paper tape. The results are given in true heights and electron density, which are then plotted to give the requisite $N(h)$ curve. The complete analysis of one $h'f$ curve is performed by the machine in approximately 20 seconds.

Approximately 200 of these calculations have been made during an investigation of travelling ionospheric disturbances.

Published data refer mainly to horizontal dimension of movements. The present investigation considers vertical dimensions and variation of characteristics with height using improved methods for the deduction of true heights. It is to be understood that the term height as used in this paper always refers to true height in the ionosphere, not virtual height.

II. Observational Data

In any study of heights of F-region travelling ionospheric disturbance phenomena it is important that the observational data do in fact pertain to that ionospheric layer, and that the effects observed are not due to disturbances in lower parts of the medium through which the probing radio ray has to pass. Briggs and Spencer (1954) have indicated that this uncertainty about precise height of measured movement is an inherent disadvantage of the fading method due to Mitra (1949), as applied to F-region measurements. There is a similar ambiguity in observations using radio star scintillations, and the height at which contributing irregularities occur does not seem to be known with certainty.

Speeds and directions of disturbances used in this paper are based on time differences of anomalies in F traces recorded at three spaced stations, a technique described by Munro (1950). A feature of these records is that the manifestations at a particular station usually occur at different times on the o- and x-ray traces (Munro and Heisler 1956*a*, 1956*b*). Moreover, the time differences so obtained are consistent with expected separations of o- and x-reflection points in the F region. The observed effects, therefore, are almost certainly due to phenomena occurring in this region at a height corresponding to the reflection height of the probing frequency.

Consideration must also be given to the validity of analysis as applied to the observational data. If θ is the angle which the probing ray makes to the vertical and t is the sweep time occupied by an ionosonde record, then in the integral method of actual height analysis $d\theta/dt$ must be zero or a very small quantity. This ensures that, for each frequency, the integration process is always along the same path through the ionized medium.

A travelling disturbance manifests itself on an ionosonde record as a complexity due in part to non-vertical reflection during portion of the frequency sweep. According to the above hypothesis, analysis of such a record would not be valid. However, in the results which follow below, ionosonde examples for analysis have been carefully chosen, either immediately before the advent of a disturbance or during that phase of the disturbance where non-vertical complexity is absent.

III. Height of Occurrence of Travelling Disturbances

(*a*) *Fixed-frequency Observations*

Most of these observations at this laboratory have been made on a fixed frequency of 5·8 Mc/s. This immediately predetermines the height of observation as that height in the ionosphere at which an electron density of $4{\cdot}17\times10^5$ electrons/cm^3 occurs, and will consequently vary with season, sunspot number, and time of day. The observations considered in this paper were made during the years 1952 to 1954 inclusive and a determination of heights from carefully selected disturbance-free ionosonde records shows that the median seasonal midday values are as follows : winter, 189 km ; equinox, 197 km ; and summer, 205 km. In each case there is a scatter of heights 10 km each side of these values.

Disturbances are identified on the film record as complexities in the F_2 trace, and are due to off-vertical reflections from curved isoionic surfaces which possess an apparent velocity relative to the observing station. Munro (1953) and Price (1959) have shown that the appearance of the disturbance as a complexity depends on the relationship between the radius of curvature r of the distorted isoionic surface and its height h above the observing point. If $r \geqslant h$ the disturbance passage will cause height and intensity changes in the record only, and these are not normally recorded as disturbance effects. Also, for a given value of r, the number of complexities and therefore recorded disturbances should increase with h. Absence of complexities therefore does not imply absence of disturbances and the film records must be carefully studied for height changes. Unless otherwise stated the statistics considered here concern only those disturbances which have produced complexities on film records.

Munro (1958) has shown that the number of disturbances observed varies considerably from day to day and indicates that, while ease of observation depends to some extent on the ionization gradient at the time, this does not account entirely for the fluctuations. A variation in occurrence of disturbances is found to be often associated with change in height of observation. This is illustrated in Figures 1 (*a*) and 1 (*b*). These are $N(h)$ curves for approximately the same time on consecutive days. On March 24, 1954 there were a large

number of 5·8 Mc/s disturbances, whereas on March 25, 1954 there were no 5·8 Mc/s disturbances and very few height rises. It will be noticed that on the disturbed day the 5·8 Mc/s reflection height was approximately 23 km lower than on the quiet day. Munro (1953) has indicated that travelling disturbances are more readily recognized on ionosonde records in a region where electron density changes slowly with height. The resultant manifestations on the film record are then more likely to be complex and hence more easily recognizable. It is possible therefore that differences in electron density gradient may influence the number of observed disturbances. On this basis, since the gradient is steeper on March 25, it would be expected that more disturbances would be observed on

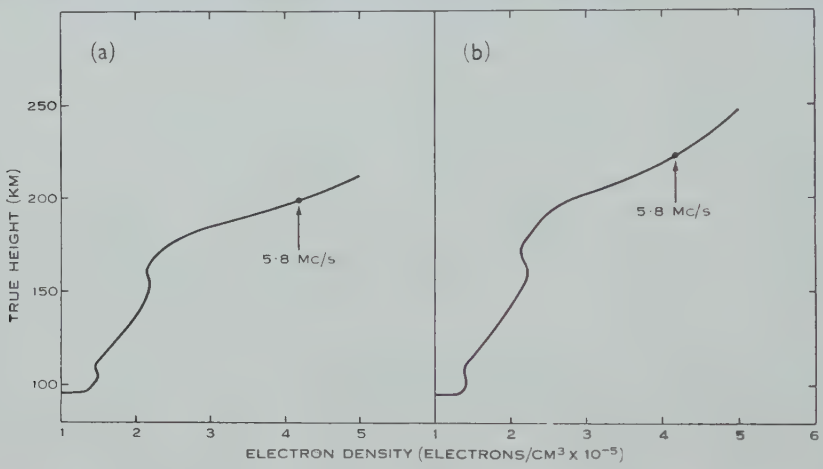

Fig. 1.—Electron density distributions illustrating relationship between height and occurrence of disturbances. (*a*) Camden 1243 hr, March 24, 1954, a day of numerous 5·8 Mc/s disturbances. (*b*) Camden 1230 hr, March 25, 1954, a day of no 5·8 Mc/s disturbances.

this day, whereas the converse is true. In this particular case therefore it would appear that gradient is not a contributory factor and height of observation governs the number of disturbances observed. Several similar cases seem to indicate that disturbances are more prevalent at lower reflection heights.

More definite information on this point was provided by a series of observations taken over a period of several months, using three frequencies simultaneously. A typical record on October 2, 1956 showed disturbed conditions on 4·5 and 5·8 Mc/s, while simultaneous observation on 9·8 Mc/s showed very few disturbances even when height rises as well as complexities were carefully checked on the film record to avoid electron density gradient influence on observational results as discussed above. The $N(h)$ curve of a typical ionosonde record for this period shown in Figure 2 places the 4·5 and 5·8 Mc/s reflection heights at 175 and 202 km respectively, whereas the 9·8 Mc/s reflection point is at the much greater height of 270 km.

The conclusion from these fixed-frequency observations is therefore that in the height range under observation there is a definite tendency for disturbances

to be more prevalent at the lower heights, with the probability of an upper boundary to the height at which they are apparent. This has been previously suggested by Heisler (1958).

(*b*) *Variable-frequency Observations*

The fixed-frequency technique described above is particularly valuable for studying small ionospheric disturbances, as it provides a very sensitive means of detection. It is limited, however, to observation of one isoionic contour and therefore cannot record the disturbance effect on a cross section of ionospheric heights. Large disturbances are more readily observed and their nature studied from sequences of ionosonde records made with a panoramic type recorder. Anomalies in such records due to travelling ionosonde disturbances have already been described (Heisler 1958). One particular type described therein as a *C* type

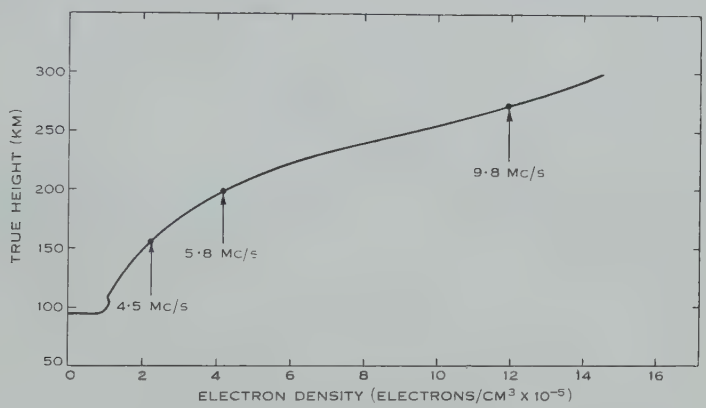

Fig. 2.—Electron density distribution at Camden for 1303 hr, October 2, 1956, showing true height of 4·5, 5·8, and 9·8 Mc/s reflection points.

anomaly occurs as a cusp-shaped trace at the top of F_1 forming a double peak, and gradually travels down the F_1 trace. An $N(h)$ curve of the ion density distribution giving rise to this type of disturbance is shown in Figure 3 (*a*). The F_1 peak in the original virtual height curve corresponds to an electron density of $3{\cdot}1\times10^5$ electrons/cm^3 and occurs at a height of 160 km. On this day there were no 5·8 Mc/s disturbances or height rises on fixed-frequency records but frequent type *C* anomalies on ionosonde records, so, while disturbances occurred at a height of 160 km and below, there were no disturbances at the 5·8 Mc/s height of 185 km.

In this case the upper boundary must be close to the F_1 peak and below the 5·8 Mc/s reflection height, i.e. at about 170 km. By contrast, records several days later, of which Figure 3 (*b*) is an $N(h)$ analysis, showed both F_1 and 5·8 Mc/s disturbances to be present. In this case the F_1 peak reflection point is at 165 km, approximately the same height as before, but the 5·8 Mc/s reflection point is at 210 km ; on this day, therefore, the upper boundary is much higher. It will be seen that the gradient is noticeably different on the two days and this may have some connexion with the change in boundary height.

IV. Height and Direction of Disturbances

The variability of direction of travel of fixed-frequency disturbances has been previously described by Munro (1958). During the summer the mean direction is 120° east of north and during winter 30° east of north with an abrupt change from winter to summer conditions during September-October and a more gradual change from summer to winter conditions during March-April.

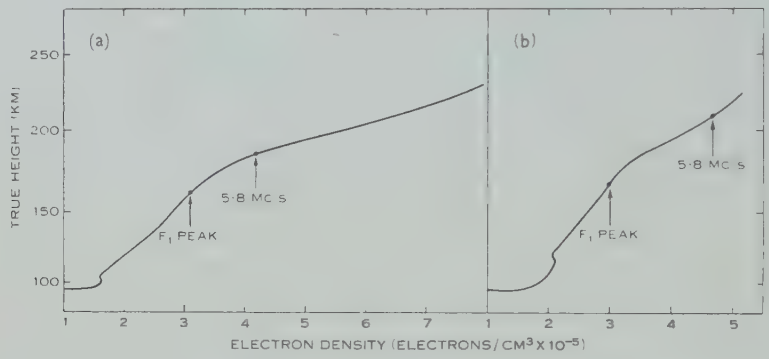

Fig. 3.—Electron density distributions illustrating change in upper bounding conditions for propagation of disturbances during equinoxial months. (*a*) Camden 1040 hr, March 18, 1952. (*b*) Camden 1327 hr, March 22, 1952.

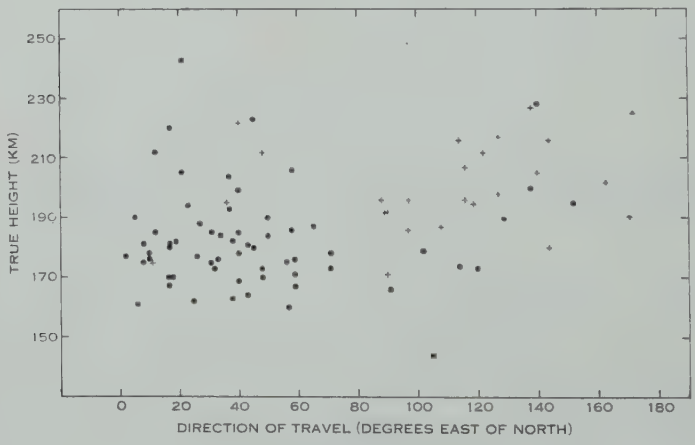

Fig. 4.—Variation of true height with direction of travel (+, summer values; ●, winter values).

Figure 4 shows a plot of direction against height of observation for disturbance cases in which summer values are plotted with crosses and winter values with dots. There are two obvious groupings; summer disturbances with heights above 190 km and directions ranging from 100 to 180°; and winter disturbances with heights below 190 km and directions ranging from 0 to 100°. This is a typical distribution, as summer heights of reflection for a particular frequency in general are higher than winter heights. However, the majority of winter disturbances observed at heights above 190 km also have directions

in the range 0–100°, and the few summer disturbances observed at heights below 190 km still have directions in the 100–180° range. It would appear therefore that change in direction is mainly seasonal and it is not valid to associate it directly with change in height of observation.

This apparent change of direction with height of observation can be further studied during equinoxial transitional periods when directions are variable. The $N(h)$ curves for such a case are shown in Figure 5. Figure 5 (*a*) is an $N(h)$ curve for 1151 hr, September 8, 1952, a day of predominant summer directions, and shows that a disturbance travelling 152° east of north at the time of this ionosonde recording was observed at a height of 195 km. However, September 11, 1952 was a day of predominant winter directions and on a similar curve shown in Figure 5 (*b*) for 1301 hr a disturbance travelling 33° east of north was observed

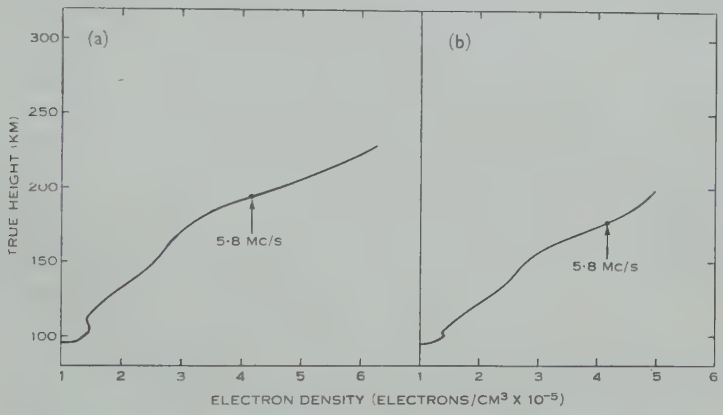

Fig. 5.—Electron density distributions illustrating relationship between height and direction of travel of disturbances. (*a*) Camden 1151 hr, September 8, 1952, a day of predominant summer directions. (*b*) Camden 1301 hr, September 11, 1952, a day of predominant winter directions.

at a height of 177 km. It will be noticed that this height is 18 km lower than previously. This difference in observational height for disturbances travelling in different directions has been observed in several equinoxial examples. In all cases low heights of observation are associated with winter directions while high heights of observation correspond to those disturbances with summer directions.

Since Figure 4 would suggest that during any particular season there is no direction gradient with height in the region of the ionosphere considered, it would appear that during the equinoxes there is some form of unstable control which not only causes the ion density distribution to fluctuate between normal summer and normal winter conditions but also governs the direction of movement of disturbances in these distributions.

A similar fluctuation in disturbance directions has been observed during summer, but only during recent sunspot maximum years when on occasional days predominant winter directions occur. A case in particular occurred on January 19, 1957 and Figure 6 (*a*) shows a typical electron density distribution

just prior to a disturbance on this day. Figure 6 (*b*) is an $N(h)$ distribution prior to a summer direction disturbance on the next day. It will be noticed that the 5·8 Mc/s reflection heights are almost identical. Moreover, in contrast to the equinoxial case of Figure 5 there is no very marked change in overall electron density distribution. Several such examples have been analysed and show the same features. It would appear, therefore, that in these cases the factors controlling direction of travel mentioned in connexion with Figure 5 are not significant and, since the particular phenomenon is observed only during sunspot maximum, some form of solar control is indicated.

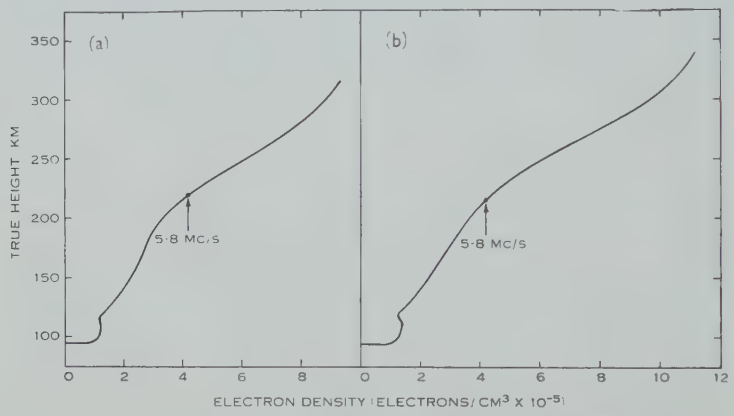

Fig. 6.—Electron density distributions illustrating relationship between height and direction of travel of disturbances during summer at sunspot maximum. (*a*) Camden 1134 hr, January 19, 1957, 5·8 Mc/s disturbance, direction 40° E. of N. (*b*) Camden 1115 hr, January 20, 1957, 5·8 Mc/s disturbance, direction 144° E. of N.

V. Height and Speed of Disturbances

As previously described (Heisler 1958), large ionospheric disturbances extend over a range of ionospheric heights and travel long distances with no apparent change in form or amplitude. Moreover, observations (Munro and Heisler 1956*a*, 1956*b*) indicate that a travelling disturbance always has an apparent vertical component of progression which is assumed to be the result of a forward tilt in the wavefront of the disturbance. If this were due to a height-speed gradient it would be difficult to understand how the disturbance could propagate without considerable change in form, particularly over large distances where tilt of the wavefront would become almost horizontal and hence vertical progression of the anomaly on the ionosonde record would be extremely slow. This is supported by the evidence of Figure 7, which shows the relationship between speeds of disturbances and height of observation. The random scatter of points suggests that in the region 160–220 km no correlation exists.

Distance of travel and duration of small fixed-frequency disturbances have not been fully investigated, but initial examination of several cases indicates that they are much less than those of the large ionospheric disturbances. It is possible, therefore, that an individual fixed-frequency disturbance could possess

a speed gradient with height. This would not be obvious on the statistic plot of Figure 7 and would restrict the scale of propagation of the disturbance.

Briggs and Spencer (1954) suggest that a height-speed gradient may exist at times of high magnetic activity, but, to arrive at this opinion, use Mitra method E and F region and radio star scintillation speed data.

As emphasized previously, there is uncertainty about precise heights of measured F-region movements using the Mitra method and a similar ambiguity exists in radio star scintillation measurements. Moreover, there is doubt as to whether the same phenomena are being observed in each case and whether indeed these phenomena are the same as those measured at this laboratory by different experimental techniques. In our observations no evidence of such an effect has been found.

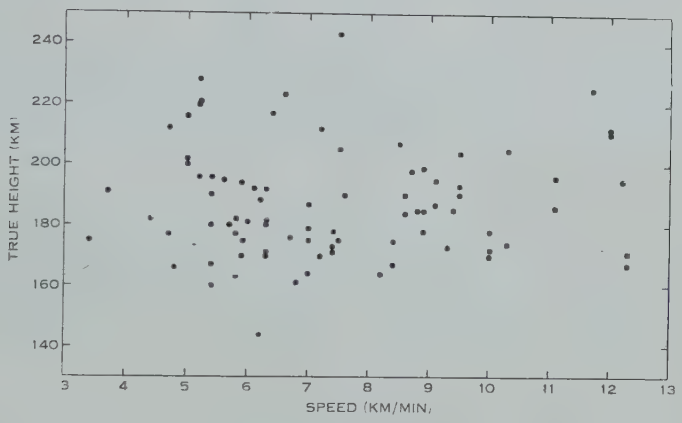

Fig. 7.—Variation of true height of occurrence with speed of disturbances.

Ratcliffe (1954) refers to a height-speed gradient in the ionosphere of 1 m sec^{-1} km^{-1}. This apparently originates in a private communication from Beynon and Thomas, quoted by Briggs and Spencer (1954). There is no indication whether this refers to all disturbance phenomena or to a particular case.

It is of little value to postulate a general gradient of speed with height in the ionosphere when there is a high variability of observed speeds in the region 160–220 km. It is probable that the inconsistency exists because of different phenomena being measured by different experimental techniques or is due to different geomagnetic observational locations. The use of virtual heights, in particular, can give very misleading results.

VI. Conclusions

The heights of observation of travelling disturbances and the mechanics of the phenomenon have been investigated by the study of associated $N(h)$ electron density profiles. Results apply particularly to the sunspot minimum years 1952–1954 and are as follows:

(1) Travelling disturbance phenomena are often contained by an upper boundary when anomalies are observed below this height only. The boundary is not always evident and may fluctuate in height from day to day.

(2) During a particular season there is no definite correlation between direction of travel of disturbances and height. Direction of travel seems to be mainly related to season, change in season being accompanied by a change in ion density distribution and a change in direction of travel of disturbances. Further, variability in direction of travel occurs during summer, but only in sunspot maximum years. There is little accompanying change in ion density distribution or height and the effect may be related to solar-geomagnetic phenomena.

(3) There is no significant correlation between speeds of disturbances and height of observation in the ionospheric region considered, which includes heights between 160 and 230 km. The observed long-distance propagation of large travelling disturbances also suggests that a height-speed gradient is improbable.

VII. Acknowledgments

This investigation has been carried out in the Electrical Engineering Department of the University of Sydney as part of the research program sponsored by the Radio Research Board. The preparation of material by the analysis staff is gratefully acknowledged. The author is particularly indebted to R. A. Duncan of the Upper Atmosphere Section of the Commonwealth Scientific and Industrial Research Organization for provision of the SILLIAC program used in analysis of data, and appreciation is expressed to the University of Sydney, in particular to Professor D. M. Myers, for provision of facilities in the Department and to Dr. G. H. Munro, Officer in Charge of the Sydney Laboratory, for helpful discussions during the preparation of this paper.

VIII. References

Booker, H. G., and Seaton, S. L. (1938).—*Phys. Rev.* **57**: 87.
Briggs, B. H., and Spencer, M. (1954).—*Rep. Progr. Phys.* **17**: 245.
Duncan, R. A. (1958).—*J. Geophys. Res.* **63**: 491.
Heisler, L. H. (1958).—*Aust. J. Phys.* **11**: 79.
Jackson, J. E. (1956).—*J. Geophys. Res.* **61**: 107.
Kelso, J. M. (1954).—*J. Atmos. Terr. Phys.* **5**: 11.
King, G. A. M. (1957).—*J. Atmos. Terr. Phys.* **11**: 209.
Manning, L. A. (1947).—*Proc. Inst. Radio Engrs., N.Y.* **35**: 1203.
Mitra, S. N. (1949).—*Proc. Inst. Elect. Engrs.* III **96**: 441.
Munro, G. H. (1950).—*Proc. Roy. Soc.* A **202**: 208.
Munro, G. H. (1953).—*Proc. Roy. Soc.* A **219**: 447.
Munro, G. H. (1957).—*J. Geophys. Res.* **62**: 325.
Munro, G. H. (1958).—*Aust. J. Phys.* **11**: 91.
Munro, G. H., and Heisler, L. H. (1956*a*).—*Aust. J. Phys.* **9**: 343.
Munro, G. H., and Heisler, L. H. (1956*b*).—*Aust. J. Phys.* **9**: 359.
Price, W. L. (1959).—*J. Atmos. Terr. Phys.* **16**: 93.
Ratcliffe, J. A. (1951).—*J. Geophys. Res.* **56**: 487.
Ratcliffe, J. A. (1954).—Report of the Physical Society Conference on The Physics of the Ionosphere.
Valverde, J. F. (1958).—Scientific Report No. 1, Radio Propagation Laboratory, Stanford University, U.S.A.

AN INTERFEROMETER FOR THE MEASUREMENT OF RADIO SOURCE SIZES

By B. R. Goddard,*† A. Watkinson,*‡ and B. Y. Mills*‡

[*Manuscript received May* 11, 1960]

Summary

Modifications have been made to the 85·5 Mc/s cross-type radio telescope at Sydney to permit the measurement of radio source sizes in the range of 10″ to 1′ arc. The basic modification involves the addition of another aerial at a distant site connected by radio link. A new form of automatic gain control ensures very good stability for the system. The modified instrument is described in general terms and calibration techniques are discussed.

I. Introduction

Knowledge of the angular sizes of discrete radio sources is of the greatest importance as an aid to the identification of the sources, for an understanding of the basic physical processes causing the emission, and in the application of radio-astronomical data to cosmology. However, the measurement of size is usually difficult, and little reliable information is available. Some of the closer and brighter sources, particularly those of galactic origin, are quite large, of the order of a degree or more, and the measurements in this case are relatively easy. Several of these were detected during 1950 and 1951 in an interferometer survey of the sky (Mills 1952*a*). However, it was clear then that the majority of detectable sources were much smaller than this and that special equipment would be needed to resolve them. Such equipment, utilizing very widely spaced interferometer aerials, was constructed in both Australia and England and almost simultaneous measurements made of the strongest unresolved sources (Brown, Jennison, and Das Gupta 1952 ; Mills 1952*b* ; Smith 1952*a*). It was shown that the five sources measured, Cassiopea A and Cygnus A in England and Cygnus A, Taurus A, Virgo A, and Centaurus A in Australia, all had angular sizes of the order of a minute to several minutes of arc, consistent with the identifications which had been made with visible nebulae. These initial measurements were extended and improved (Smith 1952*b* ; Mills 1953 ; Jennison and Das Gupta 1956) and for several years represented the only results available on the small discrete sources. Subsequent measurements extended the number of known sizes to a couple of dozen, all in the range 1′ arc or greater (Carter, personal communication ; Edge *et al.* 1959) and, more important, showed that a few sources appeared to have sizes less than 12″ arc (Morris, Palmer, and Thompson 1957).

* Division of Radiophysics, C.S.I.R.O., University Grounds, Chippendale, N.S.W.
† Present address : University of New South Wales, Sydney.
‡ Present address : School of Physics, University of Sydney.

On completion of the survey of the southern sky with the Sydney cross-type radio telescope, it became apparent that to progress in the identification of the radio sources and to apply their statistics in obtaining cosmological information it was necessary to obtain estimates of the sizes of a substantial proportion of the catalogued sources. When the catalogues are complete the total will exceed 2000.

Present results are based on the analysis of the initial catalogue between declinations $+10^\circ$ and -20°, containing nearly 1200 sources ; it appears that the majority are not resolved by the radio telescope, which is a pencil-beam instrument of beamwidth 50′ arc. The instrument has now been modified, principally by the addition of another aerial at a great distance, to study the sizes of these unresolved sources. In the present paper we describe the modified instrument and its operation ; the principal observational results will be given elsewhere.

The original instrument has been described in detail by Mills *et al.* (1958) ; briefly, it consists of a cruciform arrangement of two arrays of dipoles, each approximately 1500 ft long by effectively 15 ft wide. It operates at a wavelength of 3·5 m (85·5 Mc/s) and by combining the outputs of the arrays in a switching arrangement, produces a pencil-beam response. Analysis of some unpublished results of A. W. L. Carter, who had performed a relatively low sensitivity survey using an interferometer with spacing between arrays of 1000λ, suggested that the most useful arrangement for the present investigation would be initially an interferometer of about 3000λ spacing. With this spacing, only sources with sizes of the order of 1′ arc or less would be visible, which would enable the recognition of the very distant and small sources. The relative visibility of the sources at this spacing would also allow crude estimates of angular sizes.

However, estimation of the angular size of a radio source from measurements of its relative visibility using widely spaced interferometer aerials requires some assumption about the distribution of emission across the source. In so far as a good estimate can be made of this distribution the results of a measurement may be quite accurate ; if, however, the distribution is complex or merely elongated, quite erroneous values may be obtained. In fact, some strong radio sources which have been investigated do show complex structure and are not circularly symmetric, so that for accurate results it is necessary to make measurements with base lines of different spacing and azimuths. It is expected that the present instrument will be used in this way at the completion of a sky survey now in progress.

II. Description of the Instrument

The modified system comprises, in effect, two interferometers using the existing east-west arm of the Cross as a common aerial. The other aerials consist of (*a*) portion of the existing north-south arm of the cross 300 ft in length centred 30λ south of the centre of the east-west array and (*b*) a new array identical with (*a*) and situated 10 km distant in an east-west direction. The signal from aerial (*b*) is transmitted to the central site by means of a radio link similar to that used in an earlier investigation (Mills 1953).

The general arrangement is shown in Figure 1, together with an indication of the response patterns of the interferometers. In each case the primary

pattern is formed from the product of the response of the two arrays in the interferometer, and consists of an ellipse 0°·8 by 3°·7 to the half response points in east-west and north-south directions respectively. This response is broken up into " lobes ", 2° apart in a north-south direction for the close-spaced " local " interferometer, and 1·2′ arc apart in an east-west direction for the wide-spaced " link " interferometer. The overall gains of these interferometers are made equal so that information about the angular size of a source may be derived from the ratio of their responses.

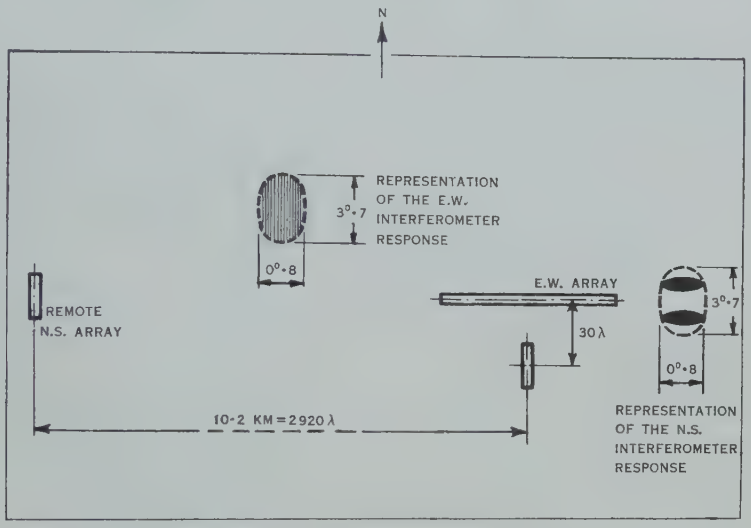

Fig. 1.—Illustrating the layout of the arrays and the form of the resulting response patterns.

The natural period of the interference pattern with the east-west interferometer varies according to the declination of the source, and is given by

$$T=\frac{12}{\pi}\,\frac{\lambda}{d}\sec\delta \text{ hours},$$

where d is the spacing between aerials and δ is the declination. With the operating wavelength 3·5 m and the actual spacing of 10·2 km (2920λ) the fastest period is about 5 sec, occurring when a source is at zero declination. If this interference pattern were recorded directly, it would not be possible to determine the relative visibilities by direct visual observation, since a very short output time constant would be needed, with consequent reduction in visibility. To overcome this, the period is increased by continually sweeping the phase of one half of the interferometer, causing the lobe pattern to follow partially the source's progression (Brown, Palmer, and Thompson 1955). In this way an interference pattern of any desired period can be obtained ; it was decided to use a standard 1 min period for all declinations. To enable direct comparison between the outputs of the long- and short-spaced interferometers, the period of the short-spaced pattern is also made 1 min by continuous phase sweeping. Some such arrangement is necessary, since a north-south interferometer has an

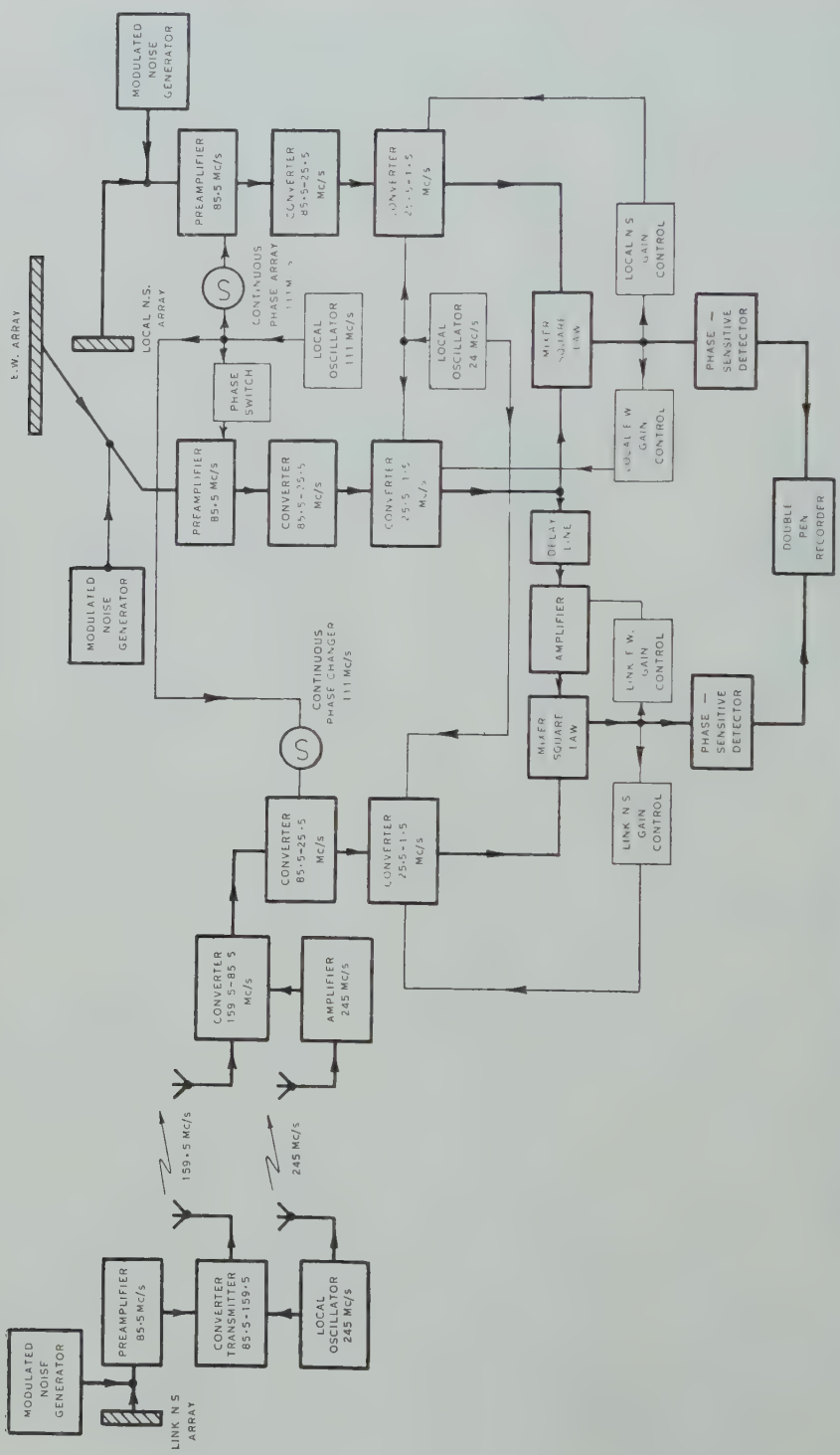

Fig. 2.—A simplified block diagram illustrating the essential functional elements of the system.

infinite period at transit and, with a fixed pattern, the response would depend on the position of the source relative to that of the pattern.

Since the accurate measurement of relative visibilities at the two spacings is required, the amplitude of the interference pattern is of prime importance. It is therefore necessary that the gain should be stable in each part of the system. The degree of stability required necessitated continuous automatic gain control on all receivers. This is achieved by maintaining constant the amplification of a " control " signal injected at the aerial inputs. The gain is then independent of variations in receiver noise factor and interfering signals.

Some of the essential parts of the system will now be discussed in more detail.

(*a*) *The Aerials*

The east-west arm of the Cross is used without alteration as the common element of the two interferometers. The constructional elements and performance of this array have been described elsewhere (Mills *et al.* 1958). Briefly, it consists of two collinear rows of half-wave dipoles separated by approximately half a wavelength and backed by a horizontal wire-mesh reflector. The overall length is approximately 1500 ft.

The remaining element in each interferometer is a north-south array of full-wave dipoles similar in arrangement to the original north-south arm of the Cross. The spacing between dipoles is $\frac{1}{2}\lambda$ and the phasing is arranged so as to produce a fan-beam response at right angles to the meridian plane. The position of this fan beam (i.e. its angle of elevation) is altered by a rearrangement of the phasing of each dipole by changing the point at which the coupling transformer is connected into the feed line, as in the original north-south arm of the Cross. However, the north-south arrays in this case have only 51, instead of 251, dipoles. With coupling and current distribution set as in the original north-south array, the aerial efficiency would be greatly reduced. To offset this, the coupling has been increased and the current distribution adjusted for rather less taper, resulting once again in an efficiency approaching 50 per cent. These alterations have caused an increase in the side-lobe responses, but they are only of the order of a few per cent. in the meridian plane and much less elsewhere: in view of the reduced sensitivity of the instrument compared with the original Cross, these are not serious.

(*b*) *The Receivers*

The overall receiving system consists of three separate receivers interconnected as shown in Figure 2. The three receivers are identical except for the inclusion of a radio link in the remote receiver and a compensating delay line in one of the local receivers. Two signals are transmitted over the radio link, one is the original 85·5 Mc/s cosmic noise signal converted to 159·5 Mc/s and re-radiated, the other is a 245 Mc/s c.w. signal derived from the local oscillator. When these are combined at the local site the original 85·5 Mc/s signal is reconstructed with phase information unaffected by the conversion processes. The 245 Mc/s signal also carries a pulse modulation for synchronizing the automatic gain control system as described later. The level of transmitted power is about $\frac{1}{2}$ W in each case.

The 85·5 Mc/s receivers use double frequency conversion, first to 25·5 Mc/s and then to 1·5 Mc/s, the delay line being inserted at the latter frequency. The system bandwidth of 250 kc/s is determined at 1·5 Mc/s after combining the signals from each aerial; the bandwidth up to that point is greater than 1 Mc/s in all receivers. Phase switching and phase-sensitive detection is used in both interferometer systems, the phase-reversing switch being inserted in the local oscillator feed to the common east-west converter (85·5 Mc/s→25·5 Mc/s). This corresponds exactly to the original Cross receivers (Mills *et al.* 1958).

The lobe sweeping of each interferometer is accomplished by continuous phase rotation of the local oscillator signal fed to each north-south receiver. The phase changer consists of a pick-up loop rotating in crossed magnetic fields excited in quadrature. The loop is driven by a small synchronous motor fed from a variable frequency oscillator, to enable the period of the interference pattern to be kept at 1 min for all declinations.

Square-law detection is achieved by an electronic multiplier at 1·5 Mc/s. This multiplier is a balanced type to improve the square law and eliminate unwanted components (Coates 1957).

(*c*) *Automatic Gain Control*

The automatic gain controls operate by keeping constant at the outputs of the receivers a standard modulated noise signal injected at the input to each preamplifier. The " control " signal is derived from a square-wave-modulated noise generator. The average noise diode current is maintained constant by a feedback control system operating on the output of the oscillator supplying power to the diode filament. The fundamental component of the control signal in the receiver output is extracted from the remaining noise by a filter and phase-sensitive detector, and a feedback control system maintains the amplitude of this component at a preset level. This action, in conjunction with the control of the injected noise, maintains a constant overall gain which can be set to any desired value by altering the comparator voltage. Since it is the fundamental Fourier component which is measured at the output and not the average value of the " square " wave, which is controlled at the input, it is important that the on-off ratio of the square wave be accurately maintained. For best performance, this ratio should be unity and to achieve this a bistable multivibrator is used, triggered by a free-running pulse generator at double the frequency.

In order that the input to the phase-sensitive detector be proportional to the gain of the system, regardless of the total level of the noise, it is necessary to extract the control signal after square-law detection.

Referring to Figure 2, it can be seen that the output of each detector contains components of:

(i) Control signal of the east-west receiver
(ii) Control signal of the north-south receiver
(iii) Coherent noise due to 429 c/s phase switching.

To avoid interaction, a modulation frequency of 1080 c/s was chosen for the east-west receiver and 632 c/s for the north-south receiver.

The phase-sensitive detector used is a gating type switched by a square wave which must be identical to the one which modulates the noise diode. In the systems located wholly at the local site this is achieved by connecting the phase-sensitive detector and the noise modulator to the same square-wave generator. In the case of the remote system it is necessary to generate another square wave at the local site, which must be coincident with the square wave modulating the noise diode at the remote site.

The double frequency triggering pulses previously referred to are used to modulate the 245 Mc/s local oscillator of the link, and these pulses are then extracted at the local site and used to trigger a similar bistable multivibrator. A sensing device in the output of the phase-sensitive detector is used to ensure that the second square wave is generated in phase with the one at the remote site. This is necessary because the bistable multivibrator has an inherent 180° ambiguity of phase.

In normal operation the automatic gain controls appear to have a stability of better than 2 or 3 per cent. over periods of 24 hours, with a long period stability over weeks of better than 10 per cent. With frequent calibration, as described in the next section, the relative sensitivities of the two interferometer receiving systems have an uncertainty of about 2 per cent.

III. Calibration

Since the measurement of angular size involves the ratio of the responses of the two interferometers, only a knowledge of relative sensitivities is required. It is convenient to consider the two main parts of the system, the aerials and the receivers, separately.

The two north-south aerials are made as nearly as possible identical. The methods of setting up have been described in detail elsewhere (Mills *et al.* 1958); briefly, the current distribution is adjusted by feeding power from a crystal-controlled oscillator into the aerial via its normal output connection, which is situated at the centre of the array. The current in each dipole is sampled in turn by a pick-up loop and fed to a detector. A reference signal is obtained by inserting a directional coupler into the feed line at a point close to the centre of the array, i.e. near the feed point. This reference signal is passed through a variable attenuator and a variable phase shift to the same detector. The magnitude and phase of the current in any dipole relative to the current at the reference point can then be determined by adjusting the attenuator and phase shift for a null. Using this technique, the individual currents are adjusted to conform with the required law and, if the corresponding reference point is used when setting up each array, the dipole currents can be adjusted for approximate equality in the two arrays; any remaining differences may be included in the overall calibration. Similar measurements made at different times have indicated an uncertainty of about 5 per cent. in the relative gains of the arrays.

To check the receivers, a standard signal of a special type is injected into each preamplifier in turn and the output is measured on the recorder. The ratios of the deflections on the recorders then give directly the ratios of the gains.

In order to include correctly the effects of the output time constant on the responses, the calibration signal is arranged to simulate the standard 1 min interferometer pattern. The standard signal is an accurately controlled noise signal, square-wave-modulated at a frequency differing from the phase-switching frequency by 1 c/min, obtained by the use of a continuously rotating goniometer. Thus, the rectified receiver output has a component at a frequency which differs from the gating frequency of the phase-sensitive detector by 1 c/min, producing the required sine-wave output on the recorder. This calibrating signal, which except for the frequency chosen is similar to the A.G.C. control signal, is injected

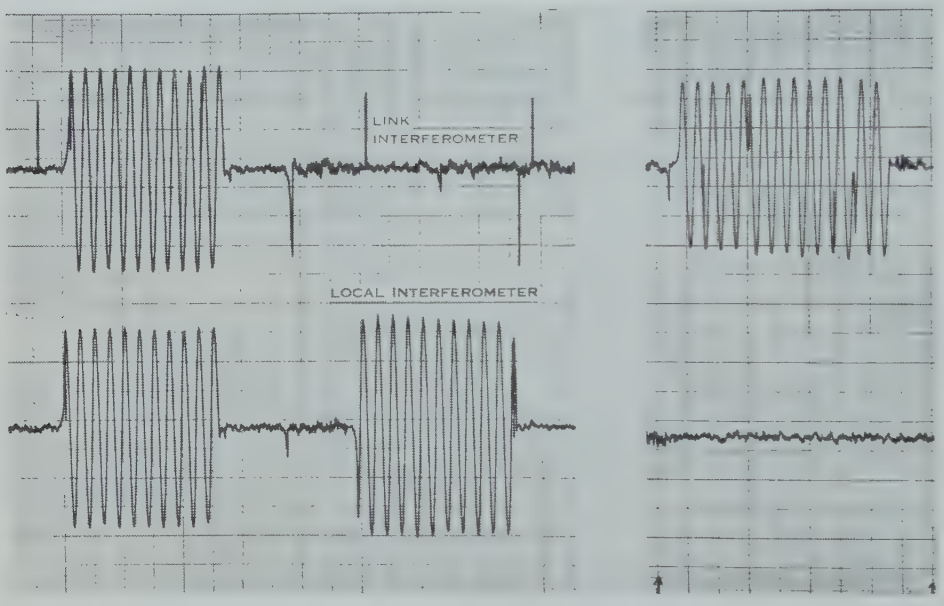

Fig. 3.—Some calibration records—on the left is shown the two east-west calibrations performed by injection of the signal into the common preamplifiers and beside them the calibration of the local north-south system. On the right is shown the corresponding calibration of the remote preamplifier transmitted over the radio link.

into the preamplifiers of each of the three systems in turn, i.e. the local and remote north-south systems and the east-west system. Typical calibrations are shown in Figure 3. When injecting into the north-south systems a pattern is produced only on the corresponding side of the record, but the common east-west system gives a response on both sides.

IV. Size Measurement

As indicated above, the chief use of the instrument in its present form is to recognize radio sources of small angular size. A further aim is to obtain estimates of the actual sizes of the sources, but, because of the expected diversity of shapes and orientations, estimates obtained with two spacings only must necessarily be very crude. However, they have proved of some use in identification work and a study of their statistics should yield information of cosmological interest.

In order to represent the measured visibility ratios by the size of an equivalent model, we assume that all sources have circularly symmetric Gaussian brightness distributions, i.e. possibilities of fine structure, elongation, and asymmetry are ignored.

This distribution is defined by

$$B(r)=B_0 \exp (1\cdot 67r/\theta_0)^2, \quad \ldots\ldots\ldots\ldots\ldots \quad (1)$$

where r is the angular distance to the centre and θ_0 is the angle between half brightness points.

It is well known (e.g. Mills 1953) that the relative visibility of a circularly symmetric distribution $B(r)$, is given by

$$A_n=\int_0^\infty I(\theta) \cos (2\pi n\theta)\mathrm{d}\theta, \quad \ldots\ldots\ldots\ldots \quad (2)$$

$$I(\theta)=2\int_\theta^\infty \frac{rB(r)}{(r^2-\theta^2)^{\frac{1}{2}}}\mathrm{d}r, \quad \ldots\ldots\ldots\ldots\ldots \quad (3)$$

where A_n is the relative visibility at a spacing of n wavelengths.

Inserting (**1**) in (**2**) and (**3**), it is readily shown that the equivalent size of the model source is given by

$$\theta_0=37\cdot 4 (\log_e X)^{\frac{1}{2}} \text{ seconds of arc}, \quad \ldots\ldots\ldots\ldots \quad (4)$$

where X is the ratio of visibilities at the two aerial spacings, i.e. $X=A_{30}/A_{2920}$. This expression is plotted in Figure 4.

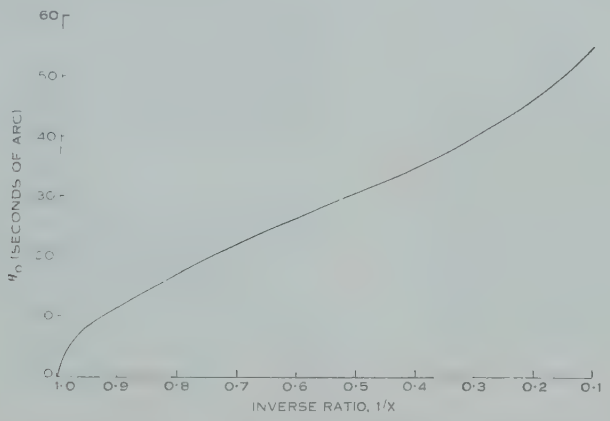

Fig. 4.—A plot of the equivalent source size against the ratio of responses on the two systems.

For large values of X the model source becomes meaningless, as fine structure in the distribution will dominate the picture: the indicated size then will be usually smaller than the actual. Below values of $X\approx 3$, however, the value of θ_0 represents approximately the half brightness angle in an east-west direction of quite a variety of distributions. As X approaches unity, the errors in measurement become important and, if the accuracy is about 10 per cent., as expected, a lower limit to the resolution is set at about 10″ arc. For the weakest sources,

statistical fluctuations reduce the accuracy considerably and, hence, also the effective resolution : for these sources the resolution limit is of the order of 30″. A substantial number of relatively strong sources have already been observed with apparently equal amplitudes at both spacings, i.e. $X \approx 1 \pm 10$ per cent. : for these we have $\theta_0 < 10''$.

In Figure 5 a record of two sources is reproduced, showing, in one case, a strong source Hydra A (09–12*4*, Mills, Slee, and Hill 1958), which has an appreciable angular size ($X = 4 \cdot 0$ and $\theta_0 = 45''$) and a weaker source (11—12*8*), which is unresolved by the equipment ($X \approx 1$, $\theta_0 < 10''$).

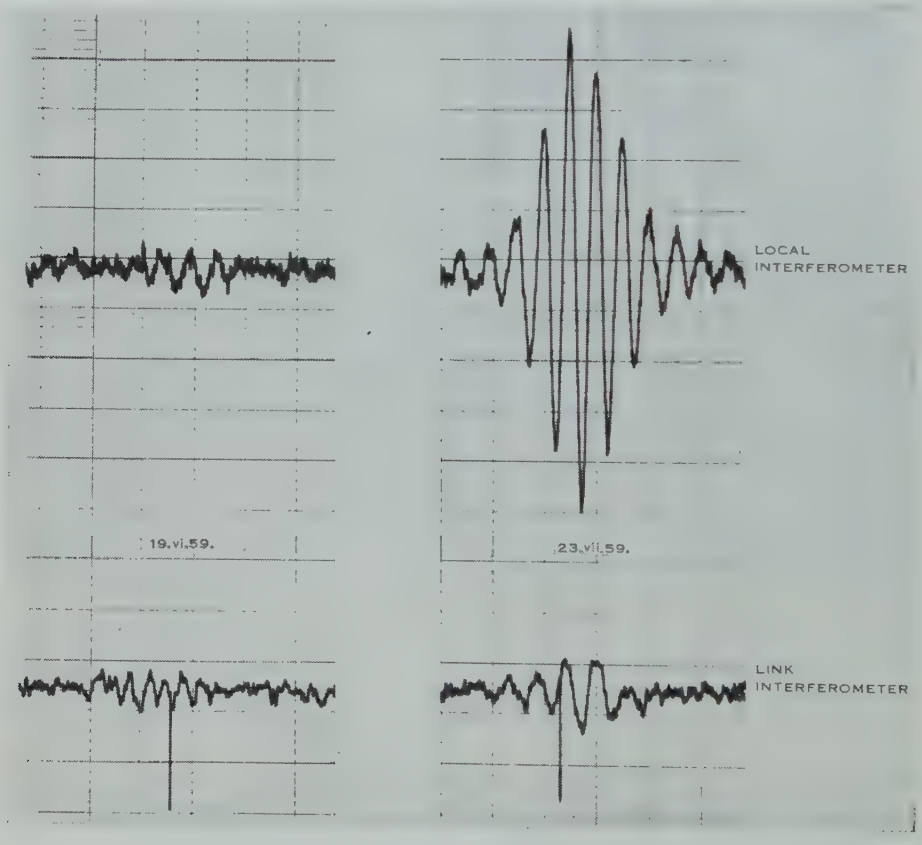

Fig. 5.—Some sample records showing, on the left, a strong source resolved by the instrument and, on the right, a weaker unresolved source.

Finally, one should mention the effects of the ionosphere on the measurement of size, since irregularities of electron density which cause the scintillation of radio sources might be expected to cause difficulties. If the ionosphere were sufficiently irregular to scatter coherent radiation into each of the widely separated aerials simultaneously, the whole basis of the method would be undermined : it is easily shown, however, from the known size of the irregularities that the scattering angle is too small by several orders of magnitude for this to occur.

Another possible cause of drastic error is the *differential* Faraday rotation at each aerial, but in this case, too, the known amounts of ionospheric refraction suggest that the effects would normally be negligible. One is therefore left with the usual effects of amplitude and phase variation, which, because of the great separation, are largely uncorrelated at the remote and local aerials. The latter variation is the more serious of the two : it can cause substantial changes in the period of the observed interference pattern and, occasionally, can be sufficiently rapid to destroy the pattern entirely, leaving it indistinguishable from random noise. To guard against the latter possibility it has been found desirable to take several observations at each declination and this has led to a considerable lengthening of the observational programme. Some of the results of this programme have already been described (Mills 1960) and others will be reported in subsequent papers.

V. References

Brown, R. H., Jennison, R. C., and Das Gupta, M. K. (1952).—*Nature* **170** : 1061.

Brown, R. H., Palmer, H. P., and Thompson, A. R. (1955).—*Phil. Mag.* **46** : 857.

Coates, H. N. (1957).—*Electron. Engng.* **29** : 41.

Edge, D. O., Shakeshaft, J. R., McAdam, W. B., Baldwin, J. E., and Archer, S. (1959).—*Mem. R. Astr. Soc.* **68** : 37.

Jennison, R. C., and Das Gupta, M. K. (1956).—*Phil. Mag.* **1** : 65.

Mills, B. Y. (1952*a*).—*Aust. J. Sci. Res.* A **5** : 266.

Mills, B. Y. (1952*b*).—*Nature* **170** : 1063.

Mills, B. Y. (1953).—*Aust. J. Phys.* **6** : 452.

Mills, B. Y. (1960).—*Aust. J. Phys.* **13** : 550.

Mills, B. Y., Little, A. G., Sheridan, K. V., and Slee, O. B. (1958).—*Proc. Inst. Radio Engrs., N.Y.* **46** : 67.

Mills, B. Y., Slee, O. B., and Hill, E. R. (1958).—*Aust. J. Phys.* **11** : 360.

Morris, D., Palmer, H. P., and Thompson, A. R. (1957).—*Observatory* **77** : 10.

Smith, F. G. (1952*a*).—*Nature* **170** : 1065.

Smith, F. G. (1952*b*).—*Proc. Phys. Soc. Lond.* B **65** : 971.

A CATALOGUE OF RADIO SOURCES BETWEEN DECLINATIONS —20° AND —50°

By B. Y. Mills,*† O. B. Slee,* and E. R. Hill*

[*Manuscript received June* 15, 1960]

Summary

A catalogue has been prepared of the radio sources observed between declinations —20° and —50°, using the Sydney cross-type radio telescope at a wavelength of 3·5 m ; a total of 892 sources is listed. This supplements an earlier catalogue in the declination zone +10° to —20°. In addition to the positions and intensities of the sources, angular sizes of 50 of the strongest are given ; several are found to have a size less than 15″ arc. As before, identifications with bright optical objects have been sought, and a number of galaxies of apparently abnormal radio emission listed. Statistical analyses of the distribution of the radio sources give results very similar to those obtained using the earlier catalogue. Within the uncertainty in the data, the distribution appears uniform in depth and there is a significantly greater number of sources of large apparent size than expected from chance blending effects.

I. Introduction

Analysis has been continuing of the records taken with the Sydney 3·5 m cross-type radio telescope. A catalogue of radio sources has now been prepared between declinations —20° and —50° to add to the previously published catalogue between +10° and —20° (Mills, Slee, and Hill 1958) ; the zone between —50° and —80°, which will complete the series, is in preparation. In the present catalogue a total of 892 radio sources is listed in the area of 2·66 steradians. The source density, 336 per steradian, is somewhat less than the previous figure of 356 per steradian, but not significantly so in view of the inclusion in the catalogue of the brightest regions of the Milky Way and the brightest southern extragalactic source : these cause a marked reduction in the listings of faint sources in their vicinity because of increased background temperatures and side-lobe effects.

The catalogue has been examined in the same manner as the earlier one for identifications with optical objects and for the statistics of the radio source distribution. Since the present data add little to the earlier conclusions and since more data will be available soon from the final catalogue zone, these results are discussed only briefly.

The present catalogue differs from the earlier one in that angular sizes are given for about 50 sources unresolvable with the pencil-beam aerial. These have been obtained with the newly developed angular size interferometer (Goddard, Watkinson, and Mills 1960). Since the sizes of many more sources

* Division of Radiophysics, C.S.I.R.O., University Grounds, Chippendale, N.S.W.
† Present Address : School of Physics, University of Sydney.

in the catalogue will be available shortly, the analysis and discussion of the results is postponed. It is interesting, however, that a number of radio sources are listed which could not be resolved by the instrument. These have been estimated to be smaller than 10–15″ arc.

II. The Catalogue

Preparation of the catalogue follows the methods described in two earlier papers (Mills and Slee 1957 ; Mills, Slee, and Hill 1958) ; subsequently these papers will be referred to as paper I and paper II respectively. The catalogue is divided into three zones covering declinations −20° to −30°, −30° to −40°, and −40° to −50° ; they are given in Tables 1, 2, and 3. The previously used scheme of reference numbers has been adopted in which the first two digits of the number denote the hour of the Right Ascension ; these are followed by the sign of the declination and the tens digit measured in degrees and, finally, an italicized serial number arranged in order of increasing Right Ascension within the 1-hr period. Only the latter italicized numbers are given in the tables, as the others are evident ; for example in Table 1, the second source would be referred to in the text as 00−*22*.

As before, the probable error in the final digit of a position is indicated by a superscript. The positions given are directly as measured, with allowances only for precession. In the catalogue of paper II the sources of highest accuracy for which the estimated probable error in R.A. was $\pm 0{\cdot}1^{m}$ were corrected by $+4^{s}$. This correction was based on the differences between the apparent radio and optical positions of six bright identified galaxies. However, two of these galaxies are of large angular size and complex structure so that differences are probably not significant, and in two other cases our uncorrected positions were confirmed by other observers. It therefore appears probable that the systematic error in our positions is negligible and no such corrections have been applied in the present catalogue. Radio sources resolved by the aerial beam have been treated as before, both their peak flux density and their integrated flux density being given, the former in parentheses. In general, only sources with apparent angular size less than 2° have been included in the catalogue, two exceptions being the well-established sources at the galactic centre, 17−*213*, and Centaurus A, 13−*42*. When the size of a source has been measured using the angular size interferometer it is given in the footnotes in units of seconds of arc. These are " equivalent " sizes and refer to a circularly symmetric source of Gaussian brightness distribution which has the same ratio of visibilities at spacings of 30λ and 2920λ (Goddard, Watkinson, and Mills 1960). The measurements are preliminary and are likely to be improved later. Possible identifications with bright nebulae are also given in the footnotes ; when the NGC number is in parentheses there appears to be no reason for thinking that this is other than an accidental coincidence in position. These and other possible identifications are discussed briefly in the next section.

A small portion of the catalogue is included in an area examined by Rishbeth (1958), who gave contour diagrams and a short catalogue of radio sources in the Vela-Puppis region near 08^{h} R.A. In general our catalogues agree quite closely,

TABLE 1

SOURCES BETWEEN DECLINATIONS —20° AND —30°

Sources which may be " extended ", that is, resolvable, are indicated by a dagger. A colon has been placed beside uncertain flux densities. Angular sizes, where available, are indicated in the footnotes. Details in Section II

Ref. No.	Position (1950) R.A. h m	Position (1950) Dec. S. ° ′	Flux Density (10^{-26} W m^{-2} (c/s)$^{-1}$)
	00		
1	01·2³	22 40⁸	6
2	02·1³	23 22⁷	10
3	07·1³	28 55⁶	8
4	10·0³	23 43⁷	8
5	16·0³	22 37⁷	13
6	17·7³	20 40⁶	13
7	20·7²	25 22⁵	21
8	21·2⁴	21 15⁸	14†
9	21·9³	29 43⁴	33[1]
10	22·0²	26 16⁶	17†
11	24·3⁴	20 47⁷	7
12	24·3⁴	27 51⁸	5
13	25·3⁴	28 21⁷	9
14	29·9³	24 32⁵	7
15	30·5⁴	22 09⁷	8
16	33·2²	20 18⁴	19
17	35·2⁵	26 41⁸	5
18	35·5²	23 12⁵	10
19	36·9⁴	29 24⁷	8
20	38·1³	27 47⁸	6
21	42·0²	22 21⁵	9
22	45·1²	25 38⁴	29[2]
23	54·4⁴	26 23⁷	9
24	56·5³	29 21⁸	8
	01		
1	00·1²	22 11⁴	35[3]
2	00·6³	27 43⁶	16
3	06·2³	29 06⁷	9
4	10·6³	22 19⁶	9†
5	13·7³	23 01⁶	8
6	13·9³	21 07⁵	*24* (18)
7	13·9⁵	28 41⁶	12
8	17·9⁴	27 25⁸	7
9	22·4⁴	25 25⁷	9
10	24·2³	22 28⁷	8
11	28·7²	26 27⁵	18
12	34·1⁴	24 05⁸	6
13	35·9⁴	23 05⁸	5
14	39·2⁴	25 57⁷	7
15	39·6³	27 21⁷	16
16	43·3⁴	24 16⁶	12
17	48·7²	29 44⁴	*63* (43)
18	50·0⁴	27 23⁷	11
19	55·0⁵	21 09⁷	10
	02		
1	02·8⁴	23 50⁸	10
2	05·2³	22 32⁷	16
3	08·5⁴	28 01⁷	8†
4	09·3⁴	23 48⁸	9
5	16·4³	24 59⁵	15
6	21·5³	28 31⁶	11
7	22·2³	23 21⁵	19
8	24·1⁵	23 58⁷	10[4]
9	26·8⁵	24 03⁷	9[4]
10	29·9⁴	20 43⁷	11
11	31·4⁴	23 43⁶	17
12	33·5²	29 11⁶	8
13	39·8⁴	28 12⁸	7
14	42·6³	21 56⁸	9
15	44·0³	23 57⁷	8
16	45·4²	29 28⁷	10†
17	46·7²	20 42⁷	14
18	53·4⁴	22 09⁷	9
19	54·2²	23 32⁶	28
20	54·7³	20 46⁶	13
21	54·7³	26 18⁷	7
22	59·8⁴	29 18⁵	8

[1] ~20″.

[2] NGC 253.

[3] ~30″.

[4] Sources 02–28, 02–29 form perhaps one extended source.

TABLE 1 (*Continued*)

Ref. No.	Position (1950) R.A. h m	Position (1950) Dec. S. ° ′	Flux Density (10^{-26} W m^{-2} (c/s)$^{-1}$)
	03		
1	04·1^{4}	24 08^{5}	7
2	05·2^{4}	22 31^{8}	17
3	13·8^{2}	27 14^{6}	23
4	25·5^{3}	23 07^{7}	15[5]
5	27·2^{3}	26 08^{7}	14
6	30·7^{3}	27 23^{7}	8
7	37·2^{3}	28 46^{5}	9
8	37·6^{5}	24 14^{8}	8
9	38·1^{4}	21 40^{7}	*14* (9)
10	45·4^{3}	29 26^{5}	15
11	46·7^{4}	21 37^{7}	9
12	49·7^{2}	27 57^{5}	53[6]
13	52·1^{4}	25 45^{7}	11†
14	58·7^{4}	24 38^{6}	9
	04		
1	06·3^{3}	24 15^{5}	14
2	06·7^{3}	22 52^{6}	10
3	12·9^{2}	29 40^{5}	17
4	13·7^{3}	21 04^{7}	26
5	14·7^{3}	22 07^{8}	8
6	20·3^{4}	26 33^{4}	11
7	22·5^{4}	20 04^{6}	7
8	26·7^{4}	27 03^{6}	15†
9	27·9^{3}	28 07^{5}	12
10	30·4^{5}	23 34^{7}	7
11	30·7^{3}	29 49^{6}	13
12	30·9^{4}	24 44^{7}	8
13	32·7^{3}	25 33^{6}	8
14	34·6^{5}	20 45^{8}	*5*
15	34·8^{3}	22 32^{6}	10
16	36·7^{5}	27 21^{8}	8
17	37·1^{5}	24 39^{8}	8
18	42·7^{1}	28 18^{3}	82[7]
19	45·9^{3}	20 40^{5}	19
20	50·4^{3}	28 36^{7}	12
21	52·9^{3}	22 04^{5}	*38* (21)
22	53·3^{3}	20 36^{4}	18
23	56·5^{4}	23 43^{7}	7

Ref. No.	Position (1950) R.A. h m	Position (1950) Dec. S. ° ′	Flux Density (10^{-26} W m^{-2} (c/s)$^{-1}$)
	05		
1	01·9^{5}	25 51^{8}	8
2	03·6^{2}	28 41^{4}	*60* (30)
3	08·4^{3}	22 06^{6}	19†
4	19·0^{3}	20 31^{6}	19:[8]
5	25·5^{4}	23 21^{7}	9
6	28·6^{4}	20 55^{7}	8
7	40·9^{4}	24 16^{6}	13
8	41·1^{4}	27 28^{6}	7
9	41·9^{3}	21 08^{6}	10
10	43·2^{3}	26 27^{5}	12
11	49·7^{3}	21 20^{5}	8
12	52·9^{4}	22 47^{8}	9
	06		
1	02·8^{4}	28 56^{6}	7
2	04·6^{2}	20 13^{5}	23
3	15·9^{3}	28 16^{7}	9
4	19·1^{4}	24 08^{8}	9
5	19·4^{3}	27 21^{6}	9[9]
6	20·1^{3}	26 05^{7}	7
7	21·0^{3}	25 18^{7}	11†
8	24·5^{4}	20 35^{7}	11
9	30·4^{4}	27 16^{6}	12
10	34·7^{1}	20 37^{4}	*85* (67)
11	37·4^{3}	27 36^{7}	17
12	37·7^{3}	28 40^{6}	17
13	51·0^{3}	21 20^{6}	9
14	51·2^{4}	22 32^{7}	8
15	55·5^{3}	26 40^{7}	16†
16	56·9^{1}	24 13^{4}	59[10]

[5] Possible confusion with IAU 03S3A side lobe.

[6] 40″.

[7] 35″.

[8] Possible confusion with IAU 05S4A side lobe.

[9] (NGC 2217).

[10] >45″.

TABLE 1 (*Continued*)

Ref. No.	Position (1950) R.A. h m	Position (1950) Dec. S. ° ′	Flux Density (10^{-26} W m^{-2} (c/s)$^{-1}$)
	07		
1	04·2^{3}	22 58^{6}	6
2	06·9^{3}	29 14^{7}	*45* (22)[11]
3	09·0^{2}	20 34^{4}	*71* (33)[11]
4	15·4^{3}	24 57^{6}	17
5	16·1^{3}	26 28^{6}	18†
6	20·1^{3}	21 55^{6}	11
7	21·9^{3}	23 28^{7}	15†
8	24·7^{3}	24 51^{6}	10
9	25·5^{3}	20 39^{6}	10
10	25·8^{4}	28 45^{7}	15†
11	27·2^{3}	22 06^{5}	16†
12	39·2^{4}	24 18^{8}	*38* (24)
13	40·7^{3}	28 15^{8}	13
14	50·5^{4}	21 47^{8}	8
15	50·9^{4}	26 20^{7}	13
16	54·4^{4}	23 28^{8}	7
	08		
1	12·3^{3}	23 33^{8}	7
2	12·9^{3}	24 48^{7}	10
3	18·3^{3}	29 46^{6}	16
4	25·1^{2}	20 15^{5}	26
5	25·1^{4}	23 13^{7}	11
6	26·7^{5}	21 30^{8}	8†
7	33·1^{4}	24 49^{8}	11
8	34·5^{3}	26 00^{7}	9
9	34·8^{3}	27 01^{6}	16
10	35·7^{4}	22 19^{7}	9
11	42·7^{5}	26 30^{8}	14†
12	43·0^{4}	23 30^{6}	15
13	43·4^{3}	29 35^{7}	12[12]
14	43·9^{4}	22 37^{8}	9
15	50·8^{4}	22 52^{7}	8
16	50·9^{3}	20 36^{6}	19
17	55·3^{3}	21 18^{7}	7
18	56·4^{3}	27 18^{6}	13
19	59·6^{2}	25 49^{5}	54[13]
	09		
1	05·7^{4}	29 21^{8}	9
2	20·4^{5}	27 24^{7}	8
3	21·5^{3}	21 05^{8}	7
4	24·5^{4}	25 57^{8}	10
5	26·2^{4}	29 48^{6}	13
6	30·7^{3}	20 07^{7}	12
7	35·3^{4}	28 50^{8}	16:†
8	36·5^{3}	25 40^{6}	12
9	42·7^{5}	27 50^{8}	8
10	47·4^{2}	24 59^{8}	19
11	51·0^{3}	23 48^{6}	9
12	56·0^{3}	28 55^{8}	*30* (18)[11]
13	56·6^{3}	20 25^{8}	6
14	59·6^{3}	23 38^{6}	15
	10		
1	02·8^{3}	21 31^{5}	48[14]
2	06·5^{4}	30 00^{6}	10
3	08·5^{4}	28 30^{8}	8[15]
4	10·9^{3}	27 50^{8}	12
5	12·5^{3}	23 38^{6}	10
6	24·6^{3}	29 46^{6}	9
7	30·8^{3}	23 37^{7}	18†
8	35·5^{4}	24 50^{8}	8
9	35·9^{4}	28 58^{7}	10
10	35·9^{3}	26 10^{6}	15
11	40·1^{4}	23 20^{7}	12
12	42·7^{3}	28 46^{7}	14†
13	43·0^{4}	22 10^{7}	9[16]
14	48·9^{4}	20 19^{7}	10
15	53·2^{3}	26 00^{7}	11
16	53·5^{4}	27 43^{8}	13†

[11] Perhaps several sources.

[12] Perhaps one extended source with 08–37.

[13] 32″.

[14] <10″.

[15] A doubtful source.

[16] Perhaps a background irregularity.

TABLE 1 (*Continued*)

Ref. No.	Position (1950) R.A. h m	Position (1950) Dec. S. ° ′	Flux Density (10^{-26} W m^{-2} (c/s)$^{-1}$)
	11		
1	03·2^{3}	24 33^{7}	8[16]
2	03·3^{3}	20 52^{5}	16
3	08·1^{3}	22 51^{6}	16
4	15·9^{3}	25 55^{7}	9
5	27·1^{3}	28 53^{6}	19†
6	29·6^{3}	26 56^{7}	8
7	38·1^{2}	26 18^{4}	28
8	39·0^{2}	28 30^{5}	27
9	49·8^{2}	30 00^{6}	7
10	51·7^{4}	28 08^{8}	9
11	52·1^{3}	28 11^{7}	13
12	55·7^{4}	22 07^{8}	15
	12		
1	08·4^{3}	25 02^{6}	14†
2	09·8^{5}	26 56^{10}	7
3	18·5^{3}	27 40^{7}	10
4	19·2^{4}	26 46^{7}	10†
5	22·7^{4}	25 51^{8}	15†
6	25·1^{3}	20 52^{6}	12
7	32·9^{2}	24 57^{4}	28:
8	37·7^{4}	20 10^{7}	9
9	38·3^{3}	23 19^{6}	9†
10	40·9^{3}	27 27^{6}	17†
11	45·0^{4}	28 58^{6}	18
12	51·7^{2}	29 03^{4}	47[17]
13	55·8^{4}	25 25^{7}	8
14	56·6^{3}	23 08^{6}	27:
15	59·0^{3}	20 09^{5}	16
	13		
1	02·7^{3}	20 53^{8}	11
2	03·5^{5}	25 00^{6}	15
3	09·0^{2}	22 00^{4}	61[18]
4	12·2^{4}	24 58^{7}	9
5	34·7^{3}	29 32^{6}	36[19]
6	36·9^{3}	21 05^{7}	14
	13		
7	45·9^{4}	25 14^{7}	17:
8	50·7^{4}	23 38^{8}	9
9	55·7^{4}	23 35^{8}	9
10	56·7^{3}	21 55^{6}	8†
	14		
1	03·8^{2}	27 18^{5}	20
2	08·0^{3}	22 27^{7}	8:
3	08·8^{3}	27 29^{7}	13
4	09·8^{3}	20 18^{6}	12:
5	10·9^{5}	23 38^{7}	19
6	14·1^{3}	21 24^{5}	17
7	19·5^{3}	29 18^{6}	15
8	20·2^{3}	27 14^{5}	40[20]
9	20·6^{3}	24 52^{6}	14
10	21·7^{4}	29 42^{6}	26
11	22·0^{4}	23 48^{7}	17
12	25·6^{3}	21 47^{10}	*18* (11)[11]
13	39·0^{3}	26 28^{5}	24
14	39·0^{3}	24 38^{7}	9:
15	54·7^{3}	28 21^{9}	7
	15		
1	03·8^{3}	22 20^{7}	10
2	05·1^{4}	26 27^{6}	9
3	05·8^{4}	29 23^{5}	*35* (20)
4	07·0^{3}	20 13^{6}	9
5	07·9^{5}	25 15^{7}	7[16]
6	11·9^{3}	22 22^{6}	9[21]
7	18·0^{5}	28 13^{6}	7
8	25·2^{4}	26 42^{6}	11
9	26·7^{4}	27 38^{6}	18†
10	26·8^{4}	20 10^{8}	8
11	44·3^{4}	22 42^{7}	13
12	50·0^{4}	25 10^{7}	12
13	56·2^{3}	21 35^{5}	36[22]
14	56·4^{3}	24 05^{6}	18

[17] ∼35″.
[18] ∼15″.
[19] NGC 5236.
[20] ⩽12″.
[21] Superimposed on background irregularity.
[22] >30″.

TABLE 1 (*Continued*)

Ref. No.	Position (1950) R.A. h m	Position (1950) Dec. S. ° ′	Flux Density (10^{-26} W m^{-2} (c/s)$^{-1}$)
	16		
1	01·9[3]	28 50[5]	35
2	05·0[4]	20 21[6]	20
3	18·2[5]	23 53[7]	14
4	19·2[3]	28 00[6]	18
5	28·7[3]	26 50[6]	27
6	35·9[6]	23 38[8]	10[15]
7	36·6[4]	21 33[7]	8
8	39·6[4]	25 25[10]	19
9	43·4[3]	22 22[5]	22
10	53·3[4]	25 40[8]	14
11	53·6[3]	20 13[6]	11
12	59·3[3]	28 43[7]	25[15]
	17		
1	01·7[4]	24 24[7]	15[15]
2	08·2[3]	20 56[6]	19
3	09·5[2]	23 18[5]	42[23]
4	09·9[3]	28 00[7]	24
5	10·8[2]	25 00[5]	47[24]
6	13·2[4]	29 50[7]	38
7	17·9[3]	28 56[8]	32[15]
8	22·1[6]	20 19[8]	17
9	22·4[4]	26 50[6]	18
10	23·0[5]	28 05[6]	14†[15]
11	27·8[1]	21 29[3]	110[25]
12	37·0[4]	21 33[7]	21
13	43·7[9]	28 41[12]	*4500*[26]
14	52·2[4]	21 30[7]	*194* (87)
15	52·4[4]	23 05[6]	82†
16	57·4[1]	23 26[3]	900[27]
17	59·9[3]	28 00[3]	35[28]
	18		
1	02·7[1]	21 23[3]	253[29]
2	02·8[4]	26 03[7]	19[15]
3	04·0[2]	20 10[4]	70
4	05·8[3]	27 00[7]	34
5	12·8[3]	24 09[5]	*114* (71)[16, 30]
6	14·9[5]	22 40[6]	24
7	16·2[3]	25 45[6]	30†
8	22·5[3]	20 05[7]	*70* (27)
9	23·8[3]	24 03[7]	31
10	24·8[3]	29 10[6]	26
11	33·6[3]	23 59[7]	39
12	48·5[3]	25 57[6]	23[16]
13	50·9[5]	26 52[7]	22[16]
14	53·0[4]	22 27[6]	10[16]
	19		
1	00·1[3]	23 33[5]	35†
2	04·0[3]	25 09[5]	17
3	12·8[3]	26 58[5]	53†
4	13·6[3]	24 49[6]	35
5	16·4[3]	21 41[7]	18
6	20·4[3]	20 37[7]	8
7	25·6[3]	25 44[5]	21†
8	29·2[4]	26 40[6]	42
9	33·4[6]	24 08[6]	9
10	34·9[3]	22 22[6]	11
11	42·6[3]	27 05[6]	12
12	46·4[4]	28 01[6]	18
13	50·4[4]	21 47[6]	11

[23] $>30''$.
[24] $\geqslant 40''$.
[25] Kepler's Supernova—size $>45''$.
[26] IAU 1782A, complex distribution—only the integrated flux is given.
[27] $>65''$.
[28] $\sim 30''$.
[29] $>60''$.
[30] $>40''$.

TABLE 1 (*Continued*)

Ref. No.	Position (1950) R.A. h m	Position (1950) Dec. S. ° ′	Flux Density (10^{-26} W m^{-2} (c/s)$^{-1}$)
	20		
1	02·8^{3}	25 03^{6}	7$^{(15)}$
2	15·1^{3}	29 40^{7}	11
3	18·3^{4}	22 23^{7}	8
4	21·1^{4}	21 11^{5}	11
5	24·3^{4}	20 34^{6}	9
6	24·5^{4}	21 44^{5}	18
7	27·4^{3}	29 40^{7}	9$^{(15)}$
8	29·9^{3}	23 00^{5}	22
9	34·8^{3}	24 18^{8}	6
10	35·7^{3}	20 16^{7}	9
11	38·8^{3}	27 57^{6}	12
12	40·6^{3}	26 43^{5}	18†
13	45·2^{3}	24 16^{7}	12
14	53·0^{3}	20 07^{5}	25
15	58·7^{2}	28 13^{4}	59:$^{(31)}$
16	59·9^{4}	21 05^{7}	8$^{(16)}$
	21		
1	04·6^{1}	25 39^{3}	100$^{(32)}$
2	06·2^{3}	23 55^{6}	21†
3	13·6^{3}	21 11^{5}	24
4	15·3^{3}	25 07^{6}	15
5	18·9^{3}	26 45^{6}	17
6	23·1^{4}	23 58^{7}	9
7	24·9^{3}	29 24^{7}	10
8	26·6^{3}	22 55^{7}	9
9	28·3^{3}	20 54^{5}	16
10	34·7^{3}	20 57^{6}	11
11	36·3^{3}	25 59^{6}	15
12	36·7^{3}	27 58^{6}	8
13	50·0^{4}	20 03^{7}	15
14	50·7^{3}	28 10^{8}	12
15	59·9^{2}	28 36^{6}	10

Ref. No.	Position (1950) R.A. h m	Position (1950) Dec. S. ° ′	Flux Density (10^{-26} W m^{-2} (c/s)$^{-1}$)
	22		
1	14·7^{4}	28 23^{6}	*23* (14)
2	16·7^{3}	20 50^{7}	11
3	22·8^{4}	27 32^{8}	9
4	26·5^{3}	29 30^{7}	9
5	32·7^{4}	23 02^{6}	9
6	45·9^{4}	24 23^{6}	9
7	46·5^{4}	26 53^{7}	8
8	47·3^{3}	23 19^{5}	13
9	48·1^{4}	22 17^{6}	7
10	55·3^{3}	23 01^{5}	9
11	59·4^{3}	26 55^{6}	8
	23		
1	03·8^{3}	25 26^{6}	13
2	07·1^{4}	28 20^{6}	7
3	10·9^{4}	21 57^{6}	8
4	17·1^{3}	27 38^{6}	23
5	17·5^{3}	22 13^{6}	13
6	18·1^{3}	24 25^{5}	12†
7	22·9^{3}	23 20^{6}	12
8	26·4^{3}	21 25^{5}	20
9	27·5^{4}	25 22^{6}	*27* (16)
10	42·5^{3}	24 10^{5}	10
11	45·8^{3}	28 20^{6}	15
12	46·7^{3}	26 25^{7}	6
13	47·9^{3}	25 16^{4}	16
14	49·8^{3}	23 19^{6}	7
15	51·9^{3}	22 25^{6}	7
16	55·4^{4}	21 30^{7}	11

(31) $\leqslant 20''$.

(32) $> 50''$.

TABLE 2

SOURCES BETWEEN DECLINATIONS —30° AND —40°

Sources which may be " extended ", that is, resolvable, are indicated by a dagger. A colon has been placed beside uncertain flux densities. Angular sizes, where available, are indicated in the footnotes. Details in Section II

Ref. No.	Position (1950) R.A. h m	Position (1950) Dec. S. ° ′	Flux Density (10^{-26} W m^{-2} (c/s)$^{-1}$)
	00		
1	00·2³	31 13⁶	17
2	02·7⁴	36 50⁸	8
3	06·9³	32 21⁸	14†
4	09·8⁴	33 16⁷	12
5	12·9³	38 27⁶	19
6	14·1³	31 28⁴	17
7	14·5³	36 41⁶	7
8	23·1³	33 07⁷	20
9	25·3⁴	39 21⁶	8
10	32·9⁵	33 41⁷	9†
11	33·7³	37 47⁶	9
12	34·3³	30 41⁷	9
13	36·2²	39 24⁵	30[1]
14	37·1³	33 06⁷	11
15	41·9²	35 38⁴	13
16	51·6³	36 38⁵	15
17	53·5⁵	38 03⁵	12[2]†
	01		
1	00·6³	31 36⁶	12
2	03·3³	38 25⁵	9
3	07·2³	37 02⁶	8
4	07·3³	39 20⁶	10
5	07·9³	35 01⁵	*30* (15)[3]
6	12·2⁴	32 30⁷	17[4]
7	12·7⁵	31 21⁸	10[4]
8	19·9³	37 49⁵	19
9	24·7³	36 41⁷	10
	01		
10	30·4³	38 31⁶	10
11	31·6²	36 44³	56†[5]
12	41·2³	39 48⁵	15[6]
13	44·3³	37 31⁷	9
14	54·2³	36 23⁵	16
15	57·9³	31 10⁴	26[7]
	02		
1	04·5³	37 52⁸	10
2	10·0⁴	34 31⁵	13
3	16·0²	36 45⁵	29†[8]
4	18·8³	38 21⁶	19
5	24·5³	30 51⁵	14
6	25·0³	34 05⁶	9
7	38·5⁴	31 13⁶	8
8	45·3³	35 34⁷	10
9	59·5³	34 36⁶	13†
	03		
1	20·6²	37 23³	*950* (825)[9]
2	32·6⁴	39 09⁶	10
3	36·2²	35 35⁵	23[10]
4	36·7³	32 01⁴	14
5	42·8⁴	31 16⁷	11
6	44·9²	34 35⁴	33[11]
7	45·7⁴	35 18⁷	8
8	55·1³	30 21⁵	12
9	57·1⁴	37 02⁵	14

[1] 15″.
[2] NGC 300.
[3] Perhaps several sources.
[4] Sources 01–36, 01–37 perhaps form one extended source.
[5] >45″.
[6] A doubtful source.
[7] <15″.
[8] ⩾40″.
[9] Fornax A ; IAU 03S3A. NGC 1316 (NGC 1317).
[10] NGC 1399 (NGC 1404).
[11] >45″.

TABLE 2 (*Continued*)

Ref. No.	Position (1950) R.A. h m	Position (1950) Dec. S. ° ′	Flux Density (10^{-26} W m^{-2} (c/s)$^{-1}$)	Ref. No.	Position (1950) R.A. h m	Position (1950) Dec. S. ° ′	Flux Density (10^{-26} W m^{-2} (c/s)$^{-1}$)
	04				06		
1	05·3[3]	32 06[7]	11	*1*	01·1[2]	34 27[4]	22
2	06·3[3]	31 11[6]	12†	*2*	02·2[3]	32 20[8]	17†
3	10·6[2]	34 33[4]	16	*3*	02·4[3]	35 24[8]	9
4	19·8[5]	31 01[8]	6	*4*	07·8[4]	30 46[7]	8
5	20·5[2]	33 26[6]	12†	*5*	14·3[4]	39 32[7]	8
6	27·1[2]	36 38[4]	35[(12)]	*6*	14·3[4]	35 06[8]	7
7	31·1[3]	39 57[6]	14	*7*	17·9[2]	37 11[5]	18
8	37·8[3]	31 09[6]	10	*8*	25·5[2]	35 26[4]	26
9	38·5[4]	36 11[6]	8	*9*	30·7[4]	36 38[6]	13†
10	41·3[4]	34 45[8]	6	*10*	31·1[4]	39 16[6]	8
11	43·8[2]	33 00[6]	8	*11*	40·7[3]	36 05[8]	7
12	45·0[5]	39 12[6]	18	*12*	46·7[2]	39 56[4]	26
13	46·4[3]	35 53[6]	10	*13*	50·2[3]	34 19[6]	9
14	54·5[2]	30 16[5]	*78* (43)[(13)]	*14*	50·2[3]	32 40[8]	9
15	55·4[3]	31 58[7]	9	*15*	58·8[4]	34 34[8]	5
	05				07		
1	03·8[4]	38 55[7]	8	*1*	00·0[3]	31 33[7]	14†
2	04·6[4]	37 51[7]	13	*2*	00·9[4]	33 34[10]	11
3	04·6[4]	32 21[8]	6[(14)]	*3*	06·0[4]	39 58[6]	12
4	04·9[2]	37 01[6]	7[(6)]	*4*	07·6[3]	35 53[6]	15
5	11·5[2]	30 34[5]	29	*5*	15·3[3]	36 27[5]	18†
6	21·4[3]	36 24[6]	66:[(15)]	*6*	17·2[4]	31 40[8]	9
7	22·9[3]	32 48[6]	18	*7*	18·9[2]	34 15[7]	18[(17)]
8	24·9[3]	30 55[7]	8	*8*	19·0[3]	35 01[8]	9[(17)]
9	34·2[3]	37 23[7]	9	*9*	25·8[3]	35 40[7]	9
10	38·1[3]	33 40[10]	*30* (16)[(16)]	*10*	27·6[3]	30 10[8]	8
11	41·9[3]	38 42[8]	8	*11*	29·7[4]	32 03[7]	14
12	45·8[4]	30 01[8]	7	*12*	35·8[3]	37 59[5]	21[(18)]
13	46·3[3]	33 04[6]	14[(16)]	*13*	36·0[3]	30 21[6]	19
14	50·0[3]	35 06[6]	13	*14*	37·9[3]	36 20[7]	11†
15	52·0[4]	36 31[7]	10[(6)]	*15*	49·4[4]	38 45[8]	*24* (13)
16	54·3[3]	32 14[7]	14	*16*	50·3[4]	35 06[8]	8†
17	58·2[5]	31 01[8]	9	*17*	51·8[3]	31 06[8]	9[(19)]
18	59·3[2]	38 40[7]	16	*18*	53·8[4]	35 40[8]	7
19	59·8[2]	39 49[5]	20	*19*	55·0[4]	30 21[8]	15[(19)]

[(12)] $\leqslant 10''$.

[(13)] Perhaps two sources.

[(14)] (NGC 1800).

[(15)] $20''$.

[(16)] Sources 05–*310*, 05–*313* perhaps form one extended source.

[(17)] Sources 07–*37*, 07–*38* perhaps form one extended source.

[(18)] Perhaps extended or superimposed on galactic emission feature.

[(19)] Sources 07–*317*, 07–*319* perhaps form one extended source.

TABLE 2 (*Continued*)

Ref. No.	Position (1950) R.A. h m	Position (1950) Dec. S. ° ′	Flux Density (10^{-26} W m^{-2} (c/s)$^{-1}$)
	08		
1	07·6[2]	38 50[5]	*38* (19)
2	25·5[4]	31 42[7]	19[(20)]
3	27·2[3]	30 31[4]	20
4	28·5[5]	32 51[7]	*30* (20)[(21)]
5	32·3[2]	34 21[6]	10
6	40·8[3]	39 42[8]	17
7	43·0[3]	30 39[6]	12[(22)]
8	43·0[3]	33 39[6]	17
9	45·4[4]	35 43[7]	8†
10	48·1[3]	34 38[6]	9†
11	50·5[3]	33 40[7]	11
12	51·8[4]	31 50[8]	9
13	59·8[4]	34 30[8]	6
	09		
1	01·9[3]	36 48[7]	15
2	02·6[3]	38 34[6]	25†
3	21·0[6]	32 11[7]	9:
4	21·1[2]	39 56[5]	9
5	34·7[4]	32 25[8]	14
6	38·8[3]	39 16[6]	8
7	41·5[3]	30 25[7]	8
8	42·3[3]	35 40[7]	8
9	44·0[4]	33 00[6]	8
10	45·3[2]	36 51[6]	11
11	50·0[3]	38 35[10]	*25* (12)
12	51·4[3]	39 26[7]	17
	10		
1	02·2[3]	36 58[7]	9[(23)]
2	03·5[4]	32 30[8]	14
3	11·5[4]	31 45[8]	10
4	14·3[3]	30 08[6]	11
5	16·5[4]	31 31[7]	14
6	17·7[3]	32 48[6]	19†
7	29·3[2]	35 58[6]	*25* (15)
8	30·8[2]	34 09[6]	20
9	35·2[4]	39 50[7]	6
10	43·9[3]	38 00[6]	7
11	45·1[3]	35 54[5]	9
	10		
12	51·7[3]	34 03[6]	12†
13	52·3[3]	37 26[5]	*18* (12)
14	56·3[2]	35 52[5]	12
15	59·5[3]	31 00[7]	10
	11		
1	00·3[3]	32 10[8]	8
2	23·0[4]	37 00[8]	7
3	23·5[3]	35 12[6]	17
4	25·8[3]	32 18[6]	10†
5	27·1[2]	34 20[7]	11
6	35·1[4]	39 02[6]	11
7	35·5[4]	36 55[8]	8
8	36·0[3]	31 58[6]	28
9	43·4[4]	35 20[6]	9[(24)]
10	43·5[2]	31 41[6]	27
11	44·1[3]	33 14[6]	16
12	46·5[3]	37 58[7]	11
13	48·7[4]	35 40[8]	8[(24)]
14	50·8[2]	34 49[6]	10[(24)]
15	55·5[3]	31 30[6]	13
	12		
1	01·2[3]	35 37[6]	13†
2	05·4[3]	33 43[7]	17
3	18·4[3]	36 56[7]	14†
4	32·3[3]	33 28[7]	22†
5	40·2[3]	38 40[6]	11†
6	41·8[5]	36 00[10]	6
7	43·2[3]	35 00[10]	7
8	54·2[3]	30 09[5]	28
9	56·2[3]	33 14[6]	18
10	59·6[3]	36 54[6]	14
	13		
1	05·3[5]	30 03[7]	12
2	09·0[4]	36 51[7]	9
3	33·9[2]	33 42[5]	70[(25)]
4	46·9[4]	39 00[7]	22
5	59·1[4]	32 45[8]	8[(6)]

[(20)] Perhaps part of 08–*34*.

[(21)] Extended parallel to galactic plane.

[(22)] Perhaps one extended source with 08–*213*.

[(23)] Perhaps a background irregularity.

[(24)] Sources 11–*39*, 11–*313*, 11–*314* perhaps form one extended source.

[(25)] $>50'$, I4296.

TABLE 2 (*Continued*)

Ref. No.	Position (1950) R.A. h m	Position (1950) Dec. S. ° ′	Flux Density (10^{-26} W m^{-2} (c/s)$^{-1}$)
	14		
1	00·6^{3}	36 16^{6}	20
2	01·5^{3}	33 53^{4}	57$^{(26)}$
3	18·8^{3}	30 55^{7}	17
4	21·7^{3}	38 10^{7}	20
5	28·1^{3}	31 53^{5}	16
6	29·6^{3}	34 54^{6}	12$^{(6)}$
7	40·3^{3}	30 28^{6}	14†
8	51·3^{2}	36 22^{4}	41
9	51·4^{3}	34 10^{7}	19
	15		
1	04·2^{3}	39 22^{6}	14
2	07·4^{3}	30 30^{7}	9$^{(6)}$
3	17·6^{3}	39 36^{6}	10
4	22·4^{3}	37 20^{7}	14
5	30·8^{3}	31 21^{6}	12$^{(23)}$
6	40·9^{3}	38 37^{6}	21:$^{(23)}$
7	53·8^{4}	35 56^{7}	10
	16		
1	04·9^{4}	32 46^{7}	19$^{(6)}$
2	10·9^{3}	39 24^{6}	*56* (28)$^{(6)}$
3	17·5^{3}	36 40^{8}	13
4	20·0^{3}	34 30^{8}	13
5	22·4^{3}	32 05^{6}	24
6	22·5^{3}	30 36^{7}	29†
7	26·6^{5}	35 09^{7}	11
8	57·8^{3}	33 57^{8}	19
	17		
1	02·1^{3}	31 54^{6}	32
2	06·6^{4}	37 10^{5}	100†
3	11·1^{2}	38 23^{4}	*500* (300)
4	19·8^{3}	35 40^{5}	75$^{(27)}$
5	21·8^{5}	38 14^{7}	75†
6	26·2^{3}	34 45^{5}	60
7	26·7^{2}	34 02^{4}	120
8	28·3^{2}	32 43^{5}	95
9	36·6^{2}	30 50^{5}	165
10	39·9^{3}	36 01^{6}	31†
	18		
1	03·7^{3}	36 20^{6}	9
2	06·9^{3}	39 52^{5}	9
3	17·8^{3}	39 11^{5}	41$^{(28)}$
4	26·1^{3}	38 11^{5}	18
5	35·2^{3}	31 51^{7}	19
6	37·7^{3}	36 17^{6}	12$^{(29)}$
7	48·6^{3}	33 26^{5}	15
8	49·4^{3}	34 41^{4}	17$^{(6)}$
9	58·6^{4}	38 24^{6}	12
	19		
1	12·8^{3}	37 03^{7}	18
2	16·9^{3}	35 44^{6}	16
3	27·0^{3}	36 06^{5}	16
4	37·1^{3}	36 11^{5}	13
5	56·4^{3}	35 49^{4}	45$^{(30)}$
	20		
1	04·5^{4}	39 00^{8}	17†$^{(31)}$
2	13·5^{3}	36 05^{7}	17
3	13·9^{4}	31 44^{6}	10
4	14·0^{3}	31 00^{7}	15†
5	24·4^{4}	32 01^{5}	18
6	29·8^{3}	37 40^{6}	7
7	32·3^{2}	35 04^{5}	41$^{(32)}$
8	48·0^{3}	37 07^{6}	19†
9	56·2^{3}	33 00^{7}	9

(26) $>45''$ (NGC 5419).
(27) $>45''$.
(28) $<20''$.
(29) Superimposed on background irregularity.
(30) Flux measurement uncertain due to Cygnus A side lobe $\sim 20''$.
(31) A doubtful source, perhaps extended or a background irregularity.
(32) $<10''$.

TABLE 2 (*Continued*)

Ref. No.	Position (1950) R.A. h m	Position (1950) Dec. S. ° ′	Flux Density (10^{-26} W m^{-2} (c/s)$^{-1}$)
	21		
1	00·3[3]	39 37[7]	12
2	07·9[3]	34 04[7]	14
3	10·4[4]	35 10[8]	8
4	14·6[3]	30 36[6]	15
5	16·0[4]	33 35[7]	8
6	28·1[3]	31 22[5]	13
7	45·5[3]	30 23[6]	14
8	57·3[4]	38 04[6]	11[(6)]
	22		
1	15·1[4]	30 45[7]	8
2	24·8[3]	30 46[5]	10
3	43·4[3]	30 42[5]	12
4	48·4[3]	33 21[6]	9
5	59·0[2]	37 33[5]	21
	23		
1	10·8[3]	32 26[7]	13
2	13·3[3]	34 31[7]	9
3	34·2[3]	32 56[6]	16
4	34·3[4]	34 58[6]	24
5	34·3[3]	37 38[6]	7[(6)]
6	48·0[3]	38 39[6]	11
7	54·6[2]	34 59[4]	39[(33)]
8	59·9[3]	36 08[5]	18

[(33)] $>40''$.

TABLE 3

SOURCES BETWEEN DECLINATIONS —40° AND —50°

Sources which may be " extended ", that is, resolvable, are indicated by a dagger. A colon has been placed beside uncertain flux densities. Angular sizes, where available, are indicated in the footnotes. Details in Section II

Ref. No.	Position (1950) R.A. h m	Position (1950) Dec. S. ° ′	Flux Density (10^{-26} W m^{-2} (c/s)$^{-1}$)
	00		
1	01·6^{3}	48 23^{6}	10
2	03·8^{3}	42 50^{6}	17
3	08·2^{2}	44 40^{4}	*60* (31)[1]
4	17·2^{3}	41 19^{5}	13
5	17·8^{3}	49 27^{6}	9
6	19·1^{3}	47 17^{5}	13
7	32·7^{4}	45 33^{6}	9
8	34·2^{3}	49 12^{6}	8
9	36·6^{4}	41 16^{7}	7[2]
10	39·8^{2}	44 37^{4}	35[3]
11	43·7^{2}	42 25^{4}	52[4]
12	44·0^{4}	49 57^{6}	6
13	48·8^{4}	44 46^{7}	16
14	50·1^{4}	43 23^{5}	23
15	52·9^{3}	49 27^{6}	9
	01		
1	03·2^{2}	45 22^{5}	41[5]
2	03·6^{3}	41 29^{4}	*25* (17)
3	07·4^{4}	48 12^{8}	5
4	12·9^{4}	44 46^{8}	8
5	14·0^{3}	47 34^{5}	34[6]
6	15·7^{3}	41 06^{6}	8[2]
7	24·3^{4}	43 25^{7}	8
8	25·2^{2}	41 17^{6}	33†
9	31·4^{3}	44 56^{8}	18
10	39·5^{3}	44 40^{7}	9
11	39·8^{4}	45 51^{8}	10
12	40·5^{4}	43 58^{7}	14
13	52·3^{3}	43 46^{6}	10

Ref. No.	Position (1950) R.A. h m	Position (1950) Dec. S. ° ′	Flux Density (10^{-26} W m^{-2} (c/s)$^{-1}$)
	02		
1	01·9^{3}	44 02^{5}	9
2	07·2^{4}	42 00^{5}	16
3	14·0^{3}	48 03^{5}	*65* (31)[7]
4	19·7^{2}	45 33^{5}	11†
5	22·6^{3}	42 03^{7}	17
6	24·2^{4}	43 15^{8}	7
7	27·4^{3}	40 14^{7}	*24* (14)[8]
8	30·5^{2}	41 22^{5}	7
9	34·6^{3}	43 49^{6}	8
10	40·2^{3}	42 03^{7}	12
11	43·5^{3}	45 07^{5}	10
12	55·0^{3}	44 05^{7}	7
13	55·3^{4}	48 49^{5}	16†
	03		
1	03·5^{2}	46 42^{7}	8
2	15·6^{3}	44 00^{6}	10
3	18·8^{3}	45 20^{7}	19[9]
4	35·5^{3}	41 28^{5}	14
5	38·4^{3}	40 37^{6}	10[2]
6	38·5^{3}	47 46^{5}	13
7	42·0^{2}	44 20^{6}	11
8	43·6^{4}	45 46^{7}	9
9	51·2^{3}	41 23^{5}	9
10	53·0^{3}	43 04^{8}	8
11	54·1^{3}	48 24^{4}	14

[1] Perhaps two sources.
[2] A doubtful source.
[3] $<15''$.
[4] $>40''$.
[5] $23''$.
[6] $>40''$.
[7] $>40''$.
[8] Perhaps several sources.
[9] Measurement subject to side-lobe influence of IAU 03S3A.

TABLE 3 (*Continued*)

Ref. No.	Position (1950) R.A. h m	Position (1950) Dec. S. ° ′	Flux Density (10^{-26} W m^{-2} (c/s)$^{-1}$)
	04		
1	08·2^{4}	47 06^{8}	9[10]
2	13·9^{3}	42 44^{6}	17
3	18·1^{3}	40 08^{6}	11
4	18·2^{3}	41 35^{8}	11
5	25·1^{3}	49 06^{6}	8
6	34·2^{3}	49 50^{7}	12
7	36·5^{3}	47 36^{6}	13
8	37·8^{3}	45 00^{6}	9
9	38·2^{3}	43 31^{5}	12
10	55·4^{3}	40 30^{5}	13
11	55·6^{3}	43 06^{6}	12
12	55·6^{3}	46 20^{7}	9[2]
	05		
1	02·0^{5}	41 50^{7}	7
2	11·9^{4}	48 32^{5}	41[11]
3	18·3^{1}	45 48^{3}	570[12]
4	25·8^{3}	40 56^{7}	14
5	31·5^{3}	45 40^{8}	19[2]
6	34·8^{3}	49 46^{6}	16
7	45·2^{3}	48 17^{5}	15
8	46·2^{3}	44 35^{6}	13
9	46·2^{4}	45 57^{6}	17
10	47·8^{2}	40 52^{4}	31†[13]
11	47·8^{4}	42 03^{8}	7
	06		
1	06·1^{3}	49 38^{7}	15†
2	07·3^{4}	42 27^{8}	9
3	12·2^{3}	47 18^{6}	27
4	16·6^{3}	48 44^{5}	9
5	19·8^{3}	45 07^{6}	12
6	20·1^{4}	47 00^{7}	7
7	27·5^{3}	41 58^{5}	12[2]
8	29·7^{3}	43 49^{7}	9
9	34·2^{5}	41 15^{8}	7
10	37·0^{5}	49 27^{8}	8
11	40·8^{4}	46 06^{8}	7[2]
12	43·0^{3}	43 55^{8}	13
13	35·0^{4}	41 53^{8}	7
	07		
1	00·1^{3}	47 30^{7}	18
2	02·5^{3}	45 22^{5}	25
3	04·3^{3}	42 46^{6}	19
4	05·3^{4}	41 08^{5}	10
5	08·8^{5}	48 26^{7}	8[2]
6	10·6^{4}	46 22^{8}	8
7	28·1^{4}	48 09^{6}	8
8	29·8^{4}	46 45^{6}	9
9	33·7^{4}	44 07^{7}	11†
10	35·0^{3}	48 56^{7}	12
11	47·3^{3}	40 36^{5}	12
12	48·1^{3}	44 00^{7}	27[14]
13	48·1^{4}	45 36^{7}	12
14	51·2^{4}	43 04^{7}	18[14]
	08		
1	09·4^{3}	49 38^{7}	27
2	09·8^{3}	43 05^{7}	10
3	16·1^{3}	47 07^{7}	10[2]
4	20·9^{3}	42 52^{4}	*690* (514)[15]
5	33·7^{2}	45 38^{5}	*1100* (276)[16]
6	54·9^{4}	41 25^{7}	10†
7	57·6^{2}	47 25^{7}	26†
8	59·3^{3}	43 26^{6}	17

[10] Perhaps extended or several sources.
[11] $\leqslant 20''$.
[12] Pictor A; IAU 05S4A 55″.
[13] $> 30''$.
[14] Sources 07–*412*, 07–*414* perhaps form one extended source.
[15] Puppis A; IAU 08S4A.
[16] $> 55''$.

TABLE 3 (*Continued*)

Ref. No.	Position (1950) R.A. h m	Position (1950) Dec. S. ° ′	Flux Density (10^{-26} W m^{-2} (c/s)$^{-1}$)
	09		
1	06·9^{4}	46 37^{8}	7
2	09·7^{3}	45 07^{6}	11
3	12·6^{3}	43 34^{7}	8†[2]
4	27·0^{4}	46 42^{8}	8
5	27·8^{5}	45 14^{7}	7
6	43·2^{4}	49 53^{7}	9
7	46·4^{3}	41 22^{7}	12†
8	49·3^{5}	46 50^{8}	*15*[8]
9	51·8^{4}	45 16^{7}	15
10	51·9^{3}	43 27^{6}	12
	10		
1	02·9^{4}	49 44^{6}	9†
2	03·3^{3}	46 27^{5}	8
3	14·9^{4}	44 25^{7}	9
4	17·9^{3}	42 26^{3}	51[17]
5	19·1^{4}	45 48^{7}	10
6	19·2^{4}	49 22^{7}	10
7	24·7^{4}	40 57^{5}	13
8	25·8^{4}	47 52^{8}	8
9	26·4^{3}	45 00^{7}	8
10	32·2^{5}	41 17^{8}	12†
11	39·3^{4}	46 05^{6}	13
12	46·4^{4}	49 15^{7}	8
13	52·2^{4}	40 00^{7}	6
	11		
1	04·4^{3}	41 56^{6}	9
2	06·7^{3}	48 23^{7}	11
3	16·1^{3}	43 24^{7}	13
4	23·0^{4}	48 13^{6}	*53* (19)
5	33·9^{3}	43 15^{7}	14
6	43·3^{3}	48 20^{6}	28
7	49·1^{3}	44 56^{7}	21[2]
8	55·5^{3}	42 16^{7}	13
	12		
1	10·7^{4}	41 43^{7}	18
2	11·5^{3}	44 56^{6}	8
3	16·2^{4}	46 01^{7}	19†
4	33·7^{4}	41 25^{7}	11
5	46·8^{3}	40 56^{5}	45[18]
6	51·9^{2}	47 43^{5}	14:†
7	55·7^{3}	41 33^{8}	16
	13		
1	02·6^{5}	49 07^{7}	20[19]
2	22·4^{3}	42 41^{4}	*8700* (2170)[20]
3	38·3^{3}	40 32^{7}	9
4	47·1^{4}	45 36^{7}	*100* (32)[21]
5	56·0^{2}	41 38^{4}	35:
	14		
1	08·9^{3}	41 33^{6}	14
2	12·6^{3}	43 23^{6}	38†[2]
3	14·4^{4}	47 23^{7}	14
4	17·6^{4}	49 44^{7}	16†
5	25·2^{3}	43 07^{5}	*90*: (30)[22]
6	25·7^{3}	47 48^{6}	29
7	32·9^{4}	45 05^{6}	10
8	42·4^{3}	42 13^{8}	15
9	45·0^{3}	46 57^{5}	33
10	45·1^{4}	48 09^{6}	10
11	47·0^{3}	40 18^{6}	14
12	50·0^{3}	41 00^{7}	9
13	51·3^{3}	42 17^{6}	19[2]
14	57·5^{2}	48 04^{6}	17†
15	59·9^{2}	41 42^{5}	55:
	15		
1	04·4^{3}	42 54^{7}	14†
2	07·6^{4}	43 56^{8}	14
3	27·4^{2}	42 21^{5}	100
4	32·4^{5}	49 44^{8}	21†
5	38·7^{3}	40 42^{7}	18
6	41·2^{3}	48 04^{7}	*47* (25)
7	45·9^{4}	45 04^{6}	24[2]
8	55·3^{3}	46 12^{7}	50†[23]

[17] ∼30″ IAU 10S4A.
[18] <15″ (NGC 4696).
[19] NGC 4945.
[20] Centaurus A; IAU 13S4A. NGC 5128.
[21] Possibly a galactic feature.
[22] Perhaps several sources, the interpretation is doubtful.
[23] >30″.

TABLE 3 (*Continued*)

Ref. No.	Position (1950) R.A. h m	Position (1950) Dec. S. ° ′	Flux Density (10^{-26} W m^{-2} (c/s)$^{-1}$)
	16		
1	03·0^{3}	44 25^{8}	19[2]
2	17·4^{4}	45 51^{7}	26:[24]
3	19·9^{4}	49 28^{7}	76[25]
4	24·9^{4}	48 40^{7}	64
5	25·1^{4}	42 10^{8}	30†
6	33·2^{3}	40 32^{7}	25[2]
7	36·3^{3}	46 31^{4}	330[26]
8	51·1^{3}	44 00^{6}	55†
9	52·1^{4}	42 25^{6}	32
10	57·6^{5}	46 22^{8}	30:
11	59·0^{4}	41 18^{5}	*90* (70)
	17		
1	03·8^{3}	44 24^{6}	25
2	10·4^{3}	45 36^{7}	35
3	14·4^{3}	44 00^{7}	18†
4	14·8^{3}	48 20^{7}	25
5	16·6^{3}	49 33^{7}	29
6	17·1^{4}	46 47^{8}	18
7	31·3^{3}	48 31^{8}	12†
8	54·4^{3}	41 33^{7}	30†
	18		
1	04·6^{5}	45 28^{6}	*77* (45)
2	12·8^{5}	48 20^{7}	16:
3	39·8^{2}	48 36^{5}	41[27]
4	40·9^{3}	40 27^{7}	22
5	43·9^{3}	49 49^{7}	12
6	44·6^{5}	43 06^{7}	8
7	53·2^{4}	43 00^{8}	7
8	59·6^{3}	41 25^{5}	13
	19		
1	12·0^{3}	46 28^{6}	11
2	13·9^{3}	45 39^{5}	13
3	21·7^{3}	43 01^{6}	17
4	25·2^{3}	41 23^{7}	17
5	31·8^{3}	49 53^{5}	9
6	32·6^{2}	46 25^{3}	141[28]
7	32·9^{3}	48 31^{7}	8
8	35·4^{3}	42 34^{7}	8
9	36·7^{4}	48 01^{6}	7
10	40·4^{3}	40 41^{6}	38†[29]
11	45·6^{3}	47 08^{5}	11
12	51·7^{3}	49 59^{6}	14
13	53·0^{3}	42 38^{5}	31†
	20		
1	03·5^{3}	47 40^{6}	9
2	05·8^{3}	42 37^{6}	15†
3	17·6^{5}	42 23^{8}	9
4	20·5^{4}	49 53^{7}	8
5	27·3^{3}	41 30^{6}	22
6	28·9^{3}	45 23^{4}	10
7	37·3^{3}	47 52^{6}	11
8	43·9^{4}	43 37^{6}	16
9	47·0^{5}	44 48^{5}	13
10	51·4^{3}	48 22^{6}	12
	21		
1	09·4^{4}	43 12^{6}	15
2	10·2^{4}	45 26^{6}	7
3	16·9^{4}	47 50^{6}	7
4	22·3^{4}	44 56^{7}	7
5	27·7^{3}	48 25^{6}	10
6	37·1^{5}	44 26^{4}	10
7	40·3^{2}	43 21^{4}	37[30]
8	50·5^{3}	46 39^{6}	14

[24] Possibly a background irregularity.
[25] $>45''$.
[26] $>45''$.
[27] $>30''$.
[28] $18''$.
[29] $>30''$.
[30] $>40''$.

TABLE 3 (*Continued*)

Ref. No.	Position (1950) R.A. h m	Position (1950) Dec. S. ° ′	Flux Density (10^{-26} W m^{-2} (c/s)$^{-1}$)	Ref. No.	Position (1950) R.A. h m	Position (1950) Dec. S. ° ′	Flux Density (10^{-26} W m^{-2} (c/s)$^{-1}$)
	22				23		
1	06·8^{4}	49 57^{6}	8	*1*	07·8^{3}	48 42^{7}	11:
2	06·8^{3}	43 59^{6}	13	*2*	10·3^{3}	44 43^{7}	10
3	25·3^{3}	40 56^{5}	28	*3*	24·2^{3}	40 34^{5}	15
4	35·0^{5}	43 44^{8}	6	*4*	31·9^{2}	41 42^{4}	50[32]
5	44·1^{4}	44 26^{7}	6:	*5*	39·0^{3}	44 50^{7}	6
6	50·1^{3}	41 10^{5}	42[31]	*6*	42·9^{3}	47 25^{8}	9
7	56·8^{3}	41 09^{6}	14	*7*	49·7^{5}	43 24^{8}	8
8	57·0^{3}	46 09^{5}	10	*8*	51·7^{3}	45 26^{7}	7[24]

[31] 30″.
[32] 26″.

although we had available a number of " non-scanning " records of high sensitivity not available to Rishbeth. His catalogue is valuable in that it is based on the contour diagram, gives information about the shapes of some extended sources, and includes several large concentrations not included in our cataloguing scheme. There are, however, often large discordances in the flux densities of weaker sources.

III. IDENTIFICATIONS

A search for identifications with bright optical objects has been carried out as in papers I and II; the atlas of Becvar (1951) has again been used in this search. Some of the area, north of declination −33°, is included in the National Geographic Society-Palomar Observatory Sky Atlas. The previous catalogue and a small portion of the present one has been compared with this Atlas in a systematic way (Mills 1960) and no doubt a similar comparison of the remaining common area will prove interesting, but it is outside the scope of the present paper.

In contrast to the earlier work, no H II regions can be unambiguously identified in the present catalogue; this arises partly as a result of their uneven distribution and partly because the zone of the catalogue crosses the galactic plane, in one of the two places, close to the galactic centre. Here the background temperature is of the same order or higher than the electron temperatures in the nebulae so that, if they are observed at all, they appear as " holes " in the background emission: some of these are listed elsewhere (Mills 1959). Coincidences with planetary nebulae and globular clusters are again not significant: there is a moderately close coincidence between the radio source 17−*21* and the globular cluster NGC 6284, but this would be expected by chance. Two other identifications with galactic objects are well known. These are Kepler's supernova, identified with 17−*211* (Mills, Little, and Sheridan 1956), and

08—44 (Puppis A) identified by Baade and Minkowski (1954) with a galactic nebulosity of a peculiar filamentary type.

There are numerous possible identifications with bright galaxies in the catalogue. Those listed include all coincidences within 1^m in Right Ascension and 20′ in declination ; there are 14 such coincidences and the chance expectation, based on the numbers of catalogued galaxies and radio sources in the area, is about 6. To reduce effects of chance we restrict attention to these coincidences within $0^m \cdot 7$ in Right Ascension and 13′ in declination, as in paper II (these numbers represent approximately twice the mean probable error in each coordinate). There are 10 such coincidences with 3 expected by chance, but since 5 of these were previously known the new information is not great. They are listed in Table 4.

TABLE 4

POSSIBLE IDENTIFICATIONS WITH BRIGHT GALAXIES

Radio Source	Galaxy		$m_{1\cdot 9}-m_p$	Notes
	NGC	Type		
00—*221*	253	Sc	1·2	
03—*31*	1316	Sa_p	—4·6	Fornax A
03—*31*	1317	SBb	—6·6	Probably a chance coincidence
03—*33*	1399	Eo	—1·6	
06—*25*	2217	SBb	—0·5	
12—*46*	4696	E1	—3·1	The angular size of the radio source is small. Probably a chance coincidence
13—*41*	4945	SBc	1·3	
13—*42*	5128	Ep	—3·9	Centaurus A, a well-known identification
13—*33*	I4296	E	—4·1	The radio size supports the identification
13—*25*	5236	Sc	0·9	

Of the previously known systems we have three " normal " galaxies NGC 253, NGC 4945, and NGC 5236, and two " radio " galaxies NGC 1316 and NGC 5128. Two of the coincidences can almost certainly be ascribed to chance, NGC 1317 and NGC 4696. In the former, the radio source is, by virtue of its position and size, almost certainly associated with the neighbouring galaxy NGC 1316 ; it would be a remarkable coincidence if NGC 1317 also were contributing to the radio emission. In the case of NGC 4696, which has been noted also by Basinki, Bok, and Gottlieb (1959), the angular size, $<15''$ arc, appears too small. There are numerous fainter galaxies in the vicinity ; but it appears most likely that the radio source is considerably more distant than any of those visible on the plate of Basinki, Bok, and Gottlieb. The galaxies NGC 1316 and NGC 5128 have been discussed extensively in the literature and will not be considered further in this paper (for the most recent results see Sheridan (1958) and Wade (1959)).

It is interesting to see whether the above coincidences might be expected assuming a radio " luminosity function " of the form suggested by Mills (1960). In this, the probability of a galaxy, chosen at random, having a ratio of

radio to optical emission, defined by $m_{1\cdot9}-m_p$, between $\underline{m}-\frac{1}{2}$ and $\underline{m}+\frac{1}{2}$ (where $\underline{m}=m_{1\cdot9}-m_p$) is given by

$$\log P=1\cdot0-0\cdot42\underline{m}.$$

Applying this result to the galaxies listed in the catalogue we have used, we would expect 6 galaxies with $m_{1\cdot9}-m_p\leqslant-2$ and 1 galaxy with $m_{1\cdot9}-m_p\leqslant-4$. In fact there are 5 coincidences in the former category and 3 in the latter, a satisfactory but not particularly significant agreement.

Two galaxies, NGC 300 and NGC 55, which are within the catalogue area, had previously been listed as probably observed (Mills 1955) but are not in Table 4. The former is listed in the footnotes to Table 2 as a possible coincidence with the source 00−3*17*, that is, it is within 1^m in Right Ascension and 20′ in declination. However, the identification is not certain because of a complex brightness distribution in the region; this difficulty was noted previously. The radio source associated with the latter galaxy is too faint for detection by the methods used in preparing the catalogue and is not included; originally it was necessary to average several records to observe it.

Finally, one should mention the two possible identifications found in the previously mentioned comparison of part of the catalogue area with the Palomar Sky Atlas. These are the sources 17−*23* and 21−*21*; they are discussed elsewhere (Mills 1960).

IV. Statistics

The question of the distribution of the radio sources has been discussed at some length in papers I and II. The present results do not alter substantially any of the earlier conclusions, so that a very brief discussion should be adequate at this stage. More useful statistical investigations may be carried out when the angular size data are complete.

Previously we had divided the analysis into two parts, the first concerned with the two-dimensional distribution over the celestial sphere in an investigation of possible clustering effects, the second with the distribution in depth of the sources. These are not independent, but the division is convenient and will be adhered to here.

(*a*) *Clustering*

Earlier analysis had provided some slight, but not conclusive, indications of large-scale clustering of the radio sources. However, addition of the present data weakens the case and, on confining attention to regions of the order of 10° to 30° across, no convincing evidence exists that the distribution is non-random.

However, in the present catalogue a curious distribution arises, namely, the density of radio sources over the last few hours of the catalogue is very much less than over the first few. For example, the number of sources between 00^h and 02^h is 103 and between 22^h and 00^h only 56. The probability of this difference arising by chance in a random distribution is less than 0·001. Since the catalogue was prepared in a number of stages each commencing at 00^h and working through to 24^h, it seems possible that the result is an artefact. However,

the catalogue of paper II was prepared in essentially the same manner and shows no such effect and, in addition, a careful re-examination of the original records supports the idea that the difference is real. The region of high source concentration includes the south galactic pole, but no reason is known why this should provide a surplus of radio sources.

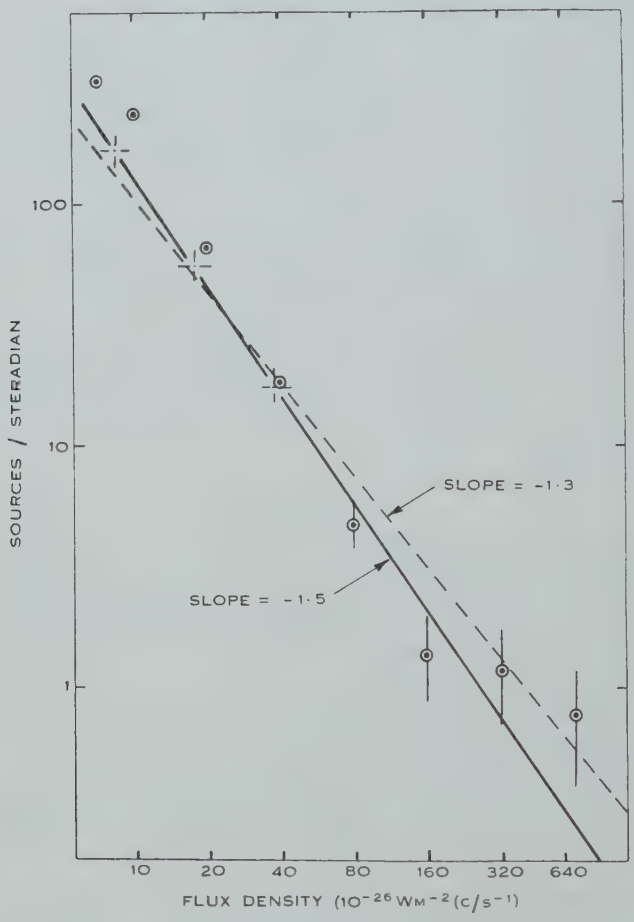

Fig. 1.—Counts of Class II radio sources.

In paper II the number of "extended" sources was compared with the number of blends of radio sources expected on the basis of a random distribution. It was concluded that there was a very significant difference, indicating that either the sources were extended regions of comparatively low brightness, or close blends of physically associated sources of small size. The present results support this conclusion although, surprisingly, the proportion of extended sources listed is much less than before. For example, between Right Ascensions of 09^h to 15^h and 21^h to 15^h (i.e. at high galactic latitudes) the numbers of extended sources with flux density greater than 40×10^{-26} W m^{-2} (c/s)$^{-1}$ is 9, and with

flux density $>20\times10^{-26}$ W m^{-2} (c/s)$^{-1}$ is 19 : the corresponding numbers expected on the basis of the previous catalogue are 16 and 29 respectively. Similarly, the number of sources with flux densities $>20\times10^{-26}$ W m^{-2} (c/s)$^{-1}$ listed as " perhaps extended " is now 7 compared with an expectation of 14 ; however, the availability of data from the angular size interferometer has helped to eliminate some doubtful examples. Since the chance blends above the same flux density limits may, from the data of paper I, be expected to be 2 and 11 respectively, the previous conclusion, that these are inadequate to explain the observations, is upheld.

(*b*) *Source Counts*

One of the most interesting questions arising from a study of the statistics of radio sources is their distribution in depth, which is investigated by means of counts of sources with fluxes above defined levels. Since there is a class of galactic source fairly closely confined to the plane it is usual to divide the analysis into two parts, dealing with the low latitude and high latitude sources separately. We will follow this procedure here, but, since the information about the galactic sources adds little or nothing to that presented in paper II and by Mills (1959), we will discuss only the high latitude or Class II sources (sources for which $|b|>12\frac{1}{2}°$).

In Figure 1 is shown the count resulting from a combination of the present catalogue and that in paper II. The actual numbers are listed in Table 5.

TABLE 5

THE NUMBERS OF CLASS II RADIO SOURCES ABOVE DEFINED FLUX DENSITIES

Flux density (10^{-26} Wm^{-2} (c/s)$^{-1}$) ..	7	10	20	40	80	160	320	640
Number of sources, N	1658	1220	332	94	24	7	6	4

The total area used in making these counts is nearly 5 steradians (2·72 steradians in paper II and 2·07 steradians in the present catalogue) and altogether there are 1658 sources with flux density $>7\times10^{-26}$ W m^{-2} (c/s)$^{-1}$ (the total number of Class II sources in the areas is 1700). Previously, the counts had been restricted at high intensities because of the fortuitous lack of such sources in the area of the catalogue ; now, however, it may be extended much further, the range of flux density being nearly 100 : 1. The standard error in each point in Figure 1 is indicated by vertical wings ; it is equal to $\sqrt{N}$, where N is the number of sources counted.

It has been shown in paper I that the counts need correction at low flux densities because of the effects of random noise and finite aerial resolution. Another effect was discovered when compiling the present catalogue, namely, a systematic tendency to over-estimate the flux density of a source when the signal-to-noise ratio is low. This appears quite distinct from the effects of noise previously considered ; it was detected by comparison of flux densities measured on " scanning " and " non-scanning " records. The former have a noise level

approximately double that of the latter and it was found that flux densities around 10×10^{-26} W m^{-2} (c/s)$^{-1}$ were, on the average, estimated higher on the scanning records by a factor of about 30 per cent. For sources of double the flux density the effect was still noticeable but much reduced. These differences appear to arise because a source position is always selected for which the noise fluctuations combine with the deflection due to the source to produce the greatest apparent flux density. This position is, in general, displaced from the true position, which, if known and adopted, would result in a lower estimate for the flux density. The effect of this type of error on the source counts is not large ; this is fortunate, since it is difficult to assess an accurate correction without re-examination of all the original records. The most likely correction for the combined counts is a reduction of 30 per cent. for sources having fluxes near 10×10^{-26} W m^{-2} (c/s)$^{-1}$, and 10 per cent. for sources having fluxes near 20×10^{-26} W m^{-2} (c/s)$^{-1}$. In Figure 1 the crosses mark the corrected points, using both the data of paper I and the above corrections.

A straight line of slope $-1\cdot5$ is shown, drawn to fit the points as closely as possible ; the fit is very good. Since this is the slope to be expected with a uniform distribution of source in a static Euclidean universe, the source counts indicate no divergence from uniformity and no obvious cosmological effects. It has been suggested by Mills (1960) that, among those sources which are associated with external galaxies, a source count having a mean slope of about $-1\cdot3$ might be expected, if account is taken of red-shift effects. A line of this slope is shown dotted ; although the agreement is not particularly good, it is not inconsistent in view of the uncertain corrections to be applied at low flux densities and the statistical uncertainties at higher fluxes. It is known, however, that not all the high latitude radio sources in the catalogues could belong to this class (unless there is physical clustering of such sources) because of the inclusion of apparently " extended " sources in the catalogue, as discussed earlier.

Finally, one should mention a slight difference in the counts if the two catalogues are analysed separately, the numbers in the present catalogue being systematically less at a given flux density. Part of the discrepancy at low flux densities may be due to the availability of more non-scanning records in the area of the present catalogue and consequently less systematic error in the weaker fluxes, whence, for a given number of sources, the flux density will be lower. The remainder may be the result of a small calibration difference ; this is likely, since the first catalogue includes zenith angles between 44° and 14°, the second includes zenith angles between 16° and 0°. A difference of 10 per cent. in the average calibrations in these areas would be adequate to explain the effect : this is about the accuracy of the calibrations, as discussed by Little (1958).

V. References

Baade, W., and Minkowski, R. L. (1954).—*Astrophys. J.* **119** : 215.

Basinki, Jane, Bok, B. J., and Gottlieb, K. (1959).—" Paris Symposium on Radio Astronomy." (Ed. R. N. Bracewell.) p. 514. (Stanford Univ. Press.)

Becvar, A. (1951).—" Atlas Coeli Skalnate Pleso." (Prirodovedecke Vydavatelstvi : Prague.)

Goddard, B. R., Watkinson, A., and Mills, B. Y. (1960).—*Aust. J. Phys.* **13** : 665.

LITTLE, A. G. (1958).—*Aust. J. Phys.* **11**: 70.
MILLS, B. Y. (1955).—*Aust. J. Phys.* **8**: 368.
MILLS, B. Y. (1959).—*Publ. Astr. Soc. Pacif.* **71**: 267.
MILLS, B. Y. (1960).—*Aust. J. Phys.* **13**: 550.
MILLS, B. Y., LITTLE, A. G., and SHERIDAN, K. V. (1956).—*Aust. J. Phys.* **9**: 84.
MILLS, B. Y., and SLEE, O. B. (1957).—*Aust. J. Phys.* **10**: 162.
MILLS, B. Y., SLEE, O. B., and HILL, E. R. (1958).—*Aust. J. Phys.* **11**: 360.
RISHBETH, H. (1958).—*Aust. J. Phys.* **11**: 550.
SHERIDAN, K. V. (1958).—*Aust. J. Phys.* **11**: 400.
WADE, C. M. (1959).—*Aust. J. Phys.* **12**: 471.

THE RADIO BRIGHTNESS OF THE QUIET SUN AT 21 CM WAVELENGTH NEAR SUNSPOT MAXIMUM

By N. R. Labrum*

[*Manuscript received June* 27, 1960]

Summary

An investigation has been made of the radio emission from the quiet Sun at 21·2 cm wavelength in 1958 (near sunspot maximum). Two different methods have been used, both involving observations with very high angular resolution, to distinguish between the quiet-Sun component and the radiation from localized active regions. In one method, the Sun was scanned with a narrow pencil-beam ; in the other, a fan-shaped aerial beam was used to give one-dimensional strip scans. In both cases it was necessary, when analysing the data, to take into account the residual effects of the very intense radiation from the localized sources. The two independent measurements gave results which agree within the limits of error. The apparent disk temperature was found to be approximately 140 000 °K, or twice the value for the same wavelength at sunspot minimum.

The fan-beam observations also provide some evidence on the distribution of quiet-Sun brightness with respect to heliographic latitude. There is limb darkening at the poles, and the distribution does not appear to have changed in shape between sunspot minimum (1953) and the time of the present series of observations.

I. Introduction

The Sun's radio emission at wavelengths of the order of 20 cm is made up of two main components. One of these varies slowly in intensity from day to day and originates in localized active regions in the solar atmosphere. These emitting regions may conveniently be termed " radio plages ", by analogy with the optical plage areas with which they are closely associated. The second component consists of thermal radiation from the undisturbed or " quiet " Sun, and remains at a constant level for periods of months or years. Radio measurements of the quiet Sun are of considerable importance, since they can provide information on temperatures and electron densities in layers of the solar atmosphere which are difficult to observe optically.

The existence of a quiet-Sun component is inferred from the fact that, at a particular wavelength, a constant base level can be recognized in the varying intensity of the solar radiation. For an experimental investigation of the quiet Sun, it is necessary to find a method of separating the fixed component from the slowly varying plage radiation. This may be done by statistical analysis of a large number of daily observations of the total power received from the whole Sun at a chosen wavelength. An alternative is to use an aerial system with sufficient angular resolution to distinguish the active regions on the solar disk from each other and from the quiet-Sun background. Pawsey and Yabsley (1949) used a statistical method. A series of daily values of the apparent disk

* Division of Radiophysics, C.S.I.R.O., University Grounds, Chippendale, N.S.W.

temperature (at 50 cm wavelength) was plotted against the corresponding projected sunspot areas. The distribution of the points on this diagram showed that the two quantities were closely correlated, and that the radiation consisted of a constant base level (quiet Sun) and a component proportional to sunspot area. The quiet-Sun temperature was estimated by drawing the line of best fit and extrapolating back to zero sunspot area.

Many quiet-Sun determinations of this kind have since been made. Taken over a period of years, they show that the temperature at a given wavelength appears to increase towards the time of sunspot maximum (Christiansen and Hindman 1951). The technique is, however, open to objections because of the underlying assumption of a linear relationship between sunspot area and radio emission. There is evidence that individual radio plages generally have a considerably longer life than the corresponding sunspot groups. The method therefore tends, especially at sunspot maximum, to ascribe to the quiet Sun some radiation from active regions which no longer contain visible sunspots.

Piddington and Davies (1953) and Dodson (1957) used alternative methods of analysis in attempts to overcome this difficulty. In each case it was found that, with the particular sets of data used, there was no clear indication of any change in quiet-Sun temperature over the sunspot cycle. On the other hand, Allen (1957) made a somewhat more elaborate analysis of the available observations and concluded that a real variation does occur. His results indicate that the greatest change (about 2 : 1 during the cycle) takes place at wavelengths near 25 cm. Christiansen, Warburton, and Davies (1957) independently confirmed Allen's conclusions. In view of these conflicting results, it is obviously desirable to make quiet-Sun observations by high resolution methods, and so avoid dependence on assumptions of correlation between radio emission and visible solar phenomena.

II. High Resolution Techniques

This paper describes two separate determinations of the quiet-Sun temperature at a wavelength of 21·2 cm (frequency = 1423 Mc/s) in 1958, shortly after sunspot maximum. Both use the high resolution Christiansen crossed grating interferometer at Fleurs, N.S.W. (see Christiansen, Mathewson, and Pawsey 1957).

This aerial system consists of two long arrays, each made up of 32 steerable paraboloid elements, 6 m in diameter and spaced 12·2 m apart on a 380 m base line. The base lines are aligned north-south and east-west respectively. The arrays can be combined in the same way as in the Mills Cross (Mills *et al.* 1958), to give a multiple response pattern of pencil beams about 3′ in half-power width and 1° apart. The separation between adjacent beams is sufficient to ensure that no more than one of them can lie on the Sun at any one time ; thus the multiple-beam response does not introduce any ambiguities in solar observations. Alternatively, either array can be used alone, to give a multiple fan-beam pattern with high resolution in only one direction. The system is thus suitable for either pencil-beam scanning over the solar disk (with the complete cross), or one-dimensional strip-scanning (with a single array).

At sunspot maximum, a large part of the quiet Sun is at any time obscured by intense radio plages. Because of this, it has not been possible to observe details of the brightness distribution of the quiet-Sun component by either of these scanning methods. Both, however, were used to determine the quiet-Sun temperature; the two independent results are in satisfactory agreement with each other. The fan-beam observations have also provided some information on the distribution of quiet-Sun radiation in heliographic latitude.

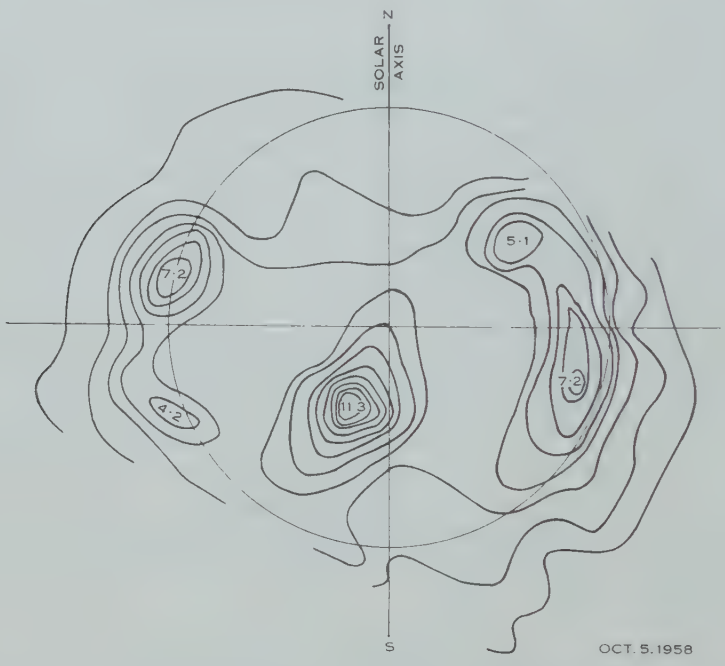

Fig. 1.—A typical contour map of the 21 cm solar brightness distribution, based on pencil-beam observations. Contour interval = 100 000 degK.

III. Pencil-beam Measurements

The solar data obtained with the crossed interferometer are summarized in daily contour maps of the radio brightness of the Sun; Figure 1 shows a typical example. It might be supposed that quiet-Sun temperatures could be read directly from each of these maps at points which on that day happened to be clear of plage areas, and that in this way a complete map of the quiet-Sun brightness distribution could be built up. The situation is, however, complicated by the presence of spurious responses to the radiation from plage areas. Like all aerials of the Mills Cross type, the crossed interferometer has rather large side lobes. The latter may be either positive or negative, and occur when a source is in a main lobe of the fan-beam pattern of one of the arrays. Their positions and magnitudes cannot be accurately predicted, as they are largely due to small accidental maladjustments in the aerial system.

Examination of the records showed that, on most days in 1958, the largest side lobes were about 4 per cent. of the main response (in terms of received power). From this, the effect of side lobes on the accuracy of quiet-Sun measurements was estimated for each of the records made between May and November 1958. It was found that in most cases the range of uncertainty was at least

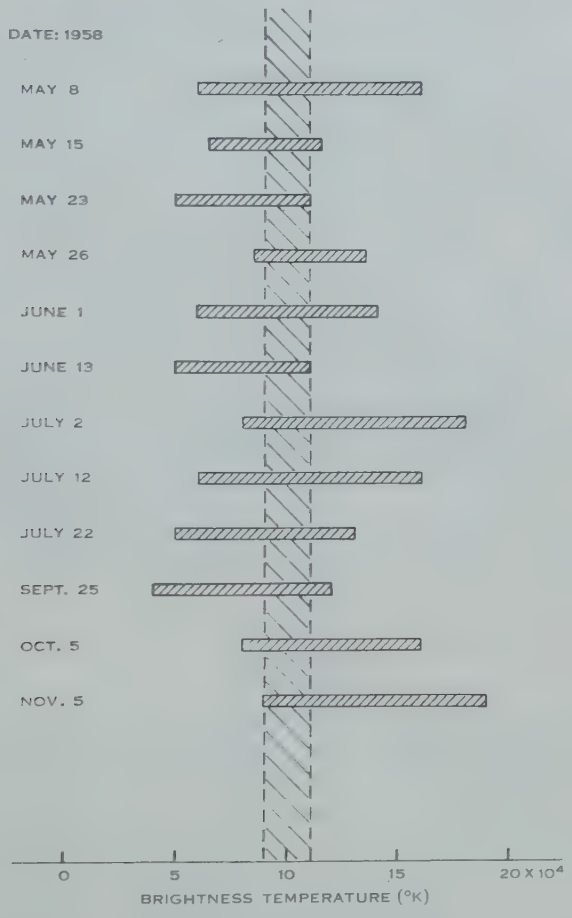

Fig. 2.—Estimation of quiet-Sun brightness temperature (at centre of visible disk) from selected pencil-beam records. The horizontal strips show the limits of error for individual records; the vertical shaded band indicates the range of temperatures which is consistent with all the observations in the group.

$\pm$100 000 degK, which is of the same order as the expected quiet-Sun temperatures. Under these conditions, it was impossible to derive any significant information on the distribution of quiet-Sun brightness; however, in a number of particularly favourable occasions there were points near the centre of the solar disk at which the quiet-Sun temperature could be determined within $\pm$50 000 degK. These selected observations were used in making an estimate of the central brightness temperature of the quiet Sun.

The temperatures were read from the original records, since the contour interval on the maps was inconveniently large for this purpose. The results are summarized in Figure 2. The mean value of the quiet-Sun temperature at the centre of the disk is 102 000 °K, and all the individual measurements are consistent with any value between 90 000 and 110 000 °K.

IV. Fan-beam Measurements

For the one-dimensional strip scans, one of the interferometer arrays was used alone, giving a multiple fan-beam response. The method is a modification of that used by Christiansen and Warburton (1953*a*, 1953*b*, 1955), who obtained sets of daily strip scans across the Sun in chosen directions and found the lower envelope of each set. These envelopes were the corresponding quiet-Sun profiles ; the area under any one of them was a measure of the flux density of the quiet-Sun component.

The plage radiation is so intense at sunspot maximum that it becomes impossible to isolate the quiet-Sun component by this simple lower-envelope technique. The active regions are, however, mainly confined to narrow bands of heliographic latitude ; it will be shown that, because of this feature of the distribution, a quiet-Sun profile can be derived even at sunspot maximum, provided that the scans are taken in a direction parallel to the solar axis.

The use of strip scans is a less direct approach to the problem than is the pencil-beam method described above. However, it avoids appreciable errors due to side-lobe responses ; in the fan-beam pattern these are always very small (less than 0·2 per cent. in received power).

(*a*) *Observations*

The aerial used was the north-south array of the crossed interferometer. In directions normal to the array, where the angular resolution is greatest, the width of the fan beams (to half-power points) is 2′ arc ; in the oblique directions in which the Sun was observed during this work, the beamwidth is about 3′. The directions of maximum response, when projected upon the celestial sphere, appear as small circles centred on the line of aerials. In Figure 3, a typical aerial beam is plotted in coordinates of declination and hour angle, together with the apparent diurnal path of the Sun across the sky. As each beam crosses the Sun, the receiver output records a one-dimensional strip scan. The direction of this scan, relative to the celestial meridian, depends on the solar hour angle and the declination, whilst the angle between this meridian and the Sun's axis varies annually over a range of $\pm 26°$. The scanning angle θ measured from the central meridian of the Sun (see Fig. 3) therefore depends on the time of day and year ; by a proper choice of observing time, scans parallel to the solar axis ($\theta = 0°$) can be obtained.

The records used for this work were made between September and November 1958. They consist of 20 strip scans taken on different days ; the scanning directions are all within $\pm 5°$ of the Sun's central meridian.

(*b*) *Method of Reduction*

(i) *Positions of Scans.*—The most precise method of locating a scan in relation to the Sun is to calculate the time at which the centre of the appropriate aerial beam crosses the centre of the solar disk. It was found to be sufficiently accurate, however, simply to determine this time by measurement on the record to the mid point of the scan. In all cases where comparisons were made, the times so estimated were within 5 sec of the calculated values.

The rate at which the aerial beam moved across the Sun was calculated for each observation. The scale of time in the original record was then converted into one giving the perpendicular distance from the centre of the scanning strip to that of the solar disk. To compensate for the small annual variation in the angular diameter of the Sun, all positions were expressed in terms of the apparent diameter of the visible disk at the time of observation.

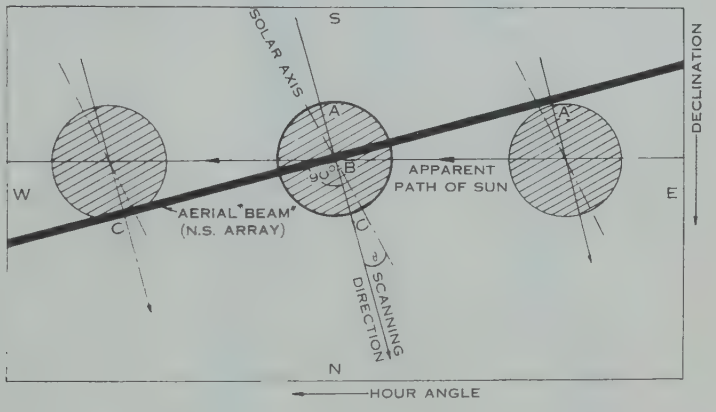

Fig. 3.—Strip-scanning across the Sun with a fan beam. The shaded circles are successive apparent positions of the Sun, at approximately 4-min intervals. θ is the scanning angle, as defined in the text.

(ii) *Intensity Calibration.*—The overall sensitivity of the equipment inevitably varied somewhat from day to day. A complete daily calibration was impracticable, owing to the difficulty in measuring losses in the complicated aerial and feeder system. Instead, a relative measure of the total energy received from the whole Sun was found for each day by integrating the strip-scan record ; this was then compared with an absolute value of the total flux density obtained from an independent direct measurement. In this way a multiplying factor was found, to bring each of the scans to a common intensity scale.

The Sydney 1420 Mc/s radiometer was unfortunately not operating continuously over the required period ; however, daily flux records at 1500 Mc/s were available from the Heinrich Hertz Institute, Berlin, Germany. These were adjusted to 1423 Mc/s on the assumption that the flux density is proportional to frequency. An examination of published data at frequencies from 1000 to 2000 Mc/s indicates that, for the small frequency change involved in this case, this procedure is unlikely to lead to errors of more than 1 per cent. in the derived values.

(iii) *The Quiet-Sun Profile.*—A typical scan with $\theta=0°$ is shown in Figure 4, while 20 such scans have been superimposed in Figure 5. These diagrams show clearly the characteristics of the distribution of plage areas with heliographic latitude. At sunspot maximum, practically all the major radio plages are centred in the middle latitudes; strong sources are unusual within $\pm 10°$ of the equator and very rare in latitudes higher than $\pm 40°$.

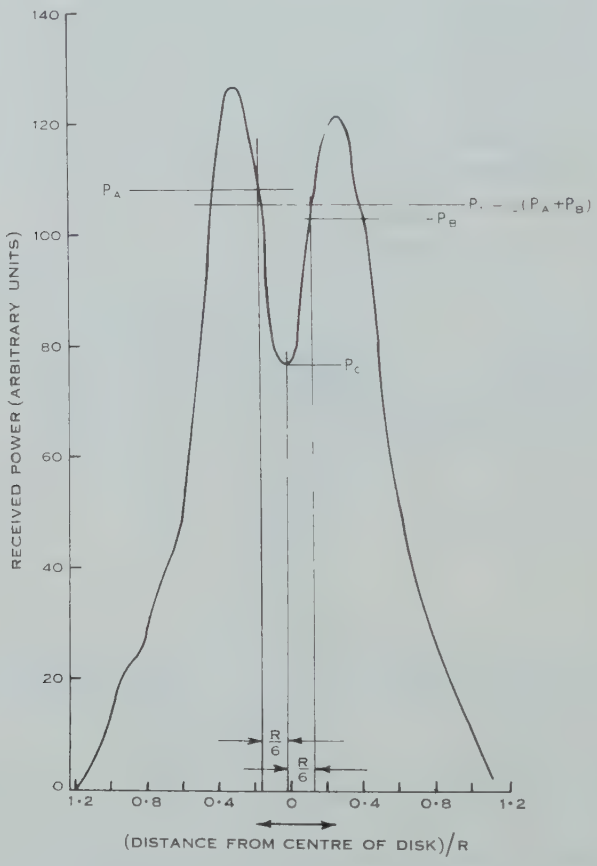

Fig. 4.—A typical strip scan, with scanning direction parallel to the central meridian ($\theta=0°$). R is the radius of the photosphere.

With the scanning direction parallel to the central meridian, therefore, the quiet-Sun profile is seriously obscured only in positions corresponding to the middle latitudes. The complete profile can be estimated by determining the equatorial and polar sections and drawing a smooth curve through the intervening unobservable region. The lower envelope is clearly defined in the polar regions; at the centre of the disk, however, there is a large scatter between individual scans, and a more elaborate method is necessary to determine the quiet-Sun value. Sources centred near the solar equator occur so infrequently that their contribution is likely to be unimportant; any excess over the quiet-Sun flux at the

central minima in the scan must be due mainly to radiation from the outer parts of the intense active regions centred in middle latitudes. The influence of these is accentuated by the smoothing effect of the finite aerial beam. The problem is, therefore, to subtract the component due to these strong sources from the observed " central " values.

Fig. 5.—A set of 20 scans at $\theta=0°$ (Sept.–Nov. 1958).

This has been done by correlating the observed minimum value, p_c, of the flux near the centre of each record with a parameter p_1, which is used as a measure of the combined effect of the middle latitude sources. The choice of p_1 is somewhat arbitrary. An obvious possibility is to use the average of the two maximum flux values on the record. The positions of these maxima, however, vary somewhat from day to day, and it appeared preferable to take p_1 as the average of the two values at equal fixed distances on either side of the minimum position. A suitable spacing was found to be one-sixth of the solar radius, which

was in all cases rather less than the distance between the positions of maximum and minimum flux density, as indicated in Figure 4.

In Figure 6, p_c is plotted against p_1. The coefficient of correlation between the two quantities is 0·80, and the points in the diagram have a clearly defined lower envelope—the straight line AB. The slope of this line is interpreted as representing the contribution of the middle latitude sources to p_c : the upward displacement from it of individual points corresponds to the occasional presence of weak sources close to the solar equator.

It is now necessary to find what part of p_c corresponds to quiet-Sun radiation. For this purpose, it is tentatively assumed that the central part of the quiet-Sun profile is flat, so that $p_c=p_1$, in the absence of any radiation from plage areas. On this assumption, the quiet-Sun value for p_c is given by the intersection of AB with the line $p_c=p_1$ (Fig. 6).

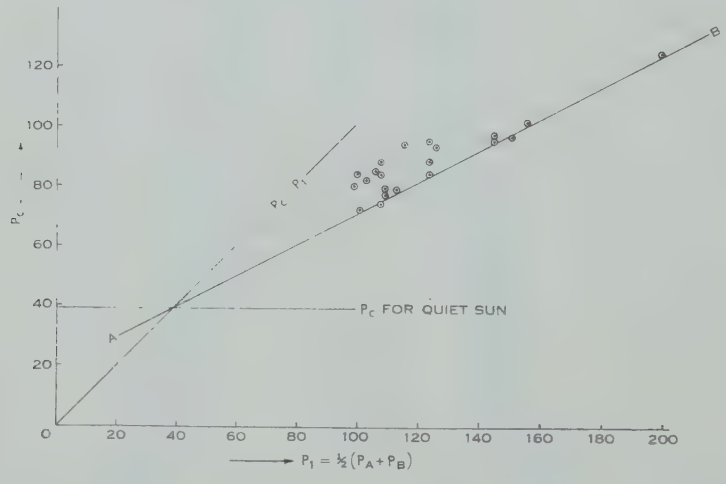

Fig. 6.—Graphical determination of central ordinate on quiet-Sun profile. The units for p_c and p_1 correspond to the vertical scales in Figures 4 and 5.

This value of p_c was combined with the polar sections of the original lower envelope, to give an estimate of the north-south profile of the quiet Sun (Fig. 7). The middle latitude part of the curve is not fixed by this procedure, but is merely interpolated by hand. It appears probable, however, that the true profile lies within the shaded area in the diagram. For any such profile, p_1 does not differ from p_c by more than 3 per cent., so that the initial assumption that $p_c=p_1$ is not invalidated.

A possible source of error in this method is the influence of sources centred near the equator on the measured value of p_1. Pencil-beam records for the dates in question show that any such sources were always too small for an effect of this kind to be appreciable.

(iv) *The Quiet-Sun Flux Density.*—The flux density of radiation from the quiet Sun can now be calculated, since it is proportional to the area under the

profile in Figure 7. The constant of proportionality is determined by comparing the area under any one of the individual daily scans (on the same scale) with the corresponding observed flux density. The results range between 5·7 and $6{\cdot}6\times10^{-21}$ Wm^{-2} $(c/s)^{-1}$ for the profiles within the shaded area of Figure 7. The corresponding apparent disk temperatures (for a uniform disk equal in size to the photosphere) are 130 000 and 150 000 °K.

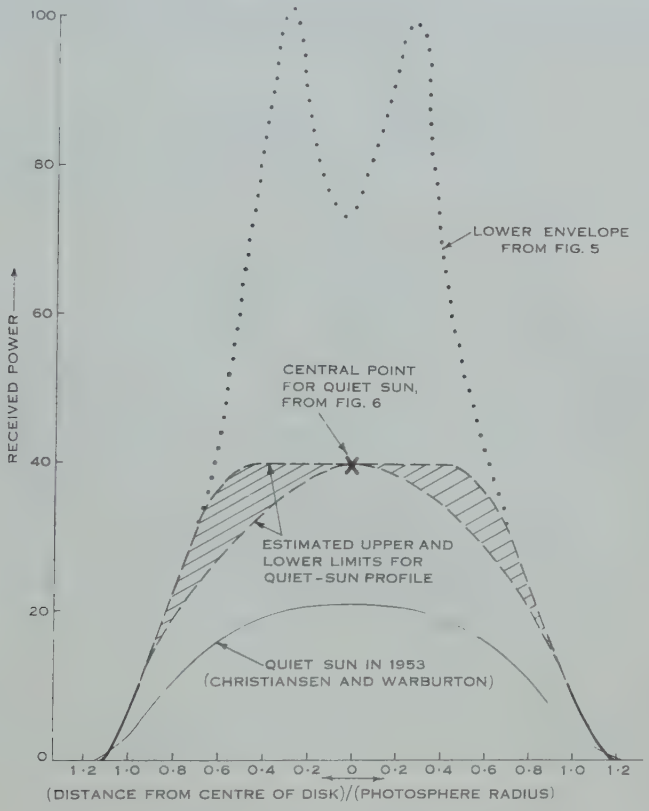

Fig. 7.—The quiet-Sun profile for $\theta=0°$. For comparison, the corresponding sunspot-minimum profile (Christiansen and Warburton 1955) is drawn on the same scale.

V. Discussion

(*a*) *Apparent Disk Temperature*

The apparent disk temperature of the quiet Sun in 1958 has now been determined, and an independent estimate has also been made of the brightness temperature at the centre of the disk. In order to compare these two results, it will be assumed that the brightness distribution in 1958 was the same as that found by Christiansen and Warburton (1955) at sunspot minimum. It will be shown later that this is a reasonable assumption. The pencil-beam value of 90 000–110 000 °K for the central temperature then gives a disk temperature of

130 000–160 000 °K. This agrees with the value derived from the fan-beam observations, within the limits of error of the two experiments. For the remainder of this discussion, the apparent disk temperature for the quiet Sun in 1958 will be taken as 140 000 °K. The corresponding flux density is $6{\cdot}2\times10^{-21}$ Wm^{-2} (c/s)$^{-1}$.

This result shows that the quiet-Sun temperature increased by a factor of 2 between sunspot minimum and sunspot maximum ; Christiansen and Warburton (1955) give a value of 70 000 °K for the apparent disk temperature in 1953. There is thus good agreement with Allen's (1957) calculations, which indicated a variation of 2·0 : 1 and were based on observations at 25 cm wavelength in the period 1947–1953. The value of the quiet-Sun flux at sunspot maximum also agrees well with an earlier estimate. Christiansen, Warburton, and Davies (1957) found the flux at 21 cm by interpolating between published 10 and 25 cm results for 1947, and obtained a value of $6{\cdot}4\times10^{-21}$ Wm^{-2} (c/s)$^{-1}$.

(*b*) *Brightness Distribution*

For sunspot minimum, Christiansen and Warburton (1955) constructed a complete map of the quiet-Sun brightness distribution from a series of profiles at various scanning angles. This was not practicable in 1958, owing to the high level of solar activity. Some inferences can, however, be drawn from a comparison of the north-south profiles for 1953 and 1958. The 1953 curve given by Christiansen and Warburton is shown in Figure 7. The two profiles are similar in shape ; the ratio of corresponding ordinates in both the equatorial and polar sections is approximately 2 : 1. It therefore seems likely that the brightness distribution is much the same at sunspot maximum and minimum. In particular, the pronounced limb darkening at the poles, which was detected from the earlier observations, was also present in 1958. The same conclusion follows from recent eclipse observations at 21 cm wavelength (Krishnan and Labrum, in preparation).

There is no detectable variation over the sunspot cycle in the polar diameter of the radio Sun at this wavelength. The 1953 profile is slightly the broader of the two, but this difference can be explained by the lower angular resolution of the earlier aerial system.

(*c*) *Interpretation of the Results*

The primary purpose of this investigation was to determine whether the observed radio emission from the quiet Sun changes during the sunspot cycle. This has been done by making measurements at a single suitable wavelength. In order to make any detailed deductions regarding the temperature and density in the solar atmosphere, similar data for a range of wavelengths would be necessary. It appears, however, that the present empirical results are consistent with other evidence. In particular, van de Hulst (1949) estimated the coronal electron density from optical measurements and found that the density at any height increases towards sunspot maximum. From this result and assuming that the kinetic temperature of the corona does not vary, he predicted that the brightness temperature of the Sun in the decimetre-wavelength region would show changes of the order of 2 : 1 during the sunspot cycle.

VI. Conclusion

The flux density of radiation from the quiet Sun at 21·2 cm in 1958 was approximately $6 \cdot 2 \times 10^{-21}$ $\mathrm{Wm^{-2}\,(c/s)^{-1}}$; this corresponds to an apparent disk temperature of 140 000 °K. The brightness of the quiet Sun at this wavelength increased by a factor of 2 : 1 from 1953 (sunspot minimum) to 1958 (slightly after sunspot maximum).

The data indicate that the distribution of quiet-Sun brightness with heliographic latitude does not change appreciably during the sunspot cycle. In 1958, as in 1953, there was substantial limb darkening near the poles of the Sun.

VII. Acknowledgments

The author wishes to thank Professor W. N. Christiansen, Dr. J. L. Pawsey, and Mr. J. P. Wild for helpful discussions of this work.

VIII. References

Allen, C. W. (1957).—*Mon. Not. R. Astr. Soc.* **117** : 174.

Christiansen, W. N., and Hindman, J. V. (1951).—*Nature* **167** : 635.

Christiansen, W. N., Mathewson, D. S., and Pawsey, J. L. (1957).—*Nature* **180** : 944.

Christiansen, W. N., and Warburton, J. A. (1953*a*).—*Aust. J. Phys.* **6** : 190.

Christiansen, W. N., and Warburton, J. A. (1953*b*).—*Aust. J. Phys.* **6** : 262.

Christiansen, W. N., and Warburton, J. A. (1955).—*Aust. J. Phys.* **8** : 474.

Christiansen, W. N., Warburton, J. A., and Davies, R. D. (1957).—*Aust. J. Phys.* **10** : 491.

Dodson, H. W. (1957).—Radio Astronomy Symposium No. IV of the International Astronomical Union. p. 327. (Cambridge Univ. Press.)

van de Hulst, H. C. (1949).—*Nature* **163** : 24.

Mills, B. Y., Little, A. G., Sheridan, K. V., and Slee, O. B. (1958).—*Proc. Inst. Radio Engrs., N.Y.* **46** : 67.

Pawsey, J. L., and Yabsley, D. E. (1949).—*Aust. J. Sci. Res.* A **2** : 168.

Piddington, J. H., and Davies, R. D. (1953).—*Mon. Not. R. Astr. Soc.* **113** : 582.

DIRECTION-FINDING ON DIFFUSE SOURCES OF ELECTROMAGNETIC RADIATION

By D. G. Cartwright*

[*Manuscript received June 27, 1960*]

Summary

It is shown that, for sources of large angular size, the response of an Adcock type direction-finder is independent of the extent of the source in altitude. On the other hand, the response of a rotating loop does depend on altitude. By combining the characteristics of both types of direction-finder, the position and size of an extended source can be found, provided that a brightness profile can be assumed.

I. Introduction

Observations of the time variations of very low frequency emissions from the Earth's upper atmosphere (Ellis 1959) have shown the need for a means of estimating the size of the apparent sources of the radiation. Investigations so far have been made at a frequency of about 5 kc/s, a long wavelength inconvenient for use with conventional high resolution antennae. However, information about the angular distribution of the recorded radiation can be obtained with relatively simple antennae such as loop and Adcock direction finders. For instance, using rotating loops, Ellis and Cartwright (1959) have found that the radiation sources have an apparent azimuthal size of between 60° and 90°.

In a recent paper (Wait 1959) it has been demonstrated that the characteristics of a downcoming radio wave may conveniently be measured by making use of rotating loop and Adcock direction-finders. Expressions were derived for finding the angle of arrival, the azimuth, and the polarization, in the case of a single plane wave-train incident on the observation point.

In the present paper the response of a loop and an Adcock system will be analysed for sources of large angular size. It will be shown that the direction-finding characteristics of an Adcock system are independent of the size of the source in elevation.

If the source is extensive in altitude as well as in azimuth, then the directional properties of a rotating loop are modified by a term containing the altitude.

II. Coordinates

The aerial systems will be considered relative to a spherical coordinate system, with the Earth a conducting surface in the x–y plane and the antenna in the x–z plane. An incident wave is specified in terms of its spherical coordinates : angle of elevation above the x–y plane, φ, and its azimuth measured from the x-axis, θ. This is shown in Figure 1.

* Upper Atmosphere Section, C.S.I.R.O., Camden, N.S.W.

III. Adcock Aerial

A pair of suitably connected antennae rotating about a vertical axis midway between them is equivalent to a conventional 4-wire Adcock and goniometer arrangement. The response of this system to a small source will be considered first. Ideally, it responds only to the vertical component of E of the incident wave. If the antennae are on the x-axis and close to a good conductor ($\sigma \gg \omega\varepsilon$, where σ is the conductivity and ε the permittivity of the surface beneath the

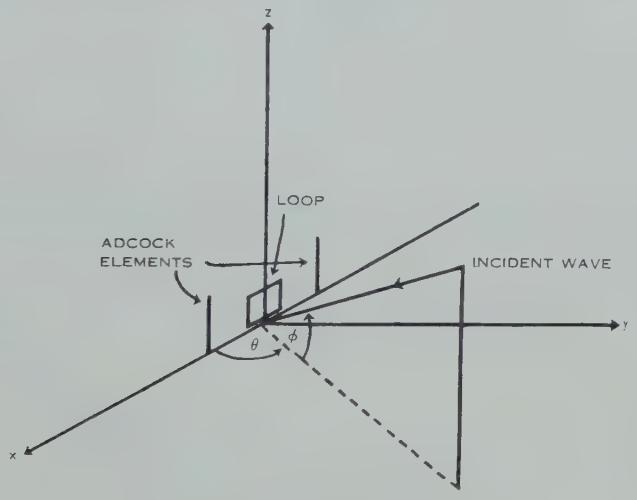

Fig. 1.—Coordinate system, showing position of loop and Adcock antennae.

loop in appropriate units, and ω is the angular frequency of the wave) the power transferred to the receiver is proportional to $\cos^4 \varphi \cos^2 \theta$, and the point source response can be written

$$p_A = \cos^4 \varphi \cos^2 \theta.$$

If the extended source is a random emitter with uniform brightness then the power at the receiver can be written

$$P_A = \int\int p_A \mathrm{d}\theta \mathrm{d}\varphi.$$

Assuming the source has a uniform brightness over an azimuthal width of 2Θ and extends in elevation from zero to Φ, then the maximum power recorded as the aerial rotates is

$$P_{\max.} = 2\int_0^{\Theta}\int_0^{\Phi} p_A \mathrm{d}\theta \mathrm{d}\varphi.$$

This gives

$$P_{\max.} = \alpha\left(\Theta + \frac{1}{2}\sin 2\Theta\right),$$

$$\alpha = \int_0^{\Phi} \cos^4 \varphi \mathrm{d}\varphi$$

$$= \frac{1}{4}\left(\frac{3}{2}\Phi + \sin 2\Phi + \frac{1}{8}\sin^4 \Phi\right),$$

and at the minimum

$$P_{\text{min.}}=2\int_{\frac{1}{2}\pi-\Theta}^{\frac{1}{2}\pi}\int_{0}^{\Phi} p_A \mathrm{d}\theta\mathrm{d}\varphi,$$

$$P_{\text{min.}}=\alpha(\Theta-\tfrac{1}{2}\sin 2\Theta).$$

Defining the modulation in power for the Adcock, M_A, resulting from the antenna rotation as

$$\frac{P_{\text{max.}}-P_{\text{min.}}}{P_{\text{max.}}+P_{\text{min.}}} \quad \ldots\ldots\ldots\ldots\ldots\ldots \quad (1)$$

gives

$$M_A=\frac{\sin 2\Theta}{2\Theta}. \quad \ldots\ldots\ldots\ldots\ldots\ldots \quad (2)$$

Since the spacing of the dipoles at very low frequency is very much smaller than a wavelength, the minimum power corresponds to the azimuthal centre of the source in the usual way.

Thus an Adcock gives information about the position and size in azimuth. The relationship is independent of the brightness profile in Φ.

IV. Loop Aerial

The case of a small rotating loop will now be considered. The magnetic components of the incident wave are H_p in the plane of incidence and H_n normal to this plane. For a loop in free space the Cartesian components due to H_p are

$$H_x=H_p \sin\varphi\cos\theta,$$
$$H_y=H_p \sin\varphi\sin\theta,$$
$$H_z=H_p \cos\varphi,$$

and those due to H_n are

$$H_x=H_n \sin\theta,$$
$$H_y=H_n \cos\theta,$$
$$H_z=0.$$

For random polarization, $H_n=H_p$ and the powers due to each component can be added. The loop absorbs power only from H_y, so the small source power response for a small loop in free space is proportional to

$$\cos^2\theta+\sin^2\varphi\sin^2\theta.$$

This is unaltered if the loop is close (in terms of the wavelength) to a good conductor in the x–y plane, so we can write

$$p_L=\cos^2\theta+\sin^2\varphi\sin^2\theta.$$

For an extended source of uniform brightness, the total power at the receiver is

$$P_L=\int\int p_L \mathrm{d}\theta\mathrm{d}\varphi.$$

If, as before, the source is of width 2Θ in azimuth and extending from 0 to Φ in elevation, the maximum power recorded is

$$P_{\max.}=(1+\beta)\Theta+\tfrac{1}{2}(1-\beta)\sin 2\Theta,$$

where

$$\beta=\int_0^{\Phi}\sin^2\varphi\,d\varphi$$
$$=\tfrac{1}{2}(\Phi-\tfrac{1}{2}\sin 2\Phi),$$

and as before

$$P_{\min.}=(1+\beta)\Theta-\tfrac{1}{2}(1-\beta)\sin 2\Theta.$$

The modulation in power for the loop then becomes

$$M_L=\left(\frac{1-\beta}{1+\beta}\right)\frac{\sin 2\Theta}{2\Theta}. \qquad \ldots\ldots\ldots\ldots\ldots\ (3)$$

M_L is indistinguishable from M_A if $\beta\ll 1$, i.e. Φ is small.

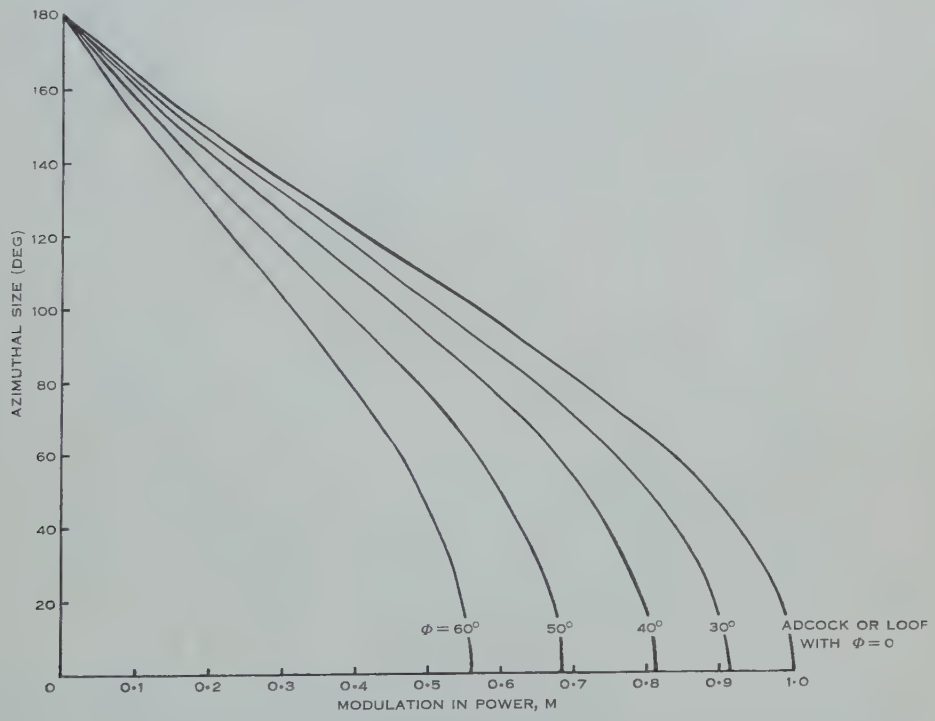

Fig. 2.—The azimuthal size 2Θ of a diffuse source, shown as a function of the modulation in power, M, produced by a rotating loop direction-finder, for different source heights Φ. The case $\Phi=0$ corresponds to an Adcock direction-finder.

V. Comparison of Loop and Adcock Results

The modulation in power of an Adcock direction-finder is independent of the brightness profile in elevation, but, if the brightness distribution in azimuth is symmetrical, the minimum recorded power corresponds to the direction of the centre of the source in the usual way.

The power modulation of a rotating loop, on the other hand, is affected by the distribution of brightness in elevation if the source extends more than about 5° above the horizon.

By comparing the records from an Adcock and a rotating loop the height of the source can easily be found.

For instance,

$$\frac{M_A}{M_L}=\frac{1+\beta}{1-\beta},$$

or

$$\frac{M_A-M_L}{M_A+M_L}=\beta=\tfrac{1}{2}(\Phi-\tfrac{1}{2}\sin 2\Phi).$$

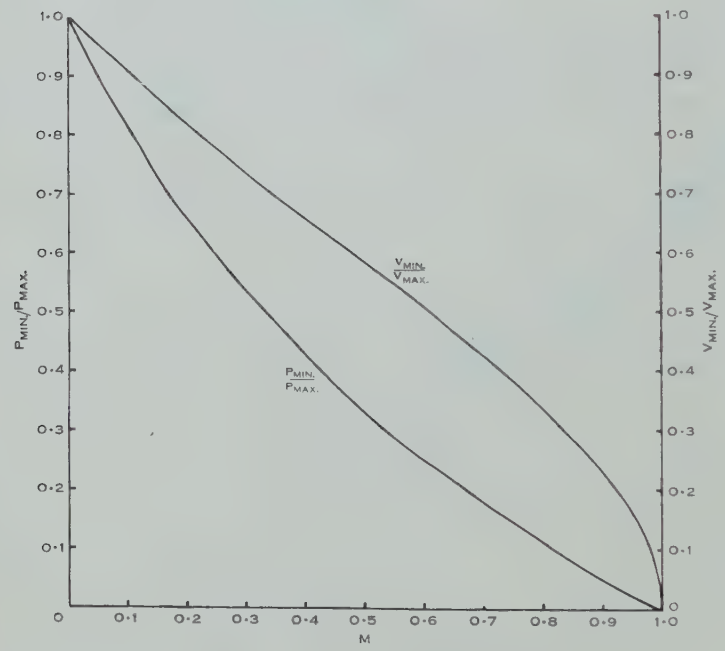

Fig. 3.—The relation between the modulation in power, $M=(P_{\max.}-P_{\min.})/(P_{\max.}+P_{\min.})$, and the ratio $P_{\min.}/P_{\max.}$, or $V_{\min.}/V_{\max.}=\sqrt{(P_{\min.}/P_{\max.})}$.

VI. Discussion

Figure 2 shows the expressions (**2**) and (**3**) with 2Θ plotted as a function of the modulation in power M. The most convenient quantity to record is the amplitude or voltage produced by the direction-finder. From (**1**) we have

$$M=(P_{\max.}-P_{\min.})/(P_{\max.}+P_{\min.}).$$

If we denote $V_{\min.}/V_{\max.}$ by v, then $v=\sqrt{(P_{\min.}/P_{\max.})}$, and so

$$v=\sqrt{\{(1-M)/(1+M)\}}. \quad \ldots\ldots\ldots\ldots\ldots \quad (4)$$

The relationship between v or $P_{\min.}/P_{\max.}$ and M is shown in Figure 3. Using either (**4**) or Figure 3 we can obtain the source size in azimuth as a function of v for any given Φ. This is shown in Figure 4.

This method is best suited to sources for which Φ is greater than about 30°. From Figure 2 it can be seen that the curves for Φ less than 30° are very closely spaced in comparison with curves for Φ greater than 30° and, in fact, the accuracy of measurement is not high enough to resolve curves for which Φ is less than 20°. An exception to this is when the source is of small size in azimuth, since the curves of Figure 4 are quite widely spaced below $2\Theta=40°$, say.

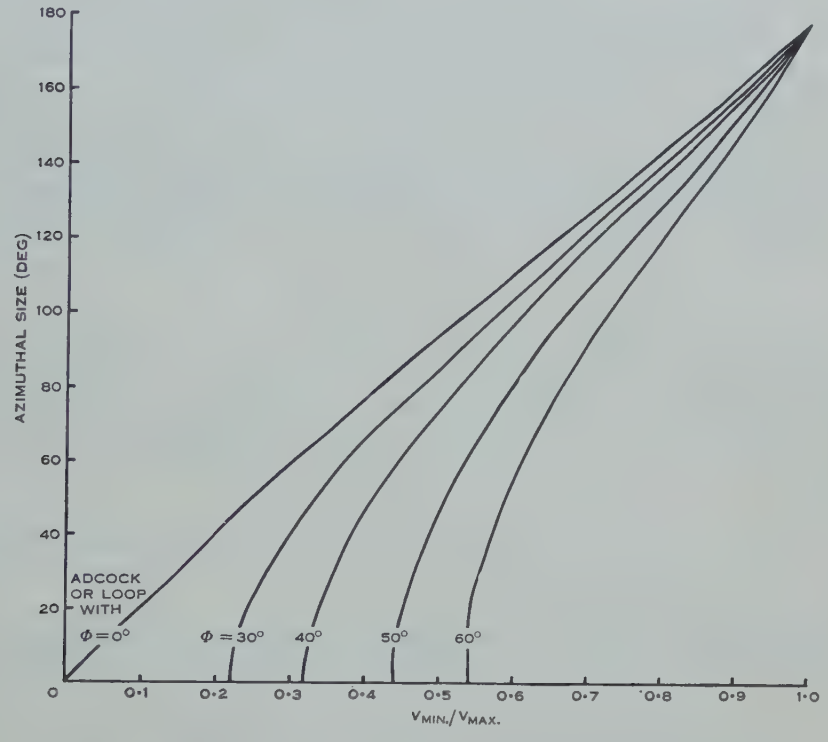

Fig. 4.—The azimuthal size 2Θ of a diffuse source shown as a function of the depth of the amplitude null, $V_{\text{min.}}/V_{\text{max.}}$, produced by a rotating loop direction-finder, for different source heights Φ. The case $\Phi=0$ corresponds to an Adcock direction-finder.

VII. Acknowledgments

The author acknowledges many suggestions made during discussions with Dr. G. R. A. Ellis of this organization.

VIII. References

Ellis, G. R. A. (1959).—Low frequency electromagnetic radiation associated with geomagnetic disturbances. *Planet. Space Sci.* **1**: 253–8.

Ellis, G. R. A., and Cartwright, D. G. (1959).—Directional observations of radio noise from the outer atmosphere. *Nature* **184**: 1307.

Wait, J. R. (1959).—Downcoming radio waves measurement of characteristics. *Electronic & Radio Engr.* **36**: 106–7.

THE GENERAL THEORY OF THE MOTIONS OF IONS AND ELECTRONS IN GASES

By L. G. H. Huxley*

[*Manuscript received June 20, 1960*]

Summary

In this paper the more important general formulae for the drift velocities and diffusion coefficients of ions and electrons in gases are derived by the application of dynamical principles. These formulae agree with those already established by a proper application of the method of free paths. Formulae for the distribution of speeds of agitation are also derived.

I. Introduction

There is an extensive literature on the theory of the motions of ions and electrons in gases but the derivations of the formulae for drift velocities, coefficients of diffusion of ions and electrons, and the conductivities of weakly ionized gases in direct or alternating electric fields accompanied or unaccompanied by a magnetic field, that find most frequent practical use, are not readily accessible.

In what follows the chief formulae are established in a general form by the application of dynamical principles. Although the treatment is purposely elementary it does not lack rigour.

The aim is to provide a compact and uniform summary of the theory of the subject in a useful form (general references : Allis 1956 ; Margenau 1958).

II. Electronic Motion in Gases

(*a*) *General*

When electrons move freely among the molecules of a gas in the absence of an electric field they interchange energy and momentum with molecules in collisions and their steady state of random agitational motion is one in which at any instant the directions of their velocities **c** are distributed isotropically and their speeds c are distributed according to Maxwell's formula which states that the proportion of a group of n electrons whose speeds exceed c but do not exceed $c+\mathrm{d}c$ is

$$\frac{\mathrm{d}n_c}{n}=\frac{4}{\alpha^3\sqrt{\pi}}\exp\left(-c^2/\alpha^2\right).c^2\mathrm{d}c, \quad \ldots\ldots\ldots\ldots \quad (1)$$

where α is the most probable speed. In addition a condition of equipartition of energy prevails in which the mean kinetic energy of agitation $\frac{1}{2}m\overline{c^2}$ of an electron is equal to that, $\frac{1}{2}M\overline{C^2}$, of a molecule.

* Commonwealth Scientific and Industrial Research Organization, Melbourne ; present address : Australian National University, Canberra.

This motion becomes modified in important respects when electrons move in a steady state of motion in a gas in the presence of a uniform and constant electric field **E**. It now comprises a steady drift velocity **W** of the centroid of the group with a superimposed random motion of agitation such that the speed W is much smaller (a few per cent.) than the mean speed of agitation $\bar{c}$.

The speeds c do not, in general, conform to Maxwell's distribution formula and the mean kinetic energy of agitation $\frac{1}{2}m\overline{c^2}$ of an electron exceeds that, $\frac{1}{2}M\overline{C^2}$, of a molecule by a factor k (Townsend's energy factor) which is a function (specific to each gas) of the ratio E/N of the electric field strength to the number of molecules N in unit volume of the gas. When the measurements are referred to a standard temperature (15 °C) the parameter E/p is more commonly employed than E/N, p being the pressure of the gas.

These and other aspects of electronic motion in gases are considered in greater detail in what follows.

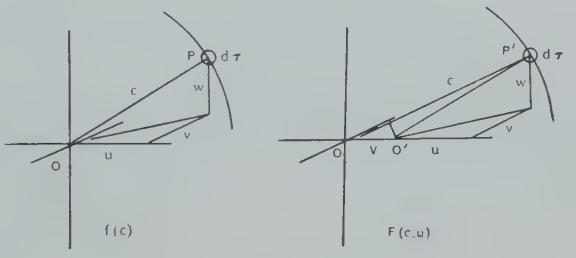

Fig. 1

(b) Nature of the Distribution Function in a Steady State of Motion

Consider a general isotropic distribution of the speeds c represented by a function $f(c)$ with the meaning that the proportion of electrons of a group n whose speeds exceed c but do not exceed $c+\mathrm{d}c$ is $\mathrm{d}n_c/n=4\pi f(c)c^2\mathrm{d}c$.

This function is represented in velocity space by a spherical distribution of points, such that the number of points contained within an element $\mathrm{d}u\ \mathrm{d}v\ \mathrm{d}w$ of velocity space at a distance $c(u,v,w)$ from the origin is $n\,f(c)\mathrm{d}u\ \mathrm{d}v\ \mathrm{d}w$. Consider the unsymmetrical distribution $F(c,u)$ obtained from $f(c)$ by increasing the u component of every velocity c by an amount $V(c)$ as shown in Figure 1. The centre of symmetry has been displaced from O to O' through a distance V, thus leaving unaltered the number of points in the element of space $\mathrm{d}\tau$ at P and P' respectively, but the velocity c increases from $c=OP$ on the left to $c=OP'$ on the right. Let θ be the angle between OP' and the u-axis and suppose that $V\ll c$, then $\cos\theta=u/c$ and $O'P'\doteq c-V\cos\theta=c-Vu/c$.

The number of representative points in $\mathrm{d}\tau$ on the right is

$$nF(c,u)\mathrm{d}\tau=nf\left(c-\frac{u}{c}V\right)\mathrm{d}\tau,$$

whence

$$F(c,u)\simeq f(c)-\frac{Vu}{c}\frac{\mathrm{d}f}{\mathrm{d}c}. \quad \ldots\ldots\ldots\ldots\ldots \quad (2)$$

It remains to determine the value of V and the form of the function $f(c)$ associated with steady electronic motion in a gas under the influence of a steady and uniform electric field **E**, it being assumed throughout that the number of electrons in unit volume is much smaller than the number of molecules in unit volume so that mutual interactions of electrons are unimportant.

(*c*) *Specification of an Encounter*

In Figure 2 (*a*) an electron or ion e with mass m approaches a molecule O with mass M at a relative velocity **g** and is deflected to leave the vicinity of O at a velocity **g′**. It is supposed that when e is sufficiently distant from a molecule its trajectory is rectilinear.

In Figure 2, b is the perpendicular distance of O from the direction of **g** and θ the angle of deflection (the angle between **g** and **g′**). $\theta(b,g)$ is a function of b and g.

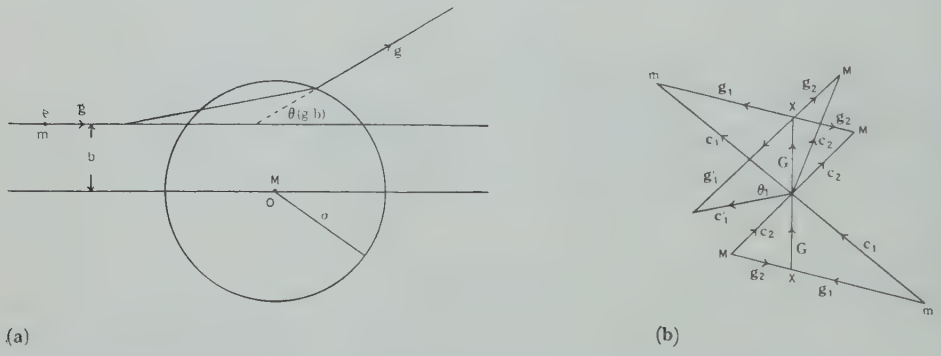

(a) (b)

Fig. 2

It will be assumed that there is a limiting distance σ such that if b exceeds σ the deflections $\theta(b,g)$ are zero or so small that even in aggregate they are unimportant.

The vector diagram of velocities relating to an encounter is (following Maxwell) depicted in Figure 2 (*b*). $\mathbf{c}_1$ and $\mathbf{c}_2$ are the velocities respectively of the ion (or electron) and the molecule before an encounter and $\mathbf{c}_1'$ and $\mathbf{c}_2'$ those after the encounter.

G is the velocity of the centroid X of m and M and $\mathbf{g}_1$ and $\mathbf{g}_2$ are those of m and M relative to X before the encounter and $\mathbf{g}_1'$ and $\mathbf{g}_2'$ those after it. It follows that $\mathbf{g}=\mathbf{g}_1+\mathbf{g}_2$ and $\mathbf{g}'=\mathbf{g}_1'+\mathbf{g}_2'$.

In a system in which the gas as a whole has no mass motion, and to which the velocities **c** refer, the actual deflection of e is the angle θ_1 between $\mathbf{c}_1$ and $\mathbf{c}_1'$ and in general this angle depends not only upon b and g, but when $\mathbf{c}_1$ is given, upon $\mathbf{c}_2$. However, when $m/M \ll 1$ and also $c_1 \gg c_2$, as is the case if e is an electron, then $\mathbf{g} \simeq \mathbf{c}_1$ and $\theta(b,g)=\theta(b,c_1)=\theta_1$. Also c_1' differs little from c_1 in most instances.

An important quantity is $\overline{\cos\theta_1}$ the average value of $\cos\theta_1$ taken over all encounters in which the ion or electron is travelling with speed c_1 before an

encounter. Since the velocities $\mathbf{c}_1'$ are distributed with axial symmetry about the direction of $\mathbf{c}_1$, in the case of an electron where $\theta_1=\theta(b,c_1)$,

$$\overline{\cos\theta_1}=\left[2\pi\int_0^\sigma \cos\theta(b,c_1)b\,db\right]/\pi\sigma^2=2/\sigma^2\int_0^\sigma \cos(\theta,c_1)b\,db.$$

The mean value of $\cos\theta_1$ averaged over the whole distribution of speeds c_1 would be written $\overline{\overline{\cos\theta_1}}$, that is to say it is the mean value of θ in an encounter of any kind.

(*d*) *Free Paths*

Consider a large number p of free paths $x_1, x_2, \ldots, x_n$ all traversed at the same speed c by the ion or electron, but not necessarily consecutively.

If l_{0c} is the mean free path, then

$$pl_{0c}=\sum_1^n x_k.$$

Let $\bar{g}$ be the mean speed of the ion (with speed c) relative to the molecules which move at random and let N be the number of molecules in unit volume.

The sum of the times spent in traversing the paths x_k is $t=pl_{0c}/c$, that is to say, $p=ct/l_{0c}$. But $p=\bar{g}t.N\pi\sigma^2$, consequently, if $l_0=1/N\pi\sigma^2$, $l_{0c}=c/\bar{g}.N\pi\sigma^2=(c/\bar{g})l_0$. For electrons $\bar{g}=c$; $l_{0c}=1/N\pi\sigma^2=l_0$. σ is the limiting value of the impact parameter beyond which deflection of the ions are unimportant.

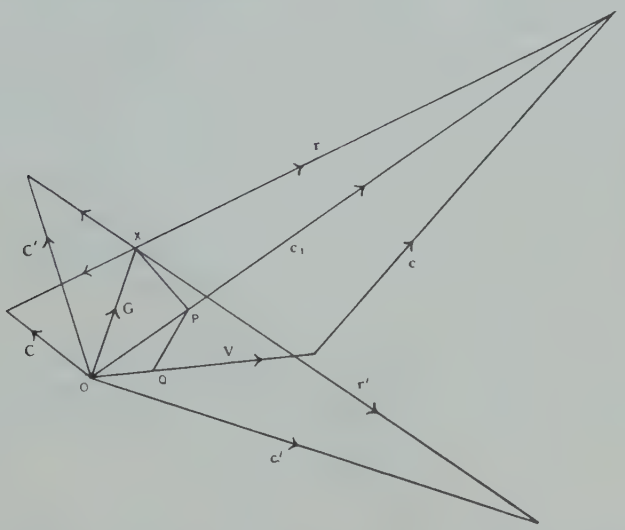

Fig. 3

(*e*) *Calculation of* V

According to Section 2 (*b*), the velocity of an electron is the vector sum $\mathbf{V}+\mathbf{c}$ of a fixed velocity $\mathbf{V}$ and velocity of agitation $\mathbf{c}$.

Consider the vector diagram of velocities of a collision of such an electron with a molecule with momentum $M\mathbf{C}$ (Fig. 3).

In Figure 3, $\mathbf{c}_1=\mathbf{V}+\mathbf{c}$; $\mathbf{G}=(m\mathbf{c}_1+M\mathbf{C})/(m+M)$ is the velocity of the centroid X of m and M, and $\mathbf{r}$ is the velocity of the electron (or ion) relative to X. These are the velocities before the encounter. After the encounter the corresponding velocities are $\mathbf{c}'$, $\mathbf{C}'$, $\mathbf{G}$, and $\mathbf{r}'$.

If no change results in the internal energy of the molecule then $r'=r$.

Consider first the case in which all directions of $\mathbf{r}'$ are equally probable when $\mathbf{C}$ and $\mathbf{c}_1$ are given, as would occur in encounters between rigid smooth spheres (Maxwell 1890).

The mean velocity of electrons and molecules ($\mathbf{c}_1$ and $\mathbf{C}$ as specified) after encounters is therefore $\mathbf{G}$. Consider next, the mean residual velocity in all encounters of electrons for which $\mathbf{c}_1$ is given but $\mathbf{C}$ is allowed to range over all possible directions. Draw XP parallel to $\mathbf{C}$ to meet $\mathbf{c}_1$ at P. Then $\mathbf{G}=\mathbf{OP}+\mathbf{PX}$. But $OP=\{m/(M+m)\}c_1$ and $XP=\{M/(M+m)\}C$, consequently P is a fixed point and XP has a fixed length when C is constant. The possible end points of $\mathbf{C}$ lie on the surface of a sphere about O and those of $\mathbf{G}$ on a sphere about P. Thus the mean projections of both $\mathbf{C}$ and $\mathbf{PX}$ on the direction of $\mathbf{c}_1$ are zero. The mean residual velocity after all such encounters is $\mathbf{OP}$. Finally $\mathbf{c}$ may assume all directions with respect to $\mathbf{V}$ and therefore $\mathbf{QP}$ does likewise. The mean residual velocity is therefore $\mathbf{OQ}=\{m/(m+M)\}\mathbf{V}$ for encounters in which the agitational speed has a fixed value c.

Suppose that all directions of $\mathbf{r}'$ are not equally probable but that $\mathbf{r}'$ is distributed with axial symmetry about $\mathbf{r}$. Since the scattering occurs with axial symmetry about the direction XQ, the mean values of the components of $\mathbf{c}'$ and $\mathbf{r}'$ normal to XQ are zero, so that the mean value of the vector $\mathbf{c}'$ when the scattering about X is not isotropic is a vector parallel to $\mathbf{r}$. It may be written $\alpha\mathbf{r}$.

But, from the triangle PXQ, $\alpha\mathbf{r}=\alpha\{M/(M+m)\}(\mathbf{c}_1-\mathbf{C})$, so that when $\mathbf{C}$ is distributed over all possible directions in space the residual mean value of $\mathbf{c}'$ is a vector parallel to $\mathbf{c}_1$ and equal to $\{\alpha M/(M+m)\}\mathbf{c}_1$. But $\mathbf{c}_1=\mathbf{V}+\mathbf{c}$, so that when $\mathbf{c}$ ranges over all possible directions the mean value of $\mathbf{c}'$ reduces to $\{\alpha M/(M+m)\}V$, where $\alpha=\overline{\cos\theta}$, where θ is an angle of deflection of the velocity $\mathbf{r}$ relative to X in an encounter when the speed of the ion or electron relative to a molecule is $g=\{(M+m)/M\}r$.

The mean residual momentum after encounters is therefore $\{(m+\alpha M)/(M+m)\}m\mathbf{V}$, which is the same as the mean momentum that the ion possesses when it enters the speed group c. The mean momentum lost in an encounter is

$$m\mathbf{V}\left(1-\frac{m+\alpha M}{M+m}\right)=\frac{mM}{M+m}\ (1-\alpha)\mathbf{V},$$

and the mean rate at which an ion or electron loses momentum in encounters is

$$\frac{mM}{M+m}(1-\alpha)\frac{g}{l_0}\mathbf{V},$$

where $l_0=1/N\pi\sigma^2$.

In a steady state of motion the mean momentum $m\mathbf{V}$ is the sum of the mean momentum $\{(m+\alpha M)/(m+M)\}m\mathbf{V}$ at entry and that acquired from the field,

namely, $\mathbf{E}el_0/g$. The mean momentum imparted by the field is therefore equal to the mean momentum lost in an encounter. Consequently,

$$\left.\begin{aligned} \frac{Eel_0}{g} &= \frac{mM}{m+M}(1-\alpha)V, \\ V &= Eel/mg, \\ l &= \frac{M+m}{M(1-\alpha)}l_0, \quad \alpha = \overline{\cos\theta}. \end{aligned}\right\} \quad \text{or} \quad \text{where} \quad \ldots\ldots\ldots\ldots\ldots (3)$$

l is an equivalent mean free path and g is the mean speed of the ion or electron with agitational speed c, relative to the molecules. For electrons, $g \simeq c$, $m/M \ll 1$, $l = l_0/(1-\alpha)$. The equivalent cross section is here

$$A(c) = 1/Nl = (1-\overline{\cos\theta})/l_0 = 2\pi\int_0^\sigma \{1-\cos\theta(b)\}b\,\mathrm{d}b.$$

When electrons and ions interact as point centres of repulsive force $P = k/r^\nu$, then, if $\nu > 2$, the integral

$$2\pi\int_0^\infty \{1-\cos\theta(b)\}b\,\mathrm{d}b$$

is convergent and defines an equivalent cross section and mean free path

$$l = 1/2\pi N\int_0^\infty (1-\cos\theta(b))b\,\mathrm{d}b = 1/NA(c),$$

where $A(c) = 2\pi BA_1(\nu)/c^{4/(\nu-1)}$, in which $B = (k/m)^{2/(\nu-1)}$ and $A_1(\nu)$ is a function of ν only (Chapman and Cowling 1952, p. 171; Huxley 1957*a*, p. 125). For instance, when $\nu = 5$; $A(c) \propto 1/c$.

If the scattering is isotropic,

$$A = 2\pi\int_0^\sigma b\,\mathrm{d}b = \pi\sigma^2 = A_0.$$

In this event, $\alpha = 0$,

$$V = \frac{Ee}{mg}\,\frac{l_0(M+m)}{M} = \frac{Eel_0}{g}\left(\frac{1}{m}+\frac{1}{M}\right). \quad \ldots\ldots\ldots\ldots (4)$$

In general, $l = l_0(M+m)/M(1-\alpha)$ may be written $l = l_0 + S$ (Huxley 1957, 1960), where

$$S = (m+\alpha M)l_0/M(1-\alpha). \quad \ldots\ldots\ldots\ldots\ldots (5)$$

(f) Formula for Drift Velocity $\mathbf{W}$ *in a Steady and Uniform Field* $\mathbf{E}$

The mean speed of drift in the direction of $\mathbf{E}$ (parallel to Ox) of the group of electrons with speeds c is the mean value of the component u of the velocities $\mathbf{c}$ averaged over all directions in space. From equation (2) it follows that the mean value of $u = c\cos\theta$ is

$$W(c) = cf(c)\,\overline{\cos\theta} - Vc\frac{\mathrm{d}f}{\mathrm{d}c}\,.\,\overline{\cos^2\theta} = -\frac{Vc}{3}\,\frac{\mathrm{d}f}{\mathrm{d}c},$$

so that, from equation (3),

$$W(c)=\frac{Eel}{3mg}c\frac{\mathrm{d}f}{\mathrm{d}c}. \quad \ldots\ldots\ldots\ldots\ldots\ldots \quad (6)$$

The mean value of $W(c)$ taken over all speeds c is the drift speed W of the centroid of the whole group. Thus,

$$\begin{aligned} W&=-\frac{Ee}{3m}\int_0^\infty 4\pi\frac{c^2lc}{g}\frac{\mathrm{d}f}{\mathrm{d}c}\mathrm{d}c \\ &=\frac{Ee}{3m}\left\{-\left[\frac{4\pi lc^3}{g}f\right]_0^\infty+4\pi\int_0^\infty\frac{1}{c^2}\frac{\mathrm{d}}{\mathrm{d}c}\left(\frac{lc^3}{g}\right)f.c^2\mathrm{d}c\right\} \\ &=\frac{Ee}{3m}\cdot\overline{c^{-2}\frac{\mathrm{d}}{\mathrm{d}c}\left(\frac{lc^3}{g}\right)}, \quad \ldots\ldots\ldots\ldots\ldots\ldots\ldots\ldots \quad (7) \end{aligned}$$

where $l=l_0+S$; (equation (5)) ; g is the mean speed of an ion or electron relative to the molecules. For electrons, $m/M\ll 1$, $g=c$, equation (7) becomes

$$W=\frac{Ee}{3m}\overline{c^{-2}\frac{\mathrm{d}}{\mathrm{d}c}(lc^2)}, \quad \ldots\ldots\ldots\ldots\ldots\ldots \quad (8)$$

the bar denoting an average with respect to c.

This formula was previously derived directly by a correct application of the method of free paths (Huxley 1957*a*, 1960).

Throughout, the atomic charge e is regarded as algebraically positive, that is to say, a negative value should be substituted in the case of electrons.

(*g*) *Drift Speed in an Alternating Electric Field*

Let the electric field be considered to be a rotating vector in the XOY plane, $E=E_0\exp \mathrm{i}pt$. It is assumed that the frequency $p/2\pi$ is sufficiently large that fluctuations in the mean energy $\frac{1}{2}m\overline{c^2}$ are unimportant. This assumption is also correct for the special case $p=0$.

An expression for the velocity $\mathbf{V}$ is first obtained. The momentum $m\mathbf{V}$ fluctuates in a time-dependent field because its rates of loss by encounters and of gain from the field are not equal. Thus, from Section II (*e*),

$$m\frac{\mathrm{d}V}{\mathrm{d}t}=E_0e\exp(\mathrm{i}pt)-\left(\frac{M}{M+m}-\alpha\right)\frac{g}{l_0}mV,$$

or

$$\frac{\mathrm{d}V}{\mathrm{d}t}+\frac{g}{l}V=\frac{E_0e}{m}\exp(\mathrm{i}pt), \quad \ldots\ldots\ldots\ldots\ldots\ldots \quad (9)$$

whence

$$V=\frac{E_0e}{m(\nu+\mathrm{i}p)}\exp(\mathrm{i}pt), \quad \ldots\ldots\ldots\ldots\ldots \quad (10)$$

where $\nu=g/l$.

When the vector **V** is not directed along an axis of coordinates the appropriate form of equation (**2**) is

$$F(c,u,v,w)=f(c)-\frac{\mathbf{V}\cdot\mathbf{c}}{c}\frac{\mathrm{d}f}{\mathrm{d}c}. \quad \ldots\ldots\ldots\ldots\ldots\ldots \quad (11)$$

So that, when $E=E_0\exp(ipt)=E_x+iE_y$ and $V=V_x+iV_y$, the appropriate form of equation (**11**) is

$$F(c,u,v)=f(c)-\frac{E_0eu\exp(ipt)}{cm(\nu+ip)}\frac{\mathrm{d}f}{\mathrm{d}c}.$$

It follows, as in Section II (*f*), that, with $E=E_0\exp(ipt)$,

$$\begin{aligned}W&=-\frac{Ee}{3m}\int_0^\infty\frac{4\pi c^3}{(\nu+ip)}\frac{\mathrm{d}f}{\mathrm{d}c}\mathrm{d}c\\&=\frac{Ee}{3m}\int_0^\infty\left[c^{-2}\frac{\mathrm{d}}{\mathrm{d}c}\left(\frac{c^3}{\nu+ip}\right)\right]4\pi c^2f\mathrm{d}c\\&=\frac{Ee}{3m}\cdot\overline{c^{-2}\frac{\mathrm{d}}{\mathrm{d}c}\left(\frac{c^3}{\nu+ip}\right)}. \quad \ldots\ldots\ldots\ldots\ldots\ldots \quad (12)\end{aligned}$$

(*h*) *Drift Velocity in the Presence of a Magnetic Field*

Let a magnetic field B act along the direction Oz and E along Ox and write $\omega=-Be/m$. Then equation (**9**) is to be replaced by

$$\frac{\mathrm{d}V}{\mathrm{d}t}+\nu V=\frac{E_0e}{m}\exp(ipt)+i\omega V,$$

or

$$\frac{\mathrm{d}V}{\mathrm{d}t}+(\nu-i\omega)V=\frac{E_0e}{m}\exp(ipt). \quad \ldots\ldots\ldots\ldots\ldots\ldots \quad (13)$$

Whence

$$V=\frac{E_0e\exp(ipt)}{m[\nu-i(\omega-p)]}, \quad \ldots\ldots\ldots\ldots \quad (14)$$

and

$$W=\frac{Ee}{3m}\overline{c^{-2}\frac{\mathrm{d}}{\mathrm{d}c}\left[\frac{c^3}{\nu-i(\omega-p)}\right]}. \quad \ldots\ldots\ldots \quad (15)$$

Equations (**12**) and (**15**) can be derived directly by use of the method of free paths (Huxley 1957*b*).

With electrons $\nu=g/l$ becomes $\nu=c/l$.

(*i*) *Magnetic Deflection of an Electron Stream in a Gas*

In equation (**15**) let $p=0$, then

$$W=W_0\exp(i\theta)=\frac{Ee}{3m}\overline{c^{-2}\frac{\mathrm{d}}{\mathrm{d}c}\left(\frac{c^3}{\nu-i\omega}\right)}=\frac{Ee}{3m}\overline{c^{-2}\frac{\mathrm{d}}{\mathrm{d}c}\left[\frac{(\nu+i\omega)c^3}{\nu^2+\omega^2}\right]}, \quad \ldots \quad (16)$$

$\omega=-Be/m$.

Choose the axes of coordinates so that $+Oy$ is parallel to **B** and $+Oz$ to **E**, then it follows from equation (**16**) that

$$\left.\begin{aligned} W &= W_z + \mathrm{i}W_x = W_0(\cos\theta + \mathrm{i}\sin\theta), \\ W_z &= \frac{Ee}{3m}\overline{c^{-2}\frac{\mathrm{d}}{\mathrm{d}c}\left(\frac{\nu c^3}{\nu^2+\omega^2}\right)}, \\ W_x &= \frac{Ee}{3m}\cdot\omega\overline{c^{-2}\frac{\mathrm{d}}{\mathrm{d}c}\left(\frac{c^3}{\nu^2+\omega^2}\right)}, \\ \tan\theta &= \frac{W_x}{W_z} = \omega\cdot\overline{c^{-2}\frac{\mathrm{d}}{\mathrm{d}c}\left(\frac{c^3}{\nu^2+\omega^2}\right)}\Big/\overline{c^{-2}\frac{\mathrm{d}}{\mathrm{d}c}\left(\frac{\nu c^3}{\nu^2+\omega^2}\right)}. \end{aligned}\right\} \quad \ldots\ (17)$$

In laboratory experiments in gases at pressures of a few millimetres of mercury and with fields B less than a few tens of gauss the condition $\omega^2 \ll \nu^2$ holds.

In this event, with electrons,

$$\left.\begin{aligned} W_z &\to \frac{Ee}{3m}\overline{c^{-2}\frac{\mathrm{d}}{\mathrm{d}c}\left(\frac{c^3}{\nu}\right)} = \frac{Ee}{3m}\overline{c^{-2}\frac{\mathrm{d}}{\mathrm{d}c}(lc^2)} = W, \\ W_x &\to \frac{Ee}{3m}\cdot\omega\overline{c^{-2}\frac{\mathrm{d}}{\mathrm{d}c}(l^2c)}, \\ \tan\theta &= \omega\cdot\overline{c^{-2}\frac{\mathrm{d}}{\mathrm{d}c}(l^2c)}\Big/\overline{c^{-2}\frac{\mathrm{d}}{\mathrm{d}c}(lc^2)} \\ &= \omega\cdot\overline{c^{-2}\frac{\mathrm{d}}{\mathrm{d}c}(l^2c)}\cdot\overline{c^{-2}\frac{\mathrm{d}}{\mathrm{d}c}(lc^2)}\Big/\left[\overline{c^{-2}\frac{\mathrm{d}}{\mathrm{d}c}(lc^2)}\right]^2 = -\frac{WB}{CE}, \end{aligned}\right\} \quad \ldots\ (18)$$

where

$$C = \frac{1}{3}\left[\overline{c^{-2}\frac{\mathrm{d}}{\mathrm{d}c}(lc^2)}\right]^2\Big/\overline{c^{-2}\frac{\mathrm{d}}{\mathrm{d}c}(l^2c)},$$

a dimensionless factor. Thus

$$|W| = \frac{CE}{B}|\tan\theta|. \quad \ldots\ (19)$$

Since $\tan\theta$ can be measured directly, W can be calculated if C is known. The value of C depends upon the distribution function $f(c)$ and the dependence $l \equiv l(c)$, of l upon c.

(*j*) *High Frequency Conductivity of a Weakly Ionized Gas*

An alternating electric field $E_x = X_0\cos(pt+\alpha)$, in the directions $\pm Ox$ can be resolved into two oppositely rotating vector fields as follows:

$$E_x = \tfrac{1}{2}X\exp(\mathrm{i}pt) + \tfrac{1}{2}X^*\exp(-\mathrm{i}pt),$$

where $X = X_0\exp(\mathrm{i}\alpha)$ and $X^* = X_0\exp(-\mathrm{i}\alpha)$.

It follows from equation (**15**) that the components of W are given by

$$W_x+\mathrm{i}W_y=(W_x^+ +\mathrm{i}W_y^+)+(W_x^- +\mathrm{i}W_y^-)$$
$$=\frac{e}{6m}c^{-2}\,\overline{\frac{\mathrm{d}}{\mathrm{d}c}\left\{c^3\left[\frac{X\exp(\mathrm{i}pt)}{\nu-\mathrm{i}(\omega-p)}+\frac{X^*\exp(-\mathrm{i}pt)}{\nu-\mathrm{i}(\omega+p)}\right]\right\}}. \quad \ldots (20)$$

The associated current densities are $J_x=neW_x$ and $J_y=neW_y$.

When the electric field also possesses components $E_y=Y\cos(pt+\beta)$ and $E_z=Z\cos(pt+\gamma)$ it can be seen that the complex current density $J(J_x,J_y,J_z)$ whose real parts give the physical current density is

$$\left.\begin{aligned}(J)=\begin{Bmatrix}J_x\\J_y\\J_z\end{Bmatrix}=|\,\sigma^+\,|\begin{Bmatrix}X\\Y\\Z\end{Bmatrix}\exp(\mathrm{i}pt)+|\,\sigma^-\,|\begin{Bmatrix}X^*\\Y^*\\Z^*\end{Bmatrix}\exp(-\mathrm{i}pt),\\ \text{in which}\\ |\,\sigma^+\,|=\begin{vmatrix}\sigma_{xx}^+&\sigma_{xy}^+&0\\\sigma_{yx}^+&\sigma_{yy}^+&0\\0&0&\sigma_{zz}^+\end{vmatrix}\quad\text{and}\quad|\,\sigma^-\,|=\begin{vmatrix}\sigma_{xx}^-&\sigma_{xy}^-&0\\\sigma_{yx}^-&\sigma_{yy}^-&0\\0&0&\sigma_{zz}^-\end{vmatrix},\\ \text{with } X=X_0\exp(\mathrm{i}\alpha),\ Y=Y_0\exp(\mathrm{i}\beta),\ Z=Z_0\exp(\mathrm{i}\gamma),\text{ and}\\ \sigma_{xx}^+=\sigma_{yy}^+=\mathrm{i}\sigma_{xy}^+=-\mathrm{i}\sigma_{yx}^+=(ne^2/6m)c^{-2}\,\overline{\frac{\mathrm{d}}{\mathrm{d}c}\,\frac{c^3}{\nu-\mathrm{i}(\omega-p)}},\\ \sigma_{xx}^-=\sigma_{yy}^-=\mathrm{i}\sigma_{xy}^-=-\mathrm{i}\sigma_{yx}^-=(ne^2/6m)c^{-2}\,\overline{\frac{\mathrm{d}}{\mathrm{d}c}\,\frac{c^3}{\nu-\mathrm{i}(\omega+p)}},\\ \sigma_{zz}^+=\sigma_{zz}^-=\sigma=\frac{ne^2}{3m}\,\overline{c^{-2}\,\frac{\mathrm{d}}{\mathrm{d}c}\left[\frac{c^3}{\nu+\mathrm{i}p}\right]}.\end{aligned}\right\} \quad \ldots (21)$$

III. Diffusion

(*a*) *General*

The agitational motion of the electrons or ions operates to diminish inequalities in their concentration n and to disperse a group of electrons throughout the gas. Across an elementary geometrical surface $\mathrm{d}\mathbf{S}$ at a position where grad n is not zero there is, due to diffusion, a net flux of electrons which is a function of the components of grad n. In practice $|\,\text{grad}\,n\,|/n$ is small and this flux is accurately proportional to $-\text{grad}\,n\cdot\mathrm{d}\mathbf{S}$ when no magnetic field is present. The coefficient of proportionality D is called the coefficient of diffusion. The flux is therefore $-D\,\text{grad}\,n\cdot\mathrm{d}\mathbf{S}=n\mathbf{w}\cdot\mathrm{d}\mathbf{S}$, where $\mathbf{w}$ is an equivalent convective velocity that would give the same flux across $\mathrm{d}\mathbf{S}$ were grad n equal to zero. The net transport of electrons across $\mathrm{d}\mathbf{S}$ in time $\mathrm{d}t$, being the difference between those that cross in opposite senses, is therefore

$$n\mathbf{w}\cdot\mathrm{d}\mathbf{S}\mathrm{d}t=-D\,\text{grad}\,n\cdot\mathrm{d}\mathbf{S}\mathrm{d}t.$$

(*b*) *Formula for the Coefficient of Diffusion* D

Let the direction of grad n be that of the coordinate axis $+Ox$ so that $n\mathbf{w}=n\mathbf{w}_x=-D\partial n/\partial x$, $w=-(D/n)\partial n/\partial x$. Let $w(c)$ and n_c refer to the electrons with speeds between c and $c+\mathrm{d}c$. Then $w(c)=-(D(c)/n_c)\partial n_c/\partial x$.

Consider a volume bounded by surfaces of unit area normal to Ox and a distance $\mathrm{d}x$ apart. The mean momentum of the electrons (or ions) with speeds c within this volume is $n_c m w(c)\mathrm{d}x$ and, according to equation (**3**), the rate at which momentum is destroyed within the volume is $n_c m w(c) g/l \mathrm{d}x$, where

$$l = l_0/[M/(M+m)-\alpha] = (l_0+S),$$

where S is defined in equation (**5**) and g is the mean velocity of an electron (or ion) with speed c relative to a molecule. When $\mathbf{w}(c)$ is constant this momentum is restored by transport of momentum across the boundaries. Let the unit boundary surfaces lie at positions x and $x+\mathrm{d}x$ on Ox. The mean momentum transported in time $\mathrm{d}t$ by electrons with speeds c in the direction $+Ox$ into the volume, across the unit boundary at x, is $\frac{1}{2}n_c m\overline{u^2}\mathrm{d}t = \frac{1}{6}n_c mc^2\mathrm{d}t$. The same quantity of momentum leaves the volume in time $\mathrm{d}t$ in the direction $-Ox$ and by Newton's third law there is an equal gain of momentum to the volume in the direction $+Ox$. Thus the total gain of momentum is $\frac{1}{3}n_c mc^2\mathrm{d}t$ in the direction $+Ox$. Similarly, the gain of momentum in the sense $+Ox$ across the boundary at $x+\mathrm{d}x$ is $-\frac{1}{3}mc^2\mathrm{d}t\{n_c+(\mathrm{d}n_c/\mathrm{d}x)\mathrm{d}x\}$.

The total gain of momentum in the sense $+Ox$ is therefore

$$-\tfrac{1}{3}mc^2(\mathrm{d}n_c/\mathrm{d}x)\mathrm{d}x\mathrm{d}t = -(\partial p_c/\partial x)\mathrm{d}x\mathrm{d}t,$$

where p_c is the partial pressure of the electrons (or ions) with speeds c. Thus the condition that $w(c)$ should not change with time is

$$-n_c m w(c) g/l - \tfrac{1}{3}mc^2\mathrm{d}n_c/\mathrm{d}x = 0,$$

or

$$\frac{-D(c)}{n_c}\frac{\mathrm{d}n_c}{\mathrm{d}c} = w(c) = -\frac{lc^2}{3g}\frac{1}{n_c}\frac{\mathrm{d}n_c}{\mathrm{d}x},$$

from which it follows that

$$\left.\begin{aligned} D(c) &= \tfrac{1}{3}(lc^2/g) \quad \text{and} \quad D = \overline{D(c)} = \tfrac{1}{3}\overline{(lc^2/g)}. \\ \text{With electrons, } g &= c \quad \text{and} \quad D = \tfrac{1}{3}(\overline{lc}). \end{aligned}\right\} \quad \ldots\ldots\ldots (22)$$

When a magnetic field B is present, the free paths of the ions or electrons are changed from straight lines between encounters to helices whose axes are parallel to B and about which they move with angular velocity $\omega = -Be/m$. The effect of the field is to reduce the coefficient of diffusion in directions normal to B to some value $D_B < D$, whereas that parallel to B retains the value D. It is necessary to obtain a formula for D_B.

Let $|\operatorname{grad} n| = \mathrm{d}n/\mathrm{d}x$, and consider the situation where $\mathbf{B}$ is parallel to $+Oy$. The Lorentz force on an electron or ion moving with velocity $\mathbf{w}$ across a magnetic field $\mathbf{B}$ is $\mathbf{F} = e\mathbf{w}\times\mathbf{B}$, consequently the direction of $\mathbf{w}$ in the presence of a magnetic field $\mathbf{B}$ does not in general coincide with that of $-\operatorname{grad} n$. In the present instance $\mathbf{w}$ has components w_x and w_z whereas $\operatorname{grad} n$ has the single component $\mathrm{d}n/\mathrm{d}x$.

The equations of dynamic equilibrium in this case become

$$\left.\begin{aligned} n_c\{-mw_z(c)g/l + w_x(c)eB\} &= 0, \\ -n_c m w_x(c) g/l - n_c w_z(c) eB - \tfrac{1}{3}mc^2\mathrm{d}n_c/\mathrm{d}x &= 0. \end{aligned}\right\} \quad \ldots\ldots (23)$$

Write, as before, $\omega=-eB/m$, then

$$w_z(c)=-w_x(c)l/g \text{ and } n_c w_x(c)=-\frac{lc^2}{3g}\cdot\frac{1}{[1+\omega^2l^2/g^2]}\frac{\mathrm{d}n}{\mathrm{d}x},$$

whence

$$D_B(c)=\frac{lc^2}{3g}\frac{1}{[1+\omega^2l^2/g^2]}=\frac{1}{3}\frac{c^2T}{[1+\omega^2T^2]},$$

where $T=l/g=1/\nu$. The coefficient of diffusion is therefore

$$D_B=\tfrac{1}{3}\overline{c^2T/[1+\omega^2T^2]}. \quad \ldots\ldots\ldots\ldots\ldots\ldots\ldots\ldots \quad (24)$$

With electrons $g=c$ and $T=l/c=1/\nu$.
Also,

$$nw_z=-\overline{\omega T}.nw_x=\overline{\omega T}D_B\mathrm{d}n/\mathrm{d}x. \quad \ldots\ldots\ldots\ldots\ldots\ldots\ldots \quad (25)$$

The more general case of diffusion in the presence of a magnetic field with **B** directed along $+Oy$ and grad n arbitrarily directed is expressible in matrix notation as follows ($\omega=-Be/m$):

$$-n\begin{Bmatrix}w_x\\w_y\\w_z\end{Bmatrix}=\begin{Bmatrix}D_B & 0 & \overline{\omega T}D_B\\ 0 & D & 0\\ -\overline{\omega T}D_B & 0 & D_B\end{Bmatrix}\begin{Bmatrix}\partial n/\partial x\\ \partial n/\partial y\\ \partial n/\partial z\end{Bmatrix}. \quad \ldots\ldots \quad (26)$$

IV. The Distribution Function f(c)

Consider first the interchange of energy in a collision between an electron (or ion) and a molecule of the gas.

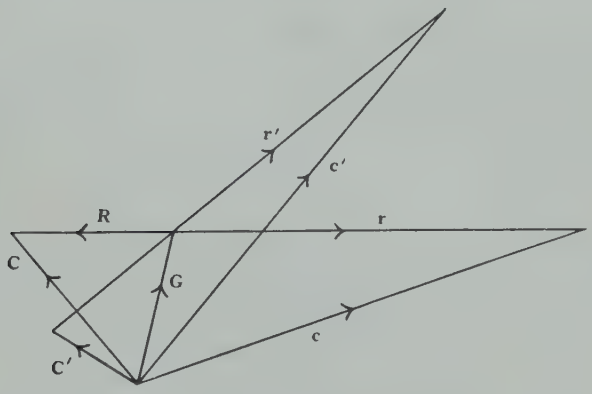

Fig. 4

(a) *Losses of Energy in Collisions*

Let **c** and **C** (Fig. 4) be the velocities respectively of an electron (or ion) and a molecule before the encounter and **c′** and **C′** the velocities following the encounter. The velocity $\mathbf{G}=m\mathbf{c}+M\mathbf{C}/(m+M)=m\mathbf{c}'+M\mathbf{C}'/(m+M)$ of the centroid X of m and M is unchanged by the encounter but the velocities **r** and **R** relative to X become **r′** and **R′**.

The following relations hold :

$$\left.\begin{aligned} \mathbf{c}=\mathbf{G}+\mathbf{r}, \qquad & \mathbf{c}'=\mathbf{G}+\mathbf{r}', \\ c^2=G^2+r^2+2\mathbf{G}\cdot\mathbf{r}, \quad & c'^2=G^2+r'^2+2\mathbf{G}\cdot\mathbf{r}', \\ c^2-c'^2=2\mathbf{G}\cdot(\mathbf{r}-\mathbf{r}')+r^2-r'^2. & \end{aligned}\right\} \quad \text{whence} \quad \ldots\ldots (27)$$

Further progress requires special assumptions.

(i) *Perfectly Elastic Collisions between Smooth Rigid Spheres.*—$r^2=r'^2$; all directions of $\mathbf{r}'$ about X are equally probable and the mean value of $\mathbf{G}\cdot\mathbf{r}'$ is zero. Then,

$$c^2-c'^2=2\mathbf{G}\cdot\mathbf{r}=2\left(\frac{m\mathbf{c}+M\mathbf{C}}{m+M}\right)\cdot\frac{M}{m+M}(\mathbf{c}-\mathbf{C}),$$

which, after reduction, gives

$$c^2-c'^2=\frac{2M}{(m+M)^2}[mc^2-MC^2+(M-m)\mathbf{c}\cdot\mathbf{C}].$$

Since $\mathbf{c}\cdot\mathbf{C}$ is zero in the mean, all directions of $\mathbf{C}$ being equally probable, it follows that the mean loss of energy in an encounter is, when c is given,

$$\tfrac{1}{2}mc^2-\tfrac{1}{2}mc'^2=\frac{2Mm}{(M+m)^2}[\tfrac{1}{2}mc^2-\tfrac{1}{2}M\overline{C^2}]. \quad \ldots\ldots (28)$$

(ii) *Scattering Elastic but not Isotropic.*—In this case $r'=r$, but with $\mathbf{c}$ and $\mathbf{C}$ given the mean value of the projection of $\mathbf{r}'$ on $\mathbf{r}$ is not zero but equal to $\beta\mathbf{r}$ where β is a function of r.

Thus, $c^2-c'^2=2\mathbf{G}\cdot(\mathbf{r}-\mathbf{r}')=2(1-\beta)\mathbf{G}\cdot\mathbf{r}$, and it follows as above, that

$$c^2-c'^2=\frac{2M}{(M+m)^2}(1-\beta)[mc^2-MC^2-(M-m)\mathbf{c}\cdot\mathbf{C}]$$

so that when $\mathbf{C}$ is given all directions and magnitudes

$$\tfrac{1}{2}mc^2-\tfrac{1}{2}mc'^2=(1-\overline{\beta})\frac{2Mm}{(M+m)^2}[\tfrac{1}{2}mc^2-\tfrac{1}{2}M\overline{C^2}], \quad \ldots\ldots (29)$$

in which $\overline{\beta}$ is the mean value of the projection of the velocities $\mathbf{r}'$ upon c, which, according to Section II (*e*), is the same as $\alpha=\overline{\cos\theta}$.

(*b*) *Derivation of the Distribution Function* f(c)

According to equations (**2**) and (**3**) the general form of the distribution function with a uniform and constant electric field $\mathbf{E}$ is,

$$F(c,u)=f(c)-\frac{Eel}{mg}\frac{u}{c}\frac{\mathrm{d}f}{\mathrm{d}c}. \quad \ldots\ldots (30)$$

In a steady state of motion the number of electrons with speeds between c and $c+\mathrm{d}c$ is $4\pi F(c,u)c^2\mathrm{d}c$ and the mean population of this group is constant. The

mean rate at which energy is supplied to the group is $nEeuF(c,u)\cdot 4\pi c^2 dc$ averaged over all values of u with c constant and is equal to

$$-\frac{E^2e^2lc}{3mg}\frac{df}{dc}4\pi c^2 dc.$$

The group transfers energy to the molecules at the same rate, otherwise its population would change.

Consider first the case in which the molecules are at rest ($\overline{C^2}=0$) and their encounters with electrons (or ions) resemble those between smooth rigid spheres ($\alpha=0$). The rate at which the group loses energy in encounters is

$$(4\pi c^2 f dc)n\cdot\frac{2Mm}{(M+m)^2}\cdot\tfrac{1}{2}mc^2\frac{g}{l_0},$$

with $l_0=Ml/(M+m)$ (Section II (e)).

It follows that

$$-\tfrac{1}{3}\left(\frac{Eel}{mg}\right)^2\frac{df}{dc}=-\frac{V^2}{3}\frac{df}{dc}=\frac{mc}{(M+m)}f, \quad \ldots\ldots\ldots (31)$$

whence

$$f(c)=\text{Const. exp}-\frac{m}{M+m}\int^c\frac{3cdc}{V^2}, \quad \ldots (32)$$

where $V=Eel/mg$.

In order to infer the form of $f(c)$ when $\frac{1}{2}M\overline{C^2}$ is not zero use is made of the fact that $f(c)$ reverts to Maxwell's distribution $f(c)=\exp(-3mc^2/2M\overline{C^2})$ when $V\to 0$. In this condition

$$df/dc=-(3mc/M\overline{C^2})f, \quad \ldots\ldots\ldots\ldots (33)$$

and the appropriate form of equation (31), when $\frac{1}{2}M\overline{C^2}$ is not zero, may be inferred to be

$$\tfrac{1}{3}\left(V^2+\frac{M}{M+m}\overline{C^2}\right)\frac{df}{dc}=-\frac{mc}{(M+m)}f. \quad \ldots\ldots\ldots (34)$$

Thus

$$\left.\begin{aligned} f(c)&=\text{const. exp}-\frac{3m}{(M+m)}\int^c\frac{cdc}{\left(V^2+\frac{M}{M+m}\overline{C^2}\right)}\\ &=\text{const. exp}-\int^c\frac{mcdc}{\frac{1}{3}(M\overline{C^2}+(M+m)V^2)}\\ &=\text{const. exp}-\int^c\frac{mcdc}{\varkappa T+\frac{1}{3}(M+m)V^2}. \end{aligned}\right\} \quad \ldots\ldots (35)$$

For electrons $M+m\simeq M$, $g\to c$, $V=Eel/mc$, and the expression for $f(c)$ is equivalent to that given by Chapman and Cowling (1952, p. 350).

The problem of the distribution function $f(c)$ has been considered by many investigators and references to their work will be found in the treatises of Chapman and Cowling (1952, p. 346) and of Loeb (1955, Ch. IV).

Equation (**31**) may also be derived as follows. The acceleration Ee/m in ordinary space corresponds to a constant velocity Ee/m in velocity space with a radial component $(Ee/m)(u/c)$. This radial component produces in the distribution given by equation (**2**) outward flux of representative points over the spherical surface with radius c, of amount

$$-4\pi c^2\left(\frac{E^2e^2}{3m}\,\frac{l}{g}\right)\frac{\mathrm{d}f}{\mathrm{d}c}\cdot n,$$

and in a permanent distribution this outward flux is balanced by an inward flux brought about by losses of energy in encounters. Let the encounters be similar to those between rigid smooth spheres, then the mean loss of speed $\Delta c=c-c'$ in an encounter is to be obtained from $c^2-c'^2=2Mmc^2/(M+m)^2$, it being supposed that the molecules are at rest. When $\Delta c/c\ll 1$ it follows that $\Delta c\simeq Mmc/(M+m)^2$. The inward flux over the surface with radius c is equal to the number of collisions in unit time that are made by all electrons in the velocity range c to $c+\Delta c$, namely,

$$nf\frac{g}{l_0}\cdot 4\pi c^2\cdot\frac{Mmc}{(M+m)^2}=nf\frac{g}{l}\cdot 4\pi c^2\frac{mc}{(M+m)},$$

from which it follows that

$$-\tfrac{1}{3}\left(\frac{Ee}{m}\,\frac{l}{g}\right)\frac{2\mathrm{d}f}{\mathrm{d}c}=\frac{mc}{M+m}f,$$

which is equation (**31**).

Equation (**34**) may also be derived with greater rigour as follows. As discussed above, the acceleration $\mathbf{E}e/m$ in ordinary space becomes a velocity $\mathbf{E}e/m$ of a representative point in velocity space with a radial component Eeu/mc at the surface of a sphere with radius c. This radial component is associated with an outward flux of representative points over the sphere equal to $4\pi c^2n\overline{F(c,u)Eeu/mc}$ where the average is taken with respect to u with c constant. Since

$$F(c,u)=f(c)-\left(\frac{Eel}{mg}\right)\frac{u}{c}\,\frac{\mathrm{d}f}{\mathrm{d}c},$$

it follows that the outward flux of points (in unit time) is

$$\frac{-4\pi c^2}{3}n\left(\frac{Ee}{m}\right)^2\,\frac{l}{g}\,\frac{\mathrm{d}f}{\mathrm{d}c}.$$

In a steady distribution this outward flux is cancelled by an equal and opposite inward flux that arises from the losses of speed in encounters. First suppose that the molecules are at rest. In Figure 5, $\mathbf{OA}=\mathbf{c}$ is the velocity of an electron (mass m) that collides with a molecule at rest (mass M). $\mathbf{OX}$ is the velocity $\mathbf{G}=m\mathbf{c}/(M+m)$ of the centroid of m and M, and $G\ll c$. Let the velocity of the electron after the collision relative to the centroid be $\mathbf{r}'=\mathbf{XQ}$, then the total velocity is $\mathbf{c}'=\mathbf{OQ}$. Since $r'=XA$, it follows that $c'<c$ and all representative points $\mathbf{c}'$ lie within the sphere with radius c. If the initial velocity

is **OB** with a speed $c+x$, where $x=AB$, then the representative points after collision lie on a sphere whose centre is at X', where

$$OX'=\frac{m}{M+m}(c+x)\simeq\frac{mc}{M+m},$$

and whose radius $r=X'B$. This sphere intersects the sphere with centre O and radius c in a circle on which lies the point P. Thus the representative points that lie on the spherical cap PBP' lie outside the sphere with centre O whereas those on the complementary arc lie within. Let $c^2\mathrm{d}\omega$ be an element of surface on which A lies. The number of velocity points within an element of volume $c^2\mathrm{d}\omega\mathrm{d}x$ at B is $nfc^2\mathrm{d}\omega\mathrm{d}x$ and the corresponding number of encounters

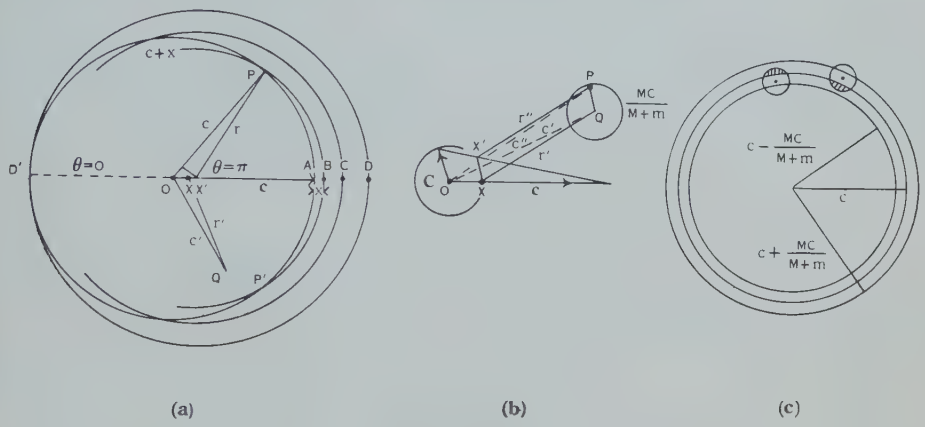

Fig. 5

in unit time is $p=c^2\mathrm{d}\omega nf(g/l_0)\mathrm{d}x$. Let the angle $D'OP=\theta$, then if the scattering is isotropic the number of encounters that give velocity points within the sphere of radius c is $\frac{1}{2}p(1-\cos\theta)$ in unit time. When the scattering is not isotropic this number becomes

$$p\frac{\varphi(\theta)(1-\cos\theta)}{2},\quad\text{with }\tfrac{1}{2}\int_0^\pi\varphi(\theta)\sin\theta\mathrm{d}\theta=1.$$

From the figure, $c^2=r^2+OX'^2-2OX'.r\cos\theta$ with $OX'=\{mc/(M+m)\}(c+x)$ and $r=\{M/(M+m)\}(c+x)$, and it can be deduced that

$$x\simeq\frac{Mmc}{(M+m)^2}(1+\cos\theta),\quad \mathrm{d}x=-\frac{Mmc}{(M+m)^2}\sin\theta\mathrm{d}\theta.$$

The number of encounters in unit time for which the initial velocity points lie within the element of velocity space $c^2\mathrm{d}\omega.AD$ and whose final points fall within the sphere c is therefore

$$\begin{aligned}nfc^2\mathrm{d}\omega\frac{g}{2l_0}\int_A^D\varphi(\theta)(1-\cos\theta)\mathrm{d}x&=\frac{nfc^2\mathrm{d}\omega g}{2l_0}\cdot\frac{Mmc}{(M+m)^2}\int_0^\pi(1-\cos\theta)\varphi(\theta)\sin\theta\mathrm{d}\theta\\&=\frac{(1-\overline{\cos\theta})}{l_0}g\cdot\frac{Mmc}{(M+m)^2}nfc^2\mathrm{d}\omega\\&=\frac{gmc}{l(M+m)}nfc^2\mathrm{d}\omega,\end{aligned}$$

where, in accordance with equation (3), $l=l_0(M+m)/M(1-\overline{\cos\theta})$. The inward flux of points across unit area in unit time is therefore $\{gmc/l(M+m)\}nf$. To estimate the influence of the molecular motions, consider Figure 5 (*b*). When the molecules are at rest the velocity of the centroid is $\mathbf{OX}=m\mathbf{c}/(M+m)=\mathbf{G}$; $G\ll c$. An encounter transforms $\mathbf{c}$ into $\mathbf{c}'=\mathbf{G}''\mathbf{r}'$. When the molecule has a velocity $\mathbf{C}$, $\mathbf{G}=\mathbf{OX}$ becomes $\mathbf{G}=\mathbf{OX}'$, $\mathbf{c}'\rightarrow\mathbf{c}''=\mathbf{G}'+\mathbf{r}''$, with $r''\simeq r'$. As $\mathbf{C}$ assumes all possible directions, the end points of c'' lie on the surface of a sphere about P and with radius $\{M/(M+m)\}C$. Thus, in velocity space (Fig. 5 (*c*)) the points which originally lay within an element of volume now become dispersed over a sphere centred on the volume and with radius $MC/(M+m)$. The spherical dispersal of velocity points about such elements of volume lying between two spherical surfaces with radii $c\pm MC/(M+m)$ give a flux of points inwards across the spherical surface with radius c. If $|y|<MC/(M+m)$ is the distance of an elementary volume from the surface with radius c, then it is readily shown that the flux of points inwards across unit surface of the sphere c is

$$(1-\cos\bar{\theta})n\frac{g}{2l_0}\times\int_{-MC/(M+m)}^{MC/(M+m)}(1-|y|)\left(f+y\frac{\mathrm{d}f}{\mathrm{d}c}\right)\mathrm{d}y$$
$$=\frac{(1-\overline{\cos\theta})M}{3(M+m)l_0}\frac{gMC^2}{(M+m)}n\frac{\mathrm{d}f}{\mathrm{d}c}=\frac{gMC^2}{3l(M+m)}n\frac{\mathrm{d}f}{\mathrm{d}c}.$$

The mean flux for all values of C is

$$\frac{ng}{3l}\frac{M\overline{C^2}}{(M+m)}\frac{\mathrm{d}f}{\mathrm{d}c}.$$

In a steady distribution of speeds c the total flux across any sphere in velocity space is zero, thus,

$$-\left(\frac{Ee}{m}\right)^2\frac{l}{3g}\frac{\mathrm{d}f}{\mathrm{d}c}-\frac{g}{l}\frac{m}{(M+m)}cf-\frac{gM\overline{C^2}}{3l(M+m)}\frac{\mathrm{d}f}{\mathrm{d}c}=0,$$

or

$$-\tfrac{1}{3}\left(V^2+\frac{M}{M+m}\overline{C^2}\right)\frac{\mathrm{d}f}{\mathrm{d}c}=\frac{mc}{(M+m)}f, \quad \ldots\ldots \quad (34)$$

which is equation (34) whose solution is equation (35).

The general case in which electrons make both elastic encounters and inelastic encounters in which a large proportion of their energy is lost, does not appear to lead to a simple formula for the distribution. Nevertheless, when electrons move in diatomic gases and their mean energies are not greater than about five times that of the gas molecules, the inelastic losses of energy in encounters are associated with changes in the rotational states of the molecules. Moreover, these transitions are produced by those electrons with energies appreciably greater than the mean energy. Let ΔQ be the energy absorbed by a molecule in changing from one rotational state to a neighbouring state. Suppose that in such collisions $\Delta Q/\frac{1}{2}mc^2\ll 1$. Since $c^2-c'^2=2\Delta Q/m$, $\Delta C\simeq\Delta Q/mc$. Let a proportion of encounters in which the speed is c and losses ΔQ occur be $x(c)$. It

follows that the inward flux of points over the sphere of radius c in velocity space now becomes, with $l_0=lM/(M+m)$,

$$nf\left[\frac{mc}{(M+m)}(1-x)g/l+\frac{xg}{l_0}\frac{\Delta Q}{mc}\right]4\pi c^2\mathrm{d}c=nf\left[(1-x)+\left(\frac{M+m}{m}\right)^2\frac{x\Delta Q}{Mc^2}\right]\frac{mc}{(M+m)}4\pi c^2\mathrm{d}c,$$

from which it follows that

$$-\tfrac{1}{3}\left(\frac{Eel}{mg}\right)^2\frac{\mathrm{d}f}{\mathrm{d}c}=\left[1-x+\left(\frac{M+m}{m}\right)^2\frac{x\Delta Q}{M\bar{C}^2}\right]\frac{mc}{M+m}f$$
$$=\frac{1}{a^2}\frac{mc}{(M+m)}f,$$

where a^2 is the reciprocal of the quantity in the square bracket. Which, when modified to allow for the influence of the agitational motions of the molecules to give Maxwell's formula when $E=0$, becomes

$$-\tfrac{1}{3}\left[(aV)^2+\frac{M\bar{C}^2}{M+m}\right]\frac{\mathrm{d}f}{\mathrm{d}c}=\frac{mc}{M+m}f,$$

whence

$$f=\text{const. exp}-\int^c\frac{3mc\mathrm{d}c}{(M+m)(aV)^2+M\bar{C}^2}. \quad \ldots\ldots \quad (36)$$

In practice $x\ll 1$; $m/M\ll 1$; $1/a^2=1+Mx\Delta Q/(mc)^2$,

$$f=\text{const. exp}-\int^c\frac{3mc\mathrm{d}c}{M[(aV)^2+\bar{C}^2]}. \quad \ldots\ldots\ldots\ldots \quad (37)$$

Suppose that $x(c)=0$ when $c<c_1$, then

$$\left.\begin{aligned} f&=\text{const. exp}-\int^c\frac{3mc\mathrm{d}c}{M(V^2+\bar{C}^2)}, \qquad c<c_1 \ldots (a),\\ f&=\text{const. exp}-\int^c\frac{3mc\mathrm{d}c}{M[(aV)^2+\bar{C}^2]}, \quad c>c_1 \ldots (b),\end{aligned}\right\} \quad \ldots\ldots \quad (38)$$

when $c_1\gg\bar{c}$, the distribution, except for the groups with large energies, is the same as if all collisions were elastic ($a=1$, $x=0$).

When c exceeds c_1, $(M/m)x\Delta Q$ soon exceeds 1 and $a\to mc/(xM\Delta Q)^{\frac{1}{2}}$,

$$f\to\text{const. exp}-\frac{3m\Delta Q}{(Ee)^2}\int^c\frac{xc\mathrm{d}c}{l}, \quad c>c_1. \quad \ldots\ldots\ldots \quad (39)$$

(c) *Limiting Form of Equations* (35) *and* (38)

When $V^2\gg\bar{C}^2$ and $c_1\gg\bar{c}$ the speeds of most electrons are distributed according to the law

$$f(c)=\text{const. exp}-\int^c\frac{3mc\mathrm{d}c}{V^2}, \quad \ldots\ldots\ldots\ldots \quad (40)$$

where $V=Eel/mc$.

When $l(c) \propto c^r$ equation (**40**) reduces to the form

$$4\pi c^2 f(c)\mathrm{d}c = \frac{4c^2}{\alpha^3 \Gamma(3/n)} \exp(-c^n/\alpha^n)\mathrm{d}c, \quad \ldots\ldots\ldots (41)$$

where α is a speed and $n = 4 - 2r$. Also

$$4\pi \int_0^\infty f(c) c^2 \mathrm{d}c = 1.$$

It follows from the standard integral

$$\int_0^\infty \exp(-y^n) y^m \mathrm{d}y = \frac{1}{n} \Gamma\left(\frac{m+1}{n}\right)$$

that the mean value of the sth power of the speeds c is

$$\overline{c^s} = \alpha^s \Gamma\left(\frac{s+3}{n}\right) / \Gamma(3/n). \quad \ldots\ldots\ldots (42)$$

The form of the distribution function in a high frequency field is obtained if V^2 in equations (**37**) and (**40**) is given the value

$$V^2 = \left(\frac{Ee}{2m}\right)^2 \left[\frac{1}{\nu^2 + (\omega - p)^2} + \frac{1}{\nu^2 + (\omega + p)^2}\right],$$

as follows from equation (**14**).

V. Ratio W/D

From the expressions for the velocity of drift **W** and the coefficient of diffusion D (equations (**7**) and (**22**)) it follows that

$$\frac{W}{D} = \frac{Ee}{m} \overline{c^{-2} \frac{\mathrm{d}}{\mathrm{d}c}\left(\frac{lc^3}{g}\right)} \Big/ \left(\overline{\frac{lc^2}{g}}\right). \quad \ldots\ldots\ldots (43)$$

In the special cases in which the speeds c are distributed according to Maxwell's formula (equation (**1**)) the factor

$$\begin{aligned}
\overline{c^{-2} \frac{\mathrm{d}}{\mathrm{d}c}\left(\frac{lc^3}{3}\right)} &= \frac{4}{\alpha^3 \sqrt{\pi}} \int_0^\infty \mathrm{e}^{-c^2/\alpha^2} \frac{\mathrm{d}}{\mathrm{d}c}\left(\frac{lc^3}{g}\right)\mathrm{d}c \\
&= \frac{8}{\alpha^5 \sqrt{\pi}} \int_0^\infty \mathrm{e}^{-c^2/\alpha^2} \frac{lc^4}{g}\mathrm{d}c \\
&= 2\left(\overline{\frac{lc^2}{g}}\right) \\
&= \frac{3}{\overline{c^2}}\left(\overline{\frac{lc^2}{g}}\right).
\end{aligned}$$

Consequently, in this case, equation (**43**) becomes

$$\frac{W}{D} = \frac{3}{2}\left(\frac{Ee}{\frac{1}{2}m\overline{c^2}}\right) = \frac{Ee}{\varkappa T} = \frac{EN_0 e}{RT}, \quad \ldots\ldots\ldots (44)$$

where N_0 is Avogadro's number (per mol), $\varkappa$ Boltzmann's constant, and R the gas constant.

The same formula results in the special case in which $l \propto g$ (inverse fifth power law of interaction).

When ions move in gases their agitational speeds are distributed according to Maxwell's law (unless E/p is very large) and equation (**44**) is satisfied, but the motions of electrons in an electric field in a gas do not conform to equation (**43**) in general. The complete expression in this case becomes (with $g=c$)

$$\left.\begin{aligned} &\frac{W}{D}=\left(\frac{Ee}{\tfrac{1}{2}m\overline{c^2}}\right)F, \\ \text{with}\quad &F=\overline{c^2}.\overline{c^{-2}\,\frac{\mathrm{d}}{\mathrm{d}c}(lc^2)/2(\overline{lc})}. \end{aligned}\right\} \quad \ldots\ldots\ldots\ldots\ (45)$$

The value of F is determined both by the law of distribution of the speeds c and the dependence $l \equiv l(c)$. When $l \propto c$ equation (**44**) is valid, but when the law of distribution assumes the more general form of equation (**43**) the values of F that correspond to values of $n=2$, 4, and 6 are $F=3/2$, $1{\cdot}312$, and 1.

VI. References

Allis, W. P. (1956).—Motions of Ions and Electrons. *In* " Handbuch der Physik ". Vol. 21. (Springer-Verlag : Berlin.)

Chapman, S., and Cowling, T. G. (1952).—" The Mathematical Theory of Non-uniform Gases." 2nd Ed. (Cambridge Univ. Press.)

Huxley, L. G. H. (1957*a*).—*Aust. J. Phys.* **10** : 125.

Huxley, L. G. H. (1957*b*).—*Aust. J. Phys.* **10** : 240.

Huxley, L. G. H. (1960).—*Aust. J. Phys.* **13** : 578.

Loeb, L. B. (1955).—"Basic Processes of Gaseous Electronics" (Univ. California Press.)

Margenau, H. (1958).—*Phys. Rev.* **109** : 6.

Maxwell, J. C. (1890).—" Collected Works." Vol. 1, p. 379. (Cambridge Univ. Press.)

SHORT COMMUNICATIONS

GRANULATION NEAR THE EXTREME SOLAR LIMB*

By R. E. Loughhead† and R. J. Bray†

Rösch (1957) found that on good photographs the photospheric granulation remains visible to within less than 10 sec of arc from the limb, and sometimes to less than 5 sec. Recently, however, these results have been contradicted by Edmonds (1960) who, on the basis of an examination of photographs obtained in "Project Stratoscope" (Schwarzschild 1959), finds that the granulation disappears almost completely at $\theta=75°$ (33 sec from the limb). Poor focus obliterates the last vestiges of the pattern closer to the limb; nevertheless, Edmonds concludes that the granulation disappears completely at $\theta=78°$ (21 sec from the limb). Since a determination of the distance from the limb at which the granulation disappears provides an estimate of the height of the top of the convection zone (Plaskett 1955; de Jager 1959), it is important to resolve this contradiction.

An examination of photographs taken with the 5-in. photoheliograph described by Loughhead and Burgess (1958) shows that the granulation remains visible very close to the limb, thus confirming Rösch's results. Plate 1 shows overlapping regions of the Sun in the neighbourhood of the west limb: both enlargements were made from the same original negative, using intermediate negatives of slightly different densities in order partially to compensate for limb darkening. The white line on Plate 1 (*b*) indicates the position of the actual limb, derived from the original negative. Apart from the much brighter *facular* granules, a number of granules can be seen less than 10 sec from the limb; in fact, one rather bright granule can be seen only 4 sec from the limb. Even in regions where individual granules are hard to distinguish, the photograph gives the impression of a low contrast, foreshortened picture of the ordinary 1–2 sec granulation. No granules are visible on the original negative in the last 4 sec to the limb; this region does not appear in Plate 1 (*b*).‡ However, observations of even higher resolution would be required to detect any possible continuation of the granulation so close to the limb.§

These results have been confirmed by other good limb photographs taken during the past three years.

* Manuscript received May 27, 1960.

† Division of Physics, C.S.I.R.O., University Grounds, Chippendale, N.S.W.

‡ Plate 1 was obtained with the aid of a "seeing monitor" (Bray, Loughhead, and Norton 1959), which is now used to trigger automatically the photoheliograph shutters when the seeing signal falls to some predetermined, acceptable value.

§ On the other hand, we have often obtained photographs showing individual *facular* granules only 1–2 sec from the limb.

GRANULATION NEAR THE EXTREME SOLAR LIMB

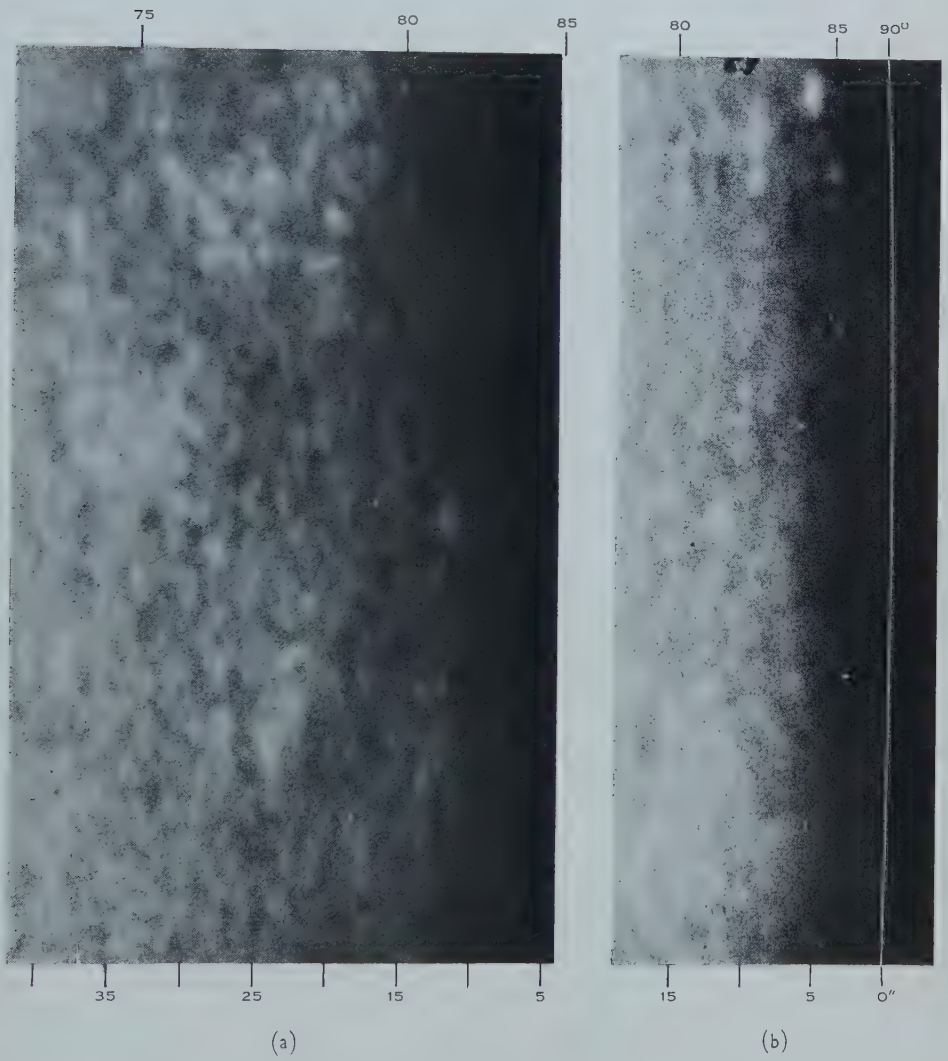

West limb photographed on February 27, 1959, at $11^h\ 44^m$ E.A.S.T. Both prints were made from the same original negative. The white line indicates the position of the actual limb, derived from the negative. The upper scale gives the value of θ, the angle between the line-of-sight and the normal to the photosphere at the point of observation ; the lower scale gives the distance from the limb in seconds of arc.

Edmonds states not only that the granulation vanishes some considerable distance from the limb but that it is replaced by a *larger-scale* pattern of brightness fluctuations with sizes in the range 2–5 sec. Its most prominent features are dark areas, which begin to appear at $\theta=60°$ and are still easily seen out to $\theta=86°$ (2 sec from the limb). We have occasionally observed a similar pattern on our own limb photographs and had previously made an independent assessment of its reality based on an examination of photographs selected from 23 limb films obtained during the last three years. However, we concluded that the effect is spurious for the following reasons :

(1) The effect is best seen on *mediocre* photographs, taken at times of only fair seeing. For example, it is particularly prominent on photographs affected by a type of seeing sometimes encountered which tends to shear the detail by 1 or 2 sec of arc—thus destroying the fine detail but leaving coarser structures more or less unaltered. On all good photographs individual granules can still be distinguished close to the limb ; the dark areas no longer seem to dominate the pattern and merely form part of the network of intergranular material.

(2) The value of θ at which the effect first becomes prominent varies from photograph to photograph.

The effect may be partly due to the fact that on photographs affected by poor definition due to seeing or other causes the ordinary granulation is smeared out, whereas the larger of the dark areas between the granules (which are characteristic features of the ordinary granulation—cf. Bray and Loughhead 1958, Plate 1) remain visible. Near the limb the crowding together of these areas due to foreshortening accentuates the impression of a coarse structure of dark areas on a grey background.

The authors wish to thank Mr. D. G. Norton for help in securing the observations and Mr. H. Gillett for processing the films and making the enlargements.

References

Bray, R. J., and Loughhead, R. E. (1958).—*Aust. J. Phys.* **11** : 507.
Bray, R. J., Loughhead, R. E., and Norton, D. G. (1959).—*Observatory* **79** : 63.
Edmonds, F. N. (1960).—*Astrophys. J.* **131** : 57.
de Jager, C. (1959).—" Handbuch der Physik." (Ed. S. Flügge.) Vol. 52. p. 83. (Springer : Berlin.)
Loughhead, R. E., and Burgess, V. R. (1958).—*Aust. J. Phys.* **11** : 35.
Plaskett, H. H. (1955).—" Vistas in Astronomy." (Ed. A. Beer.) Vol. 1. p. 646. (Pergamon : London.)
Rösch, J. (1957).—*Astronomie* **71** : 138.
Schwarzschild, M. (1959).—*Astrophys. J.* **130** : 345.

AN ATTEMPT TO DETECT LINEAR POLARIZATION IN THE GALACTIC BACKGROUND RADIATION AT 215 Mc/s*

By J. L. Pawsey† and E. Harting†

Current theories of the mode of origin of galactic radio-frequency radiation assume the main component to be due to " synchrotron " emission by relativistic electrons in interstellar magnetic fields. Such emission is almost completely linearly polarized at the point of origin. The received radiation could, however, be substantially depolarized owing to its origin in extended regions of inhomogeneous magnetic field, or to effects associated with the rotation of the plane of polarization in ionized regions with magnetic fields along the line-of-sight. The detection of polarization is a most important observation which could substantiate the " synchrotron " emission hypothesis and provide direct evidence on magnetic fields in interstellar space.

Observations show that the received radiation, both from the discrete sources and the background, is substantially randomly polarized. Linear polarization has been detected at a level of about 5 per cent. at centimetre wavelengths, for one only of the discrete sources (the Crab nebula). Careful observations of the polarization of the background have been reported by two observers: Razin (1958), who used a method based on the rotation of a plane polarized aerial, and Thomson (1957), whose method was based on the detection of correlation between the signals received on aerials polarized in mutually perpendicular planes. Razin worked at wavelengths of 1·45 m (203 Mc/s) and 3·3 m (91 Mc/s), and, in an attempt to eliminate certain sources of error, recorded the difference in apparent polarization observed with bandwidths of 200 kc/s and 5 Mc/s respectively. He reported a difference in apparent polarization on the two bandwidths of 2–4 °K at 1·45 m over all parts of the sky observed, except in the vicinity of the Milky Way where the effect was zero. He interpreted this result as a measure of the polarization of the radiation received on the narrower band, that on the wider being assumed substantially zero owing to depolarizing effects mentioned above. The 3·3 m results were substantially less on a percentage basis and were uncertain. Thomson, observing a strip of the sky at declination 22° N. on 159·5 Mc/s with a bandwidth of 4 Mc/s, set an upper limit of 1 per cent. to the possible polarization, except in two particular regions where he states, " linear polarization of the order of 1 per cent. may have been detected ". The brightness temperature was of the order of 500 °K in this case.

Razin's results, if correct, are of major importance since they imply the existence of magnetic fields and high energy electrons widely distributed throughout the galactic corona. Independent confirmation would be most valuable.

* Manuscript received September 7, 1960.

† Division of Radiophysics, C.S.I.R.O., University Grounds, Chippendale, N.S.W.

It is unfortunate that Thomson's negative results for most of the area examined cannot be directly compared with Razin's since Thomson used a wide bandwidth for which Razin claimed that the observed polarization should be inappreciable. The present paper describes an attempt to confirm Razin's observations.

Observations were made on a frequency of 215 Mc/s with bandwidths of 1 Mc/s, and 700 and 300 kc/s, using a Dicke-type receiver connected to a fixed 60 ft paraboloid directed towards the zenith. A linearly polarized feed aerial at the focus was rotated back and forth through two revolutions and the resulting changes in output recorded.

Spurious results can arise in several ways. If the directional diagram is not circularly symmetric about the axis of the aerial, output fluctuations may arise through directional effects if there are intense sources off the axis of the aerial. We attempted to minimize this effect (1) by using for the feed aerial a 2-dipole array having nearly identical directional patterns in the E and H planes and (2) by restricting observations to times when the principal intense sources, the Sun and the centre of the Galaxy, were below the horizon.

Output changes may also arise through systematic aerial impedance changes associated with the rotation of the system. Such impedance changes were observed and corrective measures employed, but apparently a residual effect remained. A periodic fluctuation of output with rotation, simulating a polarization effect of magnitude about 1·5 °K, was observed, which remained constant in phase and amplitude over the whole of the survey. A genuine polarization effect would be expected to vary with position in the sky, as well as with time owing to changing Faraday rotation in the ionosphere, and we feel confident that this effect was spurious. We have therefore subtracted the mean fluctuation from the individual observations.

A series of observations was made in the period December 1959 to February 1960. The beamwidth of the aerial was 7° and the region observed was a strip centred on declination 34° S. and ranging in right ascension from $1^h\ 30^m$ to 10^h. The noise figure of the receiver was 3·6 (5·5 dB). We consider we could detect reliably a periodic output change ranging from 1·5 °K at a bandwidth of 300 kc/s to 1 °K at 1 Mc/s. The background temperature over this region in the sky is about 150 °K. No output changes which could be attributed to polarization were observed.

These observations set an upper limit of 1 per cent. to the degree of linear polarization over the strip of sky concerned at a frequency of 215 Mc/s and for bandwidths of 1 Mc/s, and 700 and 300 kc/s. This result conforms with Thomson's negative result for most of the region he examined. It appears to contradict Razin's claim that most of the sky remote from the Milky Way shows polarization, but it must be pointed out that Razin's and our actual observations refer to different regions in the sky, Razin's to a strip about declination 56° N., ours to one about 34° S.

A detailed account of the observations is available in a laboratory report (Harting 1960).

References

Harting, E. (1960).—RPR 140. An attempt to detect linear polarization of the galactic background radiation at 215 Mc/s. (Available on request to Chief, Division of Radiophysics, C.S.I.R.O.)

Razin, V. A. (1958).—*Astr. J., Moscow* **35** : 241.

Thomson, J. M. (1957).—*Nature* **180** : 495.

A SYSTEM FOR RECORDING AND INTEGRATING PHYSICAL MEASUREMENTS*

By N. E. Rider†

Introduction

Many occasions occur when it is required to make recordings of one or more fluctuating physical quantities. When the measurements to be made, either of the same quantity at a number of positions or of various quantities at one position, exceed quite a small number, continuous recording is not a practical proposition. In any event it may not be necessary. The frequency with which it would be desirable to record a particular measurement will depend on : (*a*) the expected rate of fluctuation of the quantity concerned having regard to smoothing that may be introduced by the primary sensing device and the recorder in use ; (*b*) the magnitude of the expected fluctuations, again almost certainly modified by the apparatus ; (*c*) the resolution available in a single measurement ; (*d*) the accuracy to which a time mean value is required together with the time over which the mean is to be taken.

Very often the frequency with which individual readings can be made is dictated by the number of different observations required together with the characteristics of the available recording system. Recordings are normally made with appropriate sensing heads working in conjunction with multichannel recorders. The record finally obtained is a representation of the spot values of the quantities at time intervals depending on the switching cycle of the particular recorder. Effective multiplication of the number of recording channels with a decrease in the frequency of recording of a single variable can sometimes be achieved by external switching which is synchronized to any internal switching in the recorder. Various devices have been reported (e.g. McHugo 1959) which will provide an integrated value of at least one variable which is working into a single-channel recorder. A limit to the number of different channels that may be used on one recorder is often set by the chart record itself as this becomes too confused for convenient analysis. In all cases the chart has to be subsequently measured before the desired numerical values are available. This is often tedious and time consuming and provides opportunity for subjective error. The system

* Manuscript received May 9, 1960.

† Division of Plant Industry, C.S.I.R.O., Canberra.

to be described is fully automatic and no error of this type is possible, the individual measurements and their totals over any desired period being presented on counters. Moreover, the initial signals themselves need only be of the order of a fraction of a microvolt and, since reflecting galvanometers provide the initial signal sensing elements, the system is very flexible. It may be made to cater for a wide range of signal magnitudes. To make what is to follow specific the system as constructed to record and integrate the dry- and wet-bulb temperatures from 20 positions will be described. Modifications for other applications will readily suggest themselves.

The System in Outline

The basic idea was first developed by House, Rider, and Tugwell (1960) for use in their surface energy balance computer in which it was necessary to digitize the deflections of a reflecting galvanometer. It has not been described previously and the present system is a further development to more general use. The usual semitransparent scale of a reflecting galvanometer is replaced by a long photovoltaic selenium cell which is covered with a grid consisting of alternate opaque and transparent bands of equal width. The width of the image of the projection lamp slit at the scale distance is made the same as that of these bands. As the image of the slit moves across the photocell scale a series of pulses is produced by the cell. The number of pulses is a measure of the distance swept out by the slit image. If these pulses are applied to an electromagnetic counter via the necessary pulse amplifier a record of the change in galvanometer deflection is obtained. When a current passes through a galvanometer it takes up a position defined by the magnitude of the current and its closed circuit zero position. If the galvanometer is disconnected from the circuit in which this current originates and connected to another circuit, the bias circuit, from which a small current flows which is sufficient to move the image of the projection lamp slit off one end of the scale, the number of pulses produced will be a measure of this position with respect to the end of the scale concerned. Repetition of the operation with the galvanometer connected to its critical damping resistance in place of the signal circuit yields a measure of the zero position of the galvanometer with respect to the same end of the scale. This position is recorded on a second counter. The difference in the counter readings is then a measure of the original current which it is desired to measure and record. Suitable switching enables a sequence of signals to be applied to the one galvanometer and the resulting pulses to be passed to individual counters. The accuracy of recording will be determined by the galvanometer *v.* signal characteristics and the size of the grid spacing used. If the galvanometer and its associated circuits are allowed to pass through a number of cycles of operation the integrated deflections are obtained on the counters, which can then be photographed, or the indications can be printed out, at desired intervals.

Application to Temperature and Humidity Recording

In our present research programme we wished to record a two-dimensional grid of temperature and humidity. Absolute accuracies were relatively unimportant, but temperature and humidity differences in the vertical and

horizontal were required to be as accurate as possible consistent with the use of a reasonable amount of apparatus. Fine wire thermocouples of copper/copper-nickel were used in psychrometer units mounted on masts, there being five such units on each of four masts. Since the dry- and wet-bulb circuits are identical it is only necessary to consider one set, the addition of the other set merely requiring a duplication of the facilities to be described. The arrangement of the masts and wiring (dry bulbs only) for masts 1 and 2 is shown in Figure 1.

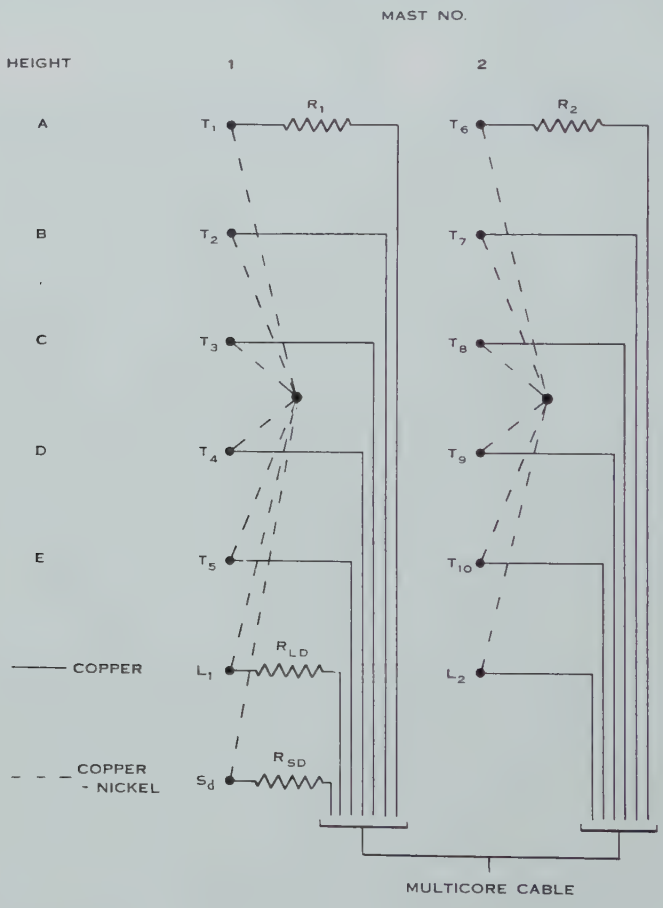

Fig. 1.—Schematic diagram of dry-bulb thermocouple circuits for two masts.

On mast No. 1 it will be seen that, as well as the five thermojunctions at heights from A to E inclusive, a standard junction (S_d) and link junction (L_1) are provided and that all the copper-nickel leads are connected together in one point. Masts Nos. 2–4 are identical and differ from the first in that they have no standard junctions. All the link junctions and the one standard junction are maintained in melting ice. Selection of any pair of copper leads from one mast provides an e.m.f. which is a measure of the small temperature difference existing between the corresponding junctions. These dry-bulb circuits use five galvanometers

and switching arrangements, to be discussed later, enabling connections to be made according to the programme given in Table 1. The time interval of 7 sec is allowed in each circuit since the galvanometers used (Tinsley type 4500, 2 sec periodic time, resistance and sensitivity approximately 50 Ω and 10 cm/μA at 33 cm scale distance respectively) required this time to take up full deflection with the fairly low resistance circuits employed, themselves necessary to obtain the required deflection per degree of temperature difference between junctions. The times not accounted for in Table 1, i.e. 8 to 11, 20 to 23 sec, etc., were occupied in sweeping the slits of the galvanometers off the ends of the scales to obtain records on the deflections at 7, 19, 31, 43, and 55 sec. With this schedule a spot value of the temperatures at each position of exposure is obtained once per minute. A faster schedule would be possible if (*a*) shorter period galvanometers, or (*b*) more galvanometers, or (*c*) higher external circuit resistances were used.

TABLE 1

SCHEDULE OF GALVANOMETER OPERATIONS FOR DRY BULB CIRCUITS

Time (sec)	Galvanometer No.				
	1	2	3	4	5
0–7	T_1 *v.* T_2	T_6 *v.* T_7	T_{11} *v.* T_{12}	T_{16} *v.* T_{17}	zero
12–19	T_1 *v.* T_3	T_6 *v.* T_8	T_{11} *v.* T_{13}	T_{16} *v.* T_{18}	T_2 *v.* S_d
24–31	T_1 *v.* T_4	T_6 *v.* T_9	T_{11} *v.* T_{14}	T_{16} *v.* T_{19}	T_2 *v.* T_7
36–43	T_1 *v.* T_5	T_6 *v.* T_{10}	T_{11} *v.* T_{15}	T_{16} *v.* T_{20}	T_2 *v.* T_{12}
48–55	zero	zero	zero	zero	T_2 *v.* T_{17}

However, the present arrangement compares favourably with what could be achieved with a reasonable number of multichannel recorders, both from the point of view of the resolution available in a single record and in the frequency of measurement at one point. It will be noted that one operation of each galvanometer is occupied in recording its zero position and that the total of 25 operations requires the use of the same number of electromagnetic counters. The link junctions are required in order to avoid the use of long lengths of copper-nickel wire between masts which would otherwise be necessary so that galvanometer No. 5 could execute its last three operations in the schedule. Since the accuracy required in the T_2 *v.* T_7, T_2 *v.* T_{12}, and T_2 *v.* T_{17} temperature difference is the same as in the T_1 *v.* T_2, T_1 *v.* T_3, etc. determinations the additional resistance that would be included in the former circuits by long lengths of copper-nickel wire would not be admissible. The link junctions would not be necessary if all measuring points were in close proximity. The resistances which have been shown in Figure 1 are provided to allow adjustment of the temperature difference *v.* galvanometer deflection characteristics of the various galvanometers and circuits. Actually they are not mounted at the masts but at the recording apparatus. These resistances are adjusted so that the sensitivity of all circuits is the same, with the exception of the T_2 *v.* S_d circuit which has a sensitivity of about one-fifth of the other circuits.

Details of Circuit Arrangements

The basic timing device which controlled the whole cycle of operations was a geared down synchronous motor which operated a 1 sec cam, this cam in turn operating a mercury-in-glass switch which energized the coil of a miniature uniselector. The uniselector had 30 output contacts per level, there being seven levels with provision for inter-level switching. This device provided the means whereby relays could be energized in time intervals down to 1 sec in the cycle of operations lasting 1 min. By grouping the uniselector output contacts any relay could be made to remain energized for any desired period during the cycle.

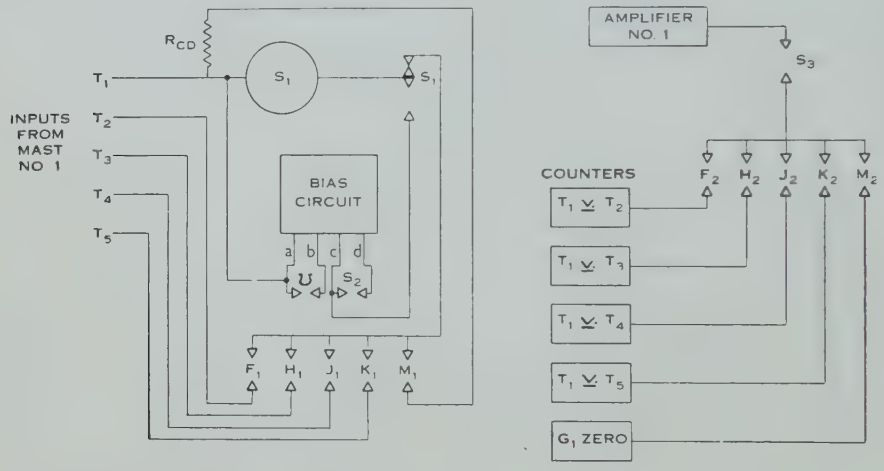

Fig. 2.—Switching circuits for galvanometer and amplifier No. 1. The contacts are shown in their normal positions. The times when they are not in the positions shown are given in Table 2.

We require that the switching arrangements should connect the correct circuits to the galvanometers at predetermined times, apply the currents required to generate the galvanometer sweeps, and select the correct electromagnetic counters to receive the outputs of the pulse amplifiers. Several other functions are also required and were arranged quite easily. The shutter of the automatic 35 mm camera used to record the counter indications must be operated at the correct time in the cycle and after the desired number of cycles have been completed, and the field illumination must be similarly controlled. If, as in the present case, the counters are fitted with reset coils these must be energized immediately following the film exposure. To cater for these operations a second uniselector of the same type as the first is driven from the latter in such a way that it moves on one step per half minute. Many arrangements are possible with these uniselectors according to the requirements of the particular application. In our case an integrated total was required after 20 cycles of operation and arrangements were made for this. We also wished to obtain on occasions an individual record of each cycle of operation and change over to this type of operation was provided for. Further, times occurred when, owing to some

emergency, it was necessary to stop a run and restart. This facility was incorporated by the use of homing arcs on the uniselectors. So many arrangements are possible that it is thought not to be worth while to detail the uniselector and relay energizing wiring and we shall confine ourselves to giving some account of the type of switching that is used in the circuit of one galvanometer (G_1) which is illustrated in Figure 2. Referring to this figure it will be seen that the copper lead from the T_1 junction is connected to one side of G_1 and that the other side of

TABLE 2
TIMES OF OPERATION OF RELAY CONTACTS SHOWN IN FIGURE 2

Contact	Time of Operation (sec)
S_1, S_2, S_3	7–11, 19–23, 31–35, 43–47, 55–59
F_1, F_2	0–11
H_1, H_2	12–23
J_1, J_2	24–35
K_1, K_2	36–47
M_1, M_2	48–59
U	8–11, 20–23, 32–35, 44–47, 56–59

the galvanometer is connected via the change-over contact S_1 to one side of a series of relay contacts marked F_1, H_1, J_1, K_1, and M_1, the other sides being connected directly to T_2, T_3, T_4, T_5, and R_{cd}, the galvanometer critical damping resistance, respectively. The times during which these and all other contacts are not in the positions shown in Figure 2 are given in Table 2. We see, for example that contact F_1 is closed in the period 0–11 sec so that G_1 is in the T_1 *v.* T_2 circuit until S_1 changes over at 7 sec, thus connecting the galvanometer into its

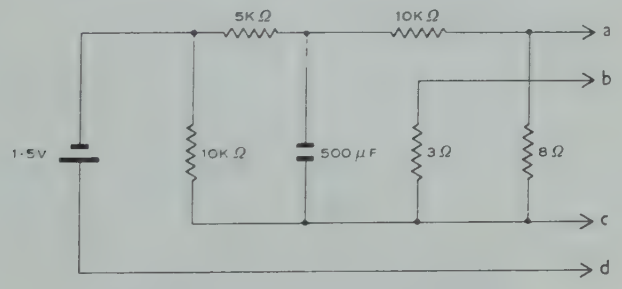

Fig. 3.—The galvanometer bias circuit.

bias circuit which produces the sweep of the slit across the cell. During the period up to 7 sec contact S_3 is open so that although F_2 is closed and the T_1 *v.* T_2 counter is in circuit no pulses which may be produced by the cell and amplifier due to fluctuations in the deflection of the galvanometer will be passed to the counter, only those arising in an actual sweep being recorded. Similar switching circuits are provided for each galvanometer and its associated amplifier and counters and each has its own bias circuit, illustrated in Figure 3, which should be considered in conjunction with Figure 2. The bias circuit consists of a 1·5 V

dry cell and a delay line which is designed to limit the rate at which the bias current rises through the galvanometer, thus ensuring that the sweep commences slowly and later speeds up. On first making contact S_2 all the current flows into the condenser and the current rises through the galvanometer and its parallel resistances as the condenser charges. This arrangement by itself was found to be insufficient to exercise enough control on the sweep speed and so two parallel resistances were used as shown, having values of around 3 and 8 Ω. At first these are both in parallel across the galvanometer but 1 sec after the start of a sweep contact U opens to increase the parallel resistance from about 2 to 8 Ω. The exact values of these two small resistances are adjusted to suit the particular galvanometer. All these bias circuit arrangements were necessary since the photovoltaic cells appear to have an initial lag to changes in light level but once they commence to operate they may be pulsed satisfactorily at speeds up to a few kc/s. The highest speed here is governed by the maximum counting rate of the electromagnetic counters used.

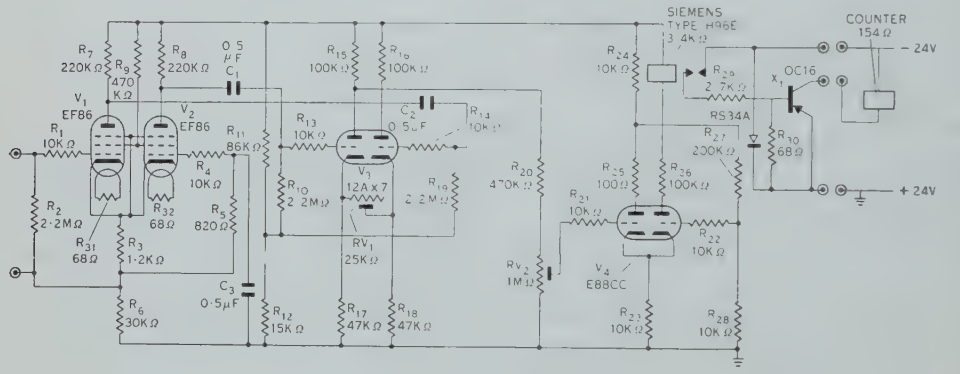

Fig. 4.—The pulse amplifier circuit.

One pulse amplifier was used with each galvanometer. Although photovoltaic cells do not lend themselves very readily to incorporation in electronic circuits (owing to their low internal impedance and small output at the low light levels used here) a satisfactory amplifier design was finally produced and is shown in Figure 4. Very briefly it consists of two EF86's connected as a long tailed pair, followed by a double triode (12AX7) to give further amplification, and the last stage is a Schmitt trigger circuit (Schmitt 1938) which operates a high speed relay. A voltage gain approaching 10^4 is obtained. RV_1 is the gain control and the relay firing point is set with RV_2. The frequency range over which the amplifier will operate is from less than 1 c/s up to a maximum determined by the relay used, in our case about 80 c/s. However, the sweep speed of the galvanometer slit must, as has already been indicated, be kept below the maximum working speed of the counters which in our case was around 35 counts/sec. Precautions have to be taken in the amplifier against oscillation at mains frequency. The valve heaters are connected in series and supplied with 24 V d.c., this supply being also required for the uniselectors, relay coils, and projection lamps. The 300 V h.t. supply must be taken from a good quality

power pack. The contacts of the high speed relay are conveniently protected by the power transistor which is shown in Figure 4. Here, with 24 V counters, the current passed by the relay contacts is completely non-inductive and is less than 10 mA, while virtually the full 24 V is dropped across the counter coil when the relay makes.

The photocells used had the dimensions 15 by 2·5 cm and the metal grids passed five pulses per 1 cm of light movement. Since the cells tend to have small weak areas it is convenient to replace the single band of light from the projector lamp by a double slit or small grid of light the image of which has the same spacing as the grid covering the cell at the scale distance.

It will be clear that the records obtained are independent of long-term galvanometer zero drift. It is only necessary for the zeros to remain fixed for the period occupied by one cycle of operation to eradicate any error which might arise on this account.

Conclusion

The particular form of the system described has been in use in a mobile laboratory for some time where it has been subjected to unusually rough treatment in travelling. All faults that have occurred can be traced to damage in transit and as a static installation the system should prove as reliable as one based on conventional recorders. If the latter had been used it is estimated that several days' work would be involved in chart analysis before a grid of temperature and humidity could be constructed for a single 30 min period. Here the basic information is immediately available in numerical form and such work as is necessary is limited to the use of the psychrometric equation to arrive at values of vapour pressure. It is not necessary to list other possible uses for the system—any application to which photographic, multichannel potentiometric or thread recorders, or pen recorders have hitherto been appropriate could be suitably served. The cost of the system is less than that of potentiometric recorders which would provide the same facilities.

References

House, G. J., Rider, N. E., and Tugwell, C. P. (1960).—*Quart. J. R. Met. Soc.* **86** : 215–31.
McHugo, J. W. (1959).—*J. Sci. Instrum.* **36** : 288–9.
Schmitt, O. H. (1938).—*J. Sci. Instrum.* **15** : 24–6.

NOISE SUPPRESSION IN PULSE RECEIVERS*

By E. C. McLauchlan†

In the course of measuring Southern Hemisphere meteor rates by radar methods, difficulty has been experienced in combating the effect on the meteor rate of a variable background, due to noise of both solar and man-made origin.

The equipment, operating at 69·5 Mc/s, radiates pulses of 23 μsec duration at a pulse recurrence frequency of 150 per sec, and a peak power of 90–100 kW. The echo is detected by a very low noise receiver and applied to the grid of a cathode-ray tube, the trace of which is completely blacked out in the absence of signal. Echoes are recorded on 35 mm film which moves continuously at the rate of 1 ft/hr past the face of the tube. Alternate sweeps of the time-base are shifted slightly in order to present echoes with more certainty as double dots.

A serious shortcoming of this fairly standard system is that any appreciable rise in background noise results in excess darkening of the film, and hence lowered recognition of echoes. This effect is somewhat aggravated by the inherent short grid base of the average cathode-ray tube. The incidence of total black-out due to man-made interference has been greatly reduced by the inclusion of a compression amplifier in the video section of the receiver.

Receiver Modifications

The compression amplifier extends the principle of a constant volume audio amplifier described by G. J. Pope (1952).‡

The essential control element is a cathode follower used as an anode load of a pentode voltage amplifier. Referring to Figure 1, V1 is arranged to give sufficient amplitude of video signal from the receiver, and to be of such a phase that the final video amplifiers V8 and V9 can be operated with positive-going signals from a near cut-off point. The gain control R1 is adjusted so that V2 will not be overloaded by the strongest video input signals.

The resistive anode load of V2 is shunted by the cathode-anode impedance of the cathode follower V5 biased towards cut-off. As the signal applied to V2 is essentially positive-going, V2 is also biased towards cut-off. The anode of V2 feeds the voltage amplifier V3, whose output is rectified by the diode V4 to provide the positive voltage necessary to offset the standing negative bias on V5.

The restricted bandwidth of the V3 circuit, together with the very long time-constant of the rectifier (V4) load circuit, serves to make the bias on V5—and hence the gain of V2—a function of the steady background noise, while it is unaffected by the signal pulses. The tendency of the cathode choke (L1) to oscillate on the receipt of very strong pulses was adequately suppressed by the

* Manuscript received May 30, 1960.

† University of Canterbury, Christchurch, New Zealand.

‡ Pope, G. J. (1952).—*Electron. Engng.* **24**: 464.

NOISE SUPPRESSION IN PULSE RECEIVERS

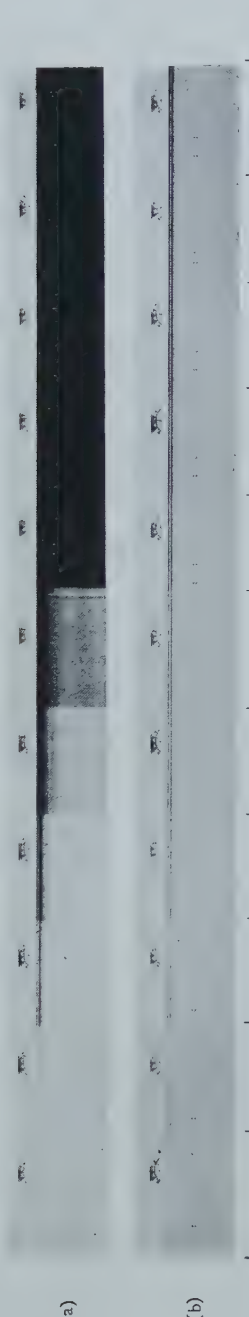

STEP NO.	1	2	3	4	5	6	7	8	9	10	11
	3·96	7·54	11·14	14·74	18·34	21·94	25·54	29·14	32·74	36·34	39·94 × 10^{-16} W

Results of tests, (*a*) without circuit modifications, (*b*) with circuit modifications.

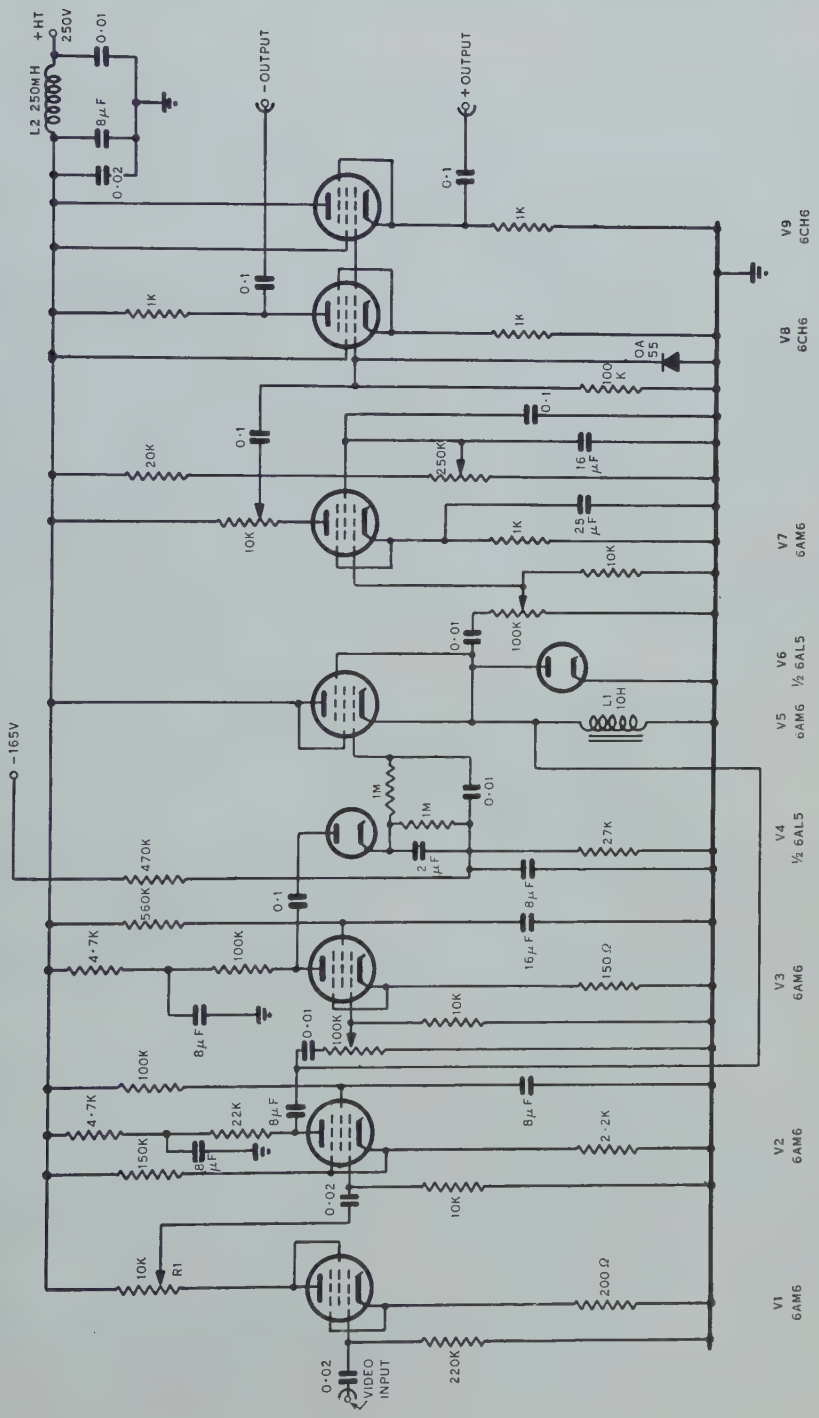

Fig. 1.—Circuit diagram of compression amplifier.

diode V6. The stage V7 acts as a conventional screen-controlled limiter, the limit level being adjusted to avoid defocusing of the cathode-ray tube under strong signal conditions.

System Efficiency

Normal conditions were synthesized for the purpose of assessing the advantage of this additional amplifier over a conventional video system. The output of a diode noise generator was injected into the receiver simultaneously with artificial echoes, of 0·2 sec duration, having the same pulse recurrence frequency and pulse width as the operational transmitter. Both the echo simulator and the noise generator were of equal output impedance.

Five echoes decreasing in amplitude from 4 to 1 μV and spaced 30 sec apart, at constant range, were recorded during each setting of the noise generator output. As the test was intended to be comparative rather than absolute, no attempt was made to match the similar impedance sources to the receiver input. (It is probable, therefore, that the minimum detectable signal power for actual echoes will be below the figures obtained in the present test.) The range of available noise power from the noise generator was less than that expected from variations of aerial noise temperature. Consequently, it was necessary to increase the receiver gain part way through the test. The results of the tests are shown in Plate 1, first for the normal video amplifier, and then with the compression amplifier added. The conditions existing at each of 11 consecutive 3-min intervals were as follows:

Step 1.— The noise generator was at zero output, and the receiver gain was adjusted to give the same detector current as when it was connected to the aerial under quiet conditions. Under these conditions the total noise power is essentially that generated by the receiver itself, which is $3{\cdot}94\times10^{-16}$ W.

Steps 2– 6.—The noise generator output was increased in five steps of $3{\cdot}6\times10^{-16}$ W.

Step 7.— The noise generator output was returned to zero and the receiver gain increased to give the same receiver detector current as had been obtained in step 6. The noise generator output was then increased to $3{\cdot}6\times10^{-16}$ W.

Steps 8–11.—The noise generator was increased in further steps as for the stages 3–6.

Thus by adding the noise power derived from the noise generator to that generated by the receiver the total noise increased from $3{\cdot}94\times10^{-16}$ W for step 1 to a final value of $39{\cdot}94\times10^{-16}$ W for step 11. The plate shows clearly the increased readability of echo rates during periods of high noise, while those obtained during periods of low noise are unaffected.

This work was carried out as part of Contract AF64(500)–6 from the U.S. Air Force Air Research and Development Command. The author is indebted to Dr. C. D. Ellyett for his assistance in preparing the paper.

INDEX

NOTICE TO CONTRIBUTORS

1. GENERAL.—Papers will be considered for publication irrespective of the organization to which the authors are attached. Intending contributors, in preparing papers for submission, should follow the general style adopted in this Journal. A "Guide to Authors" may be obtained on application to the Editor.

   Papers, which should be written as concisely as possible, should be double-space typed on one side of the paper only and with liberal side margins. Every page, including those carrying tables and illustrations, should be numbered. Lengthy manuscripts should be accompanied by a table of contents with headings appropriately numbered. The organization to which the author is attached should be indicated in a footnote.

   The original typescript and one carbon copy should be forwarded.

2. SUMMARY.—A short summary, which may be paragraphed, should precede the introduction to the paper. It should be of an informative character and written in such a way that it can be used by abstracting journals without amendment.

3. REFERENCES.—References are to be cited in the text by the year of publication, e.g. Thomson (1948), and are to be arranged alphabetically, giving the author's name and initials followed by the year of publication, title of the paper (if desired), title of the periodical, volume, and pages, thus:

   Thomson, G. P. (1948).—*Proc. Phys. Soc. Lond.* **61**: 403–16.

   Abbreviations of titles of periodicals should conform to those used in "A World List of Scientific Periodicals".

4. ILLUSTRATIONS.—Line drawings should be made with indian ink on white drawing paper (preferably bristol board), tracing paper, or graph paper. Only blue or very pale grey ruled graph paper should be used as yellow, green, and red lines are difficult to screen out. Blue linen should not be used. Lines should be sufficiently thick and symbols sufficiently large to allow of reduction to a page size of $7\frac{3}{4}$ by 5 in. (or less). It is suggested that figures be drawn approximately twice the width at which they are to be printed. Lettering and numbering should only be pencilled on the drawings as the appropriate type will be substituted before the blocks are made. Original drawings should be submitted but, where possible, photographic copies or blue-prints of the originals should also be forwarded.

   Half-tone photographs, which should be included only where essential, should be on glossy paper and show as much contrast as possible.

5. REPRINTS.—Individual authors receive 40 copies of each paper free, two authors receive 30 each, and three or more authors receive 20 each, but additional copies may be purchased.

CONTENTS

Short Communications

AUSTRALASIAN MEDICAL PUBLISHING CO. LTD.
SEAMER AND ARUNDEL STS., GLEBE, SYDNEY